Title	INCOMMENSURATE STRUCTURE AND PHASE TRANSITIONS IN SOME A_2MBr_4 SALTS AS STUDIED BY BROMINE NUCLEAR QUADRUPOLE ESONANCE
Author(s)	Nakayama, Hirokazu
Citation	大阪大学, 1985, 博士論文
Version Type	VoR
URL	https://hdl.handle.net/11094/24449
rights	
Note	

INCOMMENSURATE STRUCTURE AND PHASE TRANSITIONS

IN SOME A_2MBr_4 SALTS

AS STUDIED BY BROMINE NUCLEAR QUADRUPOLE RESONANCE

BY

Hirokazu Nakayama

M. S., Osaka University, 1981

Thesis

Submitted to

The Graduate School of Faculty of Science,

Osaka University

in Partial Fulfilment of the Requirements
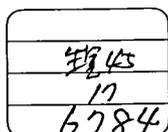
for the Degree of Doctor of Science

1985

Doctoral Committee:

Professor Hideaki Chihara, Chairman,

Professor Hiroshi Suga,

Professor |Shichio Kawai,

Associate Professor Nobuo Nakamura.

Contents

Abstract

Bromine nuclear quadrupole resonance (NQR) experiments were conducted on three isomorphous compounds, Cs_2CdBr_4, Cs_2HgBr_4, and Cs_2ZnBr_4, and $(CH_3NH_3)_2CdBr_4$ to examine the structure and dynamic properties of incommensurate (IC) phase which occurs in Cs_2CdBr_4 and Cs_2HgBr_4, and to understand the general mechanism of the incommensurate transition in materials of A_2BX_4 type from the microscopic point of view.

Efforts were made to prepare samples with high quality . Specimen with such high quality is necessary for the precise measurements of the NQR parameters such as the frequencies of otherwise weak resonance and the spin-lattice relaxation times in the substances, the behavior of which have been considered to be sensitively dependent on the sample impurity and imperfections. Hence an electric furnace with a high performance was designed and constructed and used to prepare the specimens of Cs_2CdBr_4, and Cs_2HgBr_4.

In order to detect the NQR signals and to measure the spin-lattice relaxation times (T_1) of ^{79}Br and ^{81}Br, the frequency of which are located in the VHF region, a pulsed NQR spectrometer was designed and constructed. This spectrometer was organized to a highly sensitive Fourier transform NQR spectrometer to detect very weak NQR signals in the incommensurate phases of Cs_2CdBr_4, and Cs_2HgBr_4. The ^{81}Br NQR

frequencies, and the spin-lattice relaxation times in Cs_2ZnBr_4, which is isomorphous with the above two compounds at room temperature but does not undergo any phase transition , were also measured to understand the "normal" behavior of NQR parameter in $[MBr_4]^{2-}$ type anions

NQR frequency measurements confirmed a previous phase sequence of Cs_2CdBr_4. Its normal room temperature phase changes at T_I=243 K, to an incommensurate phase, the incommensurate phase changes at T_c= 230 K to a commensurate phase, and at 156 K to another low temperature phase. NQR frequencies in the normal phase continued smoothly at T_I to those in the incommensurate phase, indicating that incommensurate phase transition is of the second-order. On the other hand the change in the NQR frequencies at T_c was discontinuous and this fact evidences that the incommensurate to commensurate phase change is of the first-order. The commensurate to the low temperature phase was revealed to be of the second-order. Cs_2HgBr_4 shows a very similar phase sequence to Cs_2CdBr_4. The NQR measurements determined the transition points and the order of the transitions T_I=252 K(second-order), T_c=237 K(first-order), and a transition from the commensurate to a low temperature phase occurs at 156 K(second-order).

In Cs_2CdBr_4, and Cs_2HgBr_4 each gave a pair of very weak resonance lines in 66.4 MHz and 92.5 MHz

regions, respectively in their incommensurate phases. The temperature dependence of the NQR frequencies in each substance was analyzed according to a phenomenological theory of the incommensurate structure and to general group theory. It was inferred that the incommensurate structure in these substances are brought about by small rotation of each $[MBr_4]^{2-}$ anions in an incommensurate manner with the underlying crystal lattice. In order to obtain the further support for the above incommensurate structure a model calculation of the electric field gradient tensor components at each bromine site was carried out by the Bertaut method for the two compounds: The calculated efg reproduced approximately the NQR frequency in each bromine site in the normal and the commensurate phases. It confirmed the above rotationally incommensurate modulation structure of the incommensurate phase, and moreover indicated that the incommensurate modulation wave is directed in the crystalline a-axis. ^{81}Br NQR spin-lattice relaxaton times in Cs_2ZnBr_4 indicated that the libration about the a-axis is mainly excited in this compound. Therefore, this and the above conclusion that the incommensurate structure occurs along the a-axis in Cs_2CdBr_4, and Cs_2HgBr_4 suggest strongly that the rotational displacement of $[MBr_4]^{2-}$ plays an important role to stabilize some special phase in these compounds.

Efforts were made to deduce some correlation

between the structural data and the presence or absence of phase transition for a series of isomorphous A_2BX_4 compounds (A=K, Na, Rb, Cs, B=Cd, Hg, Zn, Co, X=Br, Cl, I). It led to the idea that if the value of $R([BX_4]^{2-})/a$ i.e., the ionic radius of $[BX_4]^{2-}$ complex reduced by a is larger than 0.35, a phase transition should occur. If the value of $R([MX_4]^{2-})/a$ is smaller than 0.35, no phase transition may be expected to occur. This fact indicates that the interaction along the a-axis is important in these compounds in agreement with the results of ANNNI model calculation of the incommensurate structure by Bak.

The ^{81}Br and ^{79}Br NQR frequencies, and the spin-lattice relaxation times in the $(CH_3NH_3)_2CdBr_4$, which has been believed to be a candidate for an incommensurate material, were measured to examine the existence of an incommensurate phase. The results show that there is no phase transition between 78 K and 300 K in this compound. The frequencies of the lower two resonance lines show positive temperature coefficients. The NQR spin-lattice relaxation times decrease rapidly above 200 K. These results were interpreted in terms of some reorientational motion. The activation energy for this mode of reorientation is 20 kJ/mol.

Chapter 1 Introduction

1-1 Introductory remarks

Since the discovery of the structurally incommensurate-commensurate phase transition in K_2SeO_4 in 1969,[1] a large number of compounds have been found to undergo similar incommensurate phase transitions.[2] The most remarkable characteristic of the incommensurate phase is that the periodicity of the atomic or molecular arrangement does not match, i.e., it is incommensurate to the crystal lattice periodicity. An example of such incommensurate nature is described schematically in Figure 1-1.[3] In this figure a and b show normal crytals in which the periodicity of the lattice coincides with that of the atomic arrangement. In this Figure c is an example of incommensurate structure, showing the atomic displacement which is modulated in a wave-like manner independently of the lattice periodicity. This wave-like nature of the displacement is represented by so-called incommensurate modulation wave and its wavelength does not coincide with any integral number times unit cell constant. The crystal cannot therefore be described within the framework of 230 three-dimensional space groups. Translationally commensurate structure is generally restored at a lower temperature through a "lock-in" phase transition.[4]

Figure 1-1. Simple structural model of incommensurate phase. a , b, and c illustrate the atomic position in a normal phase, a commensurate phase and an incommensurate phase, respectively. The amplitude of displacement in each site is represented by u. u forms an incommensurate modulation wave in the incommensurate phase. (after Bak)

A nucleus with spin $I \geq 1$ has quadrupole moment eQ, which interacts with the electric field gradient eq produced by surrounding electrons and nuclei. This quadrupolar interaction energy is quantized into discrete energy levels, and the separation between them lies in radio frequency region. This quadrupolar splitting can be detected by Nuclear Quadrupole Resonance Spectroscopy.[5] The NQR parameters are sensitive to the electronic structure of molecule, the structure of crystal, the charge in the surrounding structure. For example, the number of resonance lines represents the number of crystallographically inequivalent sites of the resonant atomic species. And the resonance frequency is very sensitive to the site symmetry and the local environment. In addition, the nuclear quadrupole relaxation times are mainly governed by local motional states of molecules. Therefore NQR is one of the very powerful tools for investigating the crystal structure and the static and dynamic nature of phase transition in crystalline state.[6] The local structure of incommensurate substance, to which much attention has been paid over more than two decades, can be closely studied by NQR and quadrupole relaxation measurements[7] from the static as well as the dynamic points of view. This method may also throw light into the mechanism which generates incommensurate structure and the elementary excitation in it. Blinc et al.[7]

succeeded to detect NQR signals in the incommensurate phases of the number of substances and showed that the analysis of the line shapes of the NQR signals brings about much helpful information about the structure and the dynamic properties of the incommensurate phases. Blinc and his colleagues applied the NQR method mainly to Rb_2ZnCl_4, Rb_2ZnBr_4 and their analogues which have incommensurate phases characterized by "translationally" incommensurate waves.[8]

There have been known some incommensurate materials belonging to a different class from above substances. $NaNO_2$,[9] K_2SeO_4[10] and thiourea[11] belong to such a class where "rotational" incommensurate wave is responsible for the occurrence of the incommensurate phases. The ^{14}N NQR signals were detected in the incommensurate phase of $NaNO_2$ and analyzed in detail in relation to this type of incommensurate modulation.[9]

Cs_2HgBr_4[12,14-15] and Cs_2CdBr_4[12,13,15] belong also to this class of incommensurate materials. It is believed from the group theoretical point of view that the successive rotational displacements of $[MX_4]^{2-}$ form an incommensurate wave. But the true incommensurate structure, and the mechanism of the incommensurate as well as lock-in transitions in these compounds have not been clarified. It is of much interest to reveal these points and especially to examine if the methods of the data analysis proposed by Blinc et al.[7] and the

theoretical treatment presented can be applied to these materials. In the present study ^{81}Br nuclear quadrupole resonance frequencies and spin-lattice relaxation times in Cs_2HgBr_4, Cs_2CdBr_4, and their isomorphous Cs_2ZnBr_4 ,and $(CH_3NH_3)_2CdBr_4$ were measured as a function of temperature covering the incommensurate and the lock-in transition points. For Cs_2HgBr_4 and Cs_2CdBr_4 efforts were made to detect the signals and to analyze the line shapes in their incommensurate phases by the use of phenomenological theory and a simple model calculation developed in the present work. This model calculation is important in that it can elucidate the structure of the incommensurate phase. The spin-lattice relaxation times, T_1, in these materials were measured to examine the dynamic nature of the commensurate and other low temperature phases as well as the critical nature of each phase transition. The NQR frequencies and spin-lattice relaxation times were measured in Cs_2ZnBr_4 which does not undergo any phase transition[12] as a reference compound to analyze the NQR data in the above two compounds. Since $(CH_3NH_3)_2CdBr_4$ was pointed out to be a candidate of a new incommensurate material by a previous X-ray work,[16] NQR measurements were conducted to confirm the existence of phase transition in it.

The rest of this chapter will be devoted to review the incommensurate phase transition, structure of the

incommensurate phase, theoretical treatment of the incommensurate transition, and NQR and NMR in the incommensurate phase in general, and to describe the gross feature of phase transitions in and physical properties of Cs_2CdBr_4, Cs_2HgBr_4, Cs_2CdBr_4 and $(CH_3NH_3)_2CdBr_4$.

Chapter 2 will describe the instruments constructed in the present work, i.e., electric furnace, pulsed spectrometer for ^{81}Br, and pulsed FT spectrometer for ^{81}Br.

Chapter 3 will describe the method of sample preparation and of NQR measurements.

In Chapter 4 the results of the measurements of ^{81}Br nuclear quadrupole resonance frequencies and spin-lattice relaxation times in the individual salts will be given.

In Chapter 5 the line shape in incommensurate phase in each of Hg- and Cd-salts will be analyzed according to a phenomenological theory and also a model calculation which was newly developed and applied to the incommensurate structure for the first time.

In Chapter 6 classification of A_2BX_4 type of crystals will be made. The factor determining their crystal structure and governing the successive phase transitions was searched and applied to the systems, in which the existence of phase transitions have not been confirmed.

In Appendix 2 the analysis of the spin-lattice

relaxation times in $(CH_3NH_3)_2CdBr_4$ will be given.

1-2 Incommensurate phase transition

Phase transition to an incommensurate phase can be interpreted by extending generalized soft-mode theory of structural phase transitions [17]. A crystal is mechanically stable if vibrational normal mode frequencies are positive because in such a situation the restoring force acts on displaced atoms. But if the force constant for a particular mode is highly anharmonic and decrease on cooling, the frequency of that mode will be decreased to zero at a temperature, T_0. The mode undergoing such a softening is called "soft" mode and T_0 is the critical temperature. The atomic or molecular displacement accompanying the freezing of the soft mode below T_0 determines the structure of the low temperature phase. Usually the softening of a mode occurs at the center of the Brillouin zone where the wavelength of the mode is zero or at one of the zone boundaries where the wavelength is equal to the cell constant in the direction of the eigenvector of the soft mode. The former transition is often accompanied by a spontaneous polarization and in such a case the compound become ferroelectric below T_0. On the other hand, in the latter case, the unit cell becomes "doubled" and such a transition is called an

antiferroelectric transition.

Sometimes the softening occurs at some arbitary point of the Brillouin zone. If the wavelength of such a soft mode (λ_{crit}) is not an integrl multiple of the high temperature unit cell length, the resulting low temperature structure is incommensurate with the original high temperature crystal lattice, and therefore, translational lattice periodicity becomes lost.[4] This situation is shown schematically in Figure 1-2.

On further cooling a transition to a commensurate phase ($\lambda_{crit} \rightarrow \lambda_0$) usually occurs at a temperature T_c. At this transition temperature the wavelength of the soft mode is locked in to a multiple of the high temperature unit cell dimension. Therefore, this transition is called the "lock-in" transition.[4]

Iizumi et al. discovered a soft mode condensation in K_2SeO_4 for the first time by neutron scattering study as shown in Figure 1-3.[3] The incommensurate phase can be generally characterized by the soft mode wavelength λ_{crit}. The occurrence of the incommensuration can be observed also by X-ray diffraction study.[2] On cooling the sample through T_I satellite reflections appear together with the Bragg reflections which appear generally at the same place as in the high temperature normal phase. The wave number k_I ($=1/\lambda_{crit}$) corresponding to the satellite is incommensurate with the reciprocal lattice vector a^*,

Figure 1-2. Dispersion relation (Frequency plotted against the wave vector k) for a typical optical lattice mode. If mode instability occurs at a general wave vector k_I in the Brillouin zone, an incommensurate phase appears at low temperature. (after Blinc)

Figure 1-3. Condensation of the incommensurate soft mode in the high temperature normal phase of K_2SeO_4 observed by an inelastic neutron scattering study. (after Iizumi)

b^*, or c^*. k_I, the wave vector of the incommensurate modulation wave, has been determined in various compounds as listed in Figure 1-4. In an incommensurate phase, k_I varies with temperature.[2] This means that the incommensurate structure changes gradually with temperature. For example, in Rb_2ZnBr_4 k_I changes rapidly on approaching the lock-in transition temperature as shown in Figure 1-4. Such a behavior of k_I can be explained by a soliton model which will be described in the next section.

1-3 Theoretical treatment
of the incommensurate structure

In incommensurate phase, two basic problems arise: What kind of structure, which is related to the satellite reflection mentioned in the previous section, stabilizes this phase? What kind of thermal excitation exists, which corresponds to phonon in periodic crystals ? These problems are extensively studied from the theoretical aspect.

McMillan[18] reported that two kind of modulation waves could stabilize this phase. One is a plane wave and another is a soliton wave as shown in Figure 1-5

Figure 1-4. The incommensurate wave vectors k_I and the incommensurate to commensurate transition points in various compounds. (after Yamada) These temperature scale is reduced by the incommensurate transition temperature T_0.

Figure 1-5. Variation of phase p(x) of the incommensurate modulation wave $\delta u = \sin p(x)$ with distance x in the plane wave (a) and the multi-soliton (b) limits. (after Blinc)

$\delta u = A \cdot \cos \; P(x)$

(a) $P(x) = k_I x + P_0$ plane wave

(b) $P(x)$: solution of

$$\frac{d^2 P}{dx^2} - \alpha^2 \cdot \sin \, (\ell P) = 0 \qquad \text{soliton wave}$$

The static incommensurate structure is represented by either a plane wave or a soliton wave. Many incommensurate systems, however, can not be singly described by either one of the above two models. The incommensurate structure in Rb_2ZnBr_4 is described by the plane wave model in the high temperature region, whereas it is more properly described by the soliton wave[7] at lower temperature as was shown in Section 1-2.

To describe the incommensurate modulation both the amplitude and the phase of the wave are necessary. Thus, the excitation associated with the incommensurate structure consists of two modes: One is the "amplitudon" mode, which corresponds to the space and time variation of the displacement, that is, oscillation of the amplitude as shown in Figure 1-6a. The other elementary excitation is the "phason"[19] mode which corresponds to the oscillation of the phase of each displacement as shown in Figure 1-6b. The amplitudon mode behaves like an optic soft mode but its frequency increases with decreasing temperature. The phason mode is like an acoustic mode and is gapless in the continuous limit, and it consumes no energy to slide the whole modulation wave throughout the crystal.

Figure 1-6. Amplitudon and phason fluctuation modes and the corresponding dispersion relations in the plane wave model of an incommensurate system. (after Blinc)

These two aspects ,that is, the static and dynamic properties of incommensurate phase, can be both examined by NMR and NQR effectively, as shown in

1-4 NQR and NMR in incommensurate phase

As was mentioned in a previous section the NQR frequency depends on the arrangement of atoms or molecules which reflects the site symmetry of the resonant nucleus. Hence NQR is one of the most powerful tools to study subtle changes associated with phase transition phenomena in crystals.[6] When the substance of interest undergoes a second-order phase transition, irrespective of structural, displacive type or order-disorder type, the crystal symmetry as well as the site symmetry is lowered on cooling in most cases: In such cases the NQR lines split into some multiplets on the transition, corresponding to the site symmetries of the lower temperature phase. The NQR frequency shows, however, no discrete change at the transition point but varies continuously through the transition. An example of such second-order transition is shown Figure 1-7.[6] The magnitude of the splitting of the these lines has the property of the order-parameter of the transition and the number of multiplets can be used to learn the symmetry of the lower temperature phase. In some cases

phase transition is accompanied with only a change of temperature coefficient of the frequency but with no line splitting. On the other hand, first order phase transition is generally accompanied with a change in the number of lines and also discontinuous change in the resonance frequency at the transition point as shown in Figure 1-8, for example.[8] Thus one can distinguish the order of the phase transition by looking at the behavior of resonance lines near T_c.

The second-order phase transition is usually accompanied with so-called critical fluctuation of the order parameter near T_c.[6] The critical fluctuation has the long wavelength components and causes the fluctuation of the electric field gradient around the resonant nucleus which acts to increase the spin-lattice relaxation rate dramatically near T_c. So a sharp dip in T_1 is usually detected in the vicinity of T_c. Thus, the spin-lattice relaxation measurement near T_c sheds light into the mechanism of the second-order phase transition.

Next, we consider the incommensurate phase from the NQR aspect. Blinc et al.[7] investigated the line shape of ^{87}Rb resonance in the incommensurate phase in Rb_2ZnBr_4 and Rb_2ZnBr_4 and developed a method to analyze the NMR data phenomenologically. They determined the soliton densities near the lock-in transition by the use of the line shape data and also showed a method to detect the phason in the spin-lattice relaxation time

Figure 1-7. Temperature dependence of the ^{35}Cl frequencies in chloroanil.

Figure 1-8. Temperature dependence of ^{79}Br frequencies in K_2PtBr_6

measurements.

1-5 A_2BX_4 type of compounds

Since the discovery of the incommensurate phase in K_2SeO_4,[1] many compounds which assume β-K_2SO_4 type of crystal structure (Pnma) have been systematically studied.[2] These are classified into two groups. The first group is A_2BX_4 (A=K, Rb, Cs B=Se, Zn, Cd, Hg, X=O, Cl, Br, I) and the second is A'_2BX_4 A'=NH$_4$, $(CH_3)_4N$, B=Co, Mn, Zn, Cu, Ni). Among substances which belong to the first group K_2SeO_4,[10] Rb_2ZnCl_4,[20] Rb_2ZnBr_4,[21] and K_2ZnCl_4[22] have been extensively studied. Cs_2CdBr_4 also belongs to the first group. Its crystal structure is shown in Figure 1-9 as an example of the first group of the compounds. The mirror planes exist perpendicularly to the y-axis at y=1/4 and y=3/4.[16] Two Cs^+ cations are inequivalent, and are in the mirror plane with the site symmetry m. The B and X1 and X2 atoms in a distorted tetrahedron, BX_4, are also in the mirror plane with the site symmetry m. Two X3 atoms are at general positions and related to each other by the mirror plane. The B-X1 bond axis is approximately parallel to the a-axis. The most compounds in group 1 undergo cell tripling transition into the commensurate phase at T_c. Therefore,

(D.Altermatt, et al., 1979)

Figure 1-9. Projection of A_2BX_4 structure on the y-z (b-c) plane (Pnma, Z=4). Mirror planes perpendicular to the b-axis and to the plane of the paper exist at y=1/4 and 3/4. Two cations(A), the central metal(B), and two of the X atoms(X_1 and X_2) are in one of these mirror planes.

modulation wave vector is about $a^*/3$ in these materials.[2] It is interesting to see that the existence of the soliton, phason excitation and amplitudon excitation , was also confirmed by NMR .[23] The translational displacement of cation is responsible for the modulated structure for these compounds.

1-6 Cs_2MBr_4 (M= Hg, Cd, Zn) and $(CH_3NH_3)_2CdBr_4$

Cs_2CdBr_4

An X-ray diffraction study[16] has shown that at room temperature the crystal structure of Cs_2CdBr_4 is orthorhombic and its space group is Pnma (Z=4). The lattice constants are a=10.235 Å, b=7.946 Å, c=13.977 Å. At room temperature three NQR signals have been observed.[12,13] On cooling the sample through the transition at 252 K, the incommensurate phase is observed. In this phase the incommensurate modulation wave number k_I was determined to be about 0.15 a^* by X-ray diffraction[12] and NQR signals are very weak. On further cooling through the lock-in transition at 237 K, strong four NQR signals were observed again. the space group of this commensurate phase is $P2_1/n$ and four bromines of $[HgBr_4]^{2-}$ tetrahedron are all inequivalent by the loss of mirror plane symmetry. On further cooling through the transition at 156 K, each of four NQR lines splits into two lines. Recently,

Yamada et al. reported the result of their X-ray and dielectric measurements.[2] They pointed out that the third transition occurs at 208 K in contrast to 156 K reported earlier.[12] It is therefore necessary to establish the phase relation of this material.

Cs_2HgBr_4

An X-ray diffraction study[24] revealed that this substance is isomorphous to Cs_2CdBr_4 at room temperature. The lattice constants are a=10.248 Å, b=7.927 Å, and c=13.901 Å. The phase relation is similar to that of Cs_2CdBr_4. On cooling through the transition at 243 K, incommensurate phase was observed. The incommensurate wave number k_I of this phase is about 0.15 a^* by X-ray diffraction.[12] NQR signal is very weak in this phase. On further cooling through the lock-in transition at 230 K four NQR signals were observed again. And the space group of this phase is $P2_1/n$. On further cooling through the transition at 165 K, each of four lines splits into two lines. As in Cs_2CdBr_4, the rotational incommensurate modulation of $[HgBr_4]^{2-}$ is suggested[12] but has not been confirmed yet.

Cs_2ZnBr_4

An X-ray diffraction study[25] found that this crystal is also isomorphous to the above two compounds at room temperature with the lattice constants $a=10.196$ Å, $b=7.770$ Å, and $c=13.517$ Å. An NQR study[12] did not detect any phase transition between 4 and 300 K.

$(CH_3NH_3)_2CdBr_4$

An X-ray diffraction study[16] showed that the crystal structure at room temperature is monoclinic of unit cell of the space group $P2_1/c$ which is a subgroup of Pnma. The lattice constants are $a=8.1227$ Å, $b=13.4355$ Å, $c=11.4194$ Å, and $\beta=96.194°$. The atomic parameters of Br and C were not determined due probably to some disorder. Recently, differential scanning calorimetric and Infrared measurements[26] of this compound showed that two successive phase transitions occur at 167 K and 400 K with the transition enthalpies 3.0 kJ/mol and 1.1 kJ/mol respectively. Therefore, this substance is a possible candidate of an incommensurate structure. The nature of the two transitions has not been clarified, but may be closely related to the $CH_3NH_3^+$ group.

References

1. M. Iizumi, J.D. Axe, G Shirane, and K. Shimaoka,
   Phys. Rev., B$\underline{15}$, 4392 (1977).

2. Y. Yamada, and N. Hamaya; J. Phys. Soc. Jpn., $\underline{52}$,
   3466 (1983).

3. P. Bak, Rep. Prog. Phys., $\underline{45}$, 587 (1982).

4. A.D. Bruce, R.A. Cowley, and A.F. Murray, J. Phys.
   C, $\underline{11}$, 3591 (1978).

5. T.P. Das, and E.L. Hahn, "Nuclear Quadrupole
   Resonance Spectroscopy", Solid State Physics,
   Supplement 1, Seitz and Turnball, ed. New York:
   Academic Press Inc., 1958.

6. H. Chihara, and N. Nakamura, "Advances in Nuclear
   Quadrupole Resonance", vol. 4, J. A. S. Smith ed.
   London: Heyden & Son Ltd, 1980.

7. S. Zumer, and R. Blinc, J. Phys. C, $\underline{14}$, 465 (1981);
   R. Blinc, I.P. Aleksandrova, A.S. Chaves, F. Milia,
   V. Rutar, J. Seliger, B. Topic, and S. Zumer,
   J. Phys. C, $\underline{15}$, 547 (1982).

8. R. L. Armstrong, Phys. Rep., $\underline{57}$, 343 (1980)

9. I.P. Aleksandrova, R. Blinc, B. Topic, S. Zumer,
   and A. Rigamonti, Phys. Status Solidi, (a)$\underline{61}$, 95
   (1980).

10. N. Yamada, and T. Ikeda, J. Phys. Soc. Jpn., $\underline{53}$,
    2555 (1984).

11. K. Gesi, and M. Iizumi, J. Phys. Soc. Jpn., $\underline{51}$,
    1047 (1982).

12. S. Plesko, R. Kind, and H. Arend, Phys. Status Solidi, (a)61, 87 (1980).

13. S. Plesko, R. Kind, and H. Arend, Ferroelectrics, 26, 703 (1980).

14. S. Plesko, V. Dvorak, R. Kind, and A. Treindl, Ferroelectrics, 36, 331 (1981).

15. D. Altermatt, H. Arend, V. Gramlich, A. Niggli, and W. Petter, Acta Cryst., B40, 347 (1984).

16. D. Altermatt, H. Arend, A. Niggli, and W. Petter, Mat. Res. Bull., 14, 1391 (1979).

17. W. Cochran, Adv. Phys., 9, 387 (1960).

18. W.L. McMillan, Phys. Rev., B14, 1496 (1976).
    W.L. McMillan, Phys. Rev., B12, 1187 (1975).

19. W.A. Overhauser, Phys. Rev., B3, 3173 (1971).

20. T. Ueda, S. Iida, and H. Terauchi, J. Phys. Soc. Jpn., 51, 3953 (1982).

21. M. Wada, A. Sawada, and Y. Ishibashi, J. Phys. Soc. Jpn., 50, 531 (1981).

22. F. Milia, R. Kind, and J. Slak, Phys. Rev. 27, 6662 (1982).

23. R. Blinc, Phys. Rep., 79, 331 (1981).

24. G.K. Semin, I.M. Alymov, V.M. Burbelo, V.I. Pakhomov, and P.M. Fedorov, Izv. Akad. Nauk. SSSR, Ser. Fiz. 42, 2095 (1978).

25. B. Morosin, and E.C. Lingafelter, Acta. Cryst., 12, 744 (1959).

26. C.N.R. Rao, S. Ganguly, H.R. Swamy, and I.A. Oxton, J Chem. Soc., Faraday Trans. 2, 77, 1825 (1981).

Chapter 2 Instruments

2-1 Introduction

As was mentioned in the preceding Chapter the magnetic resonance methods[1] have widely been applied to investigate the incommensurate systems in which translationally modulated incommensurate structure is realized. But only a few resonance works were done on materials having incommensurate phases due to rotational modulation of molecules or ions.[2,3] Since NQR parameters are very sensitive to small angle molecular rotation[4] and the methods of analyses of the NQR data with respect to the so-called rotational transitions have been established,[5] NQR is one of the most effective methods to examine the mechanism of incommensurate transition associated with the local rotational modulation. In order to examine the mechanism of the rotational incommensurate phase transition I have applied the NQR method to Cs_2HgBr_4 and Cs_2CdBr_4 which are reported to undergo an incommensurate transition accompanied with the rotation of $[HgBr_4]^{2-}$ and $[CdBr_4]^{2-}$ groups.[6] In order to perform NQR measurements on these compounds, the following three components were constructed:

1. Electric furnace,

2. Pulsed spectrometer for ^{81}Br and ^{79}Br,

and,

3. FT pulsed spectrometer for ^{81}Br and ^{79}Br.

2-2 Electric furnace

2-2-1 Organization of furnace

According to the phase diagrams of the ternary systems, (CsBr-MBr$_2$-H$_2$O, M=Hg,Cd), Cs$_2$MBr$_4$[7,8] (M=Hg, Cd) do not crystallize in aqueous solution. But the phase diagrams of binary systems (CsBr-MBr$_2$, M=Hg,Cd)[9,10] indicate that the above compounds can be prepared from congruent melting solutions. The melting points of Hg- and Cd-salts are 708 K[9] and 712 K,[10] respectively. Therefore, an electric furnace which works up to 1100 K was constructed. The schematic diagram of electric furnace is shown in Figure 2-1. This apparatus is of Bridgeman type[11] and consists of four components; furnace, temperature controller, multimeter, and sample holder. In order to obtain crystals with very high quality essential for NQR measurements, a furnace was designed which will satisfy the following conditions.

1. It works between 800 K and 1100 K.

2. The temperature is controlled within to ±1 K for a week or more.

3. Temperature gradient larger than 10 K/cm can be realized and is controlled to within ±1 K for a week.

Figure 2-1. Block diagram of electric furnace. H-OUT, H-1 - H-4 are heaters. T-B and T-C are thermocouples for temperature control. The actual position of these heaters and thermocouples in the furnace are shown in Figure 2-3.

The details of the furnace and the temperature controller are described in Sections 2-2-2 and 2-2-3. The temperature at various points of the furnace was measured by the multimeter (Hewlett-Packard, 3465B) and stability of temperature was checked by recording emf of thermocouple with a pen recorder (National, VP-6521A).

2-2-2 Furnace

The structure of the furnace is shown in Figure 2-2. It consists of three tubes (C,D,E) with different diameters and a Dewar vessel (F). Its length is about 1.0 m, and maximum diameter is 0.15 m. The inside diameter of a pyrex glass tube (C) is 30 mm. Therefore maximum diameter of a sample tube (K) is about 20 mm. The outermost stainless-steel dewar vessel was surrounded by asbestos to prevent thermal leakage due to conduction and radiation. Inside this dewar vessel (F) a stainless-steel tube (E) was set which holds an outer heater (G) and a thermocouple (J) as shown in Figure 2-3a. The outer heater (G) is made from zonal nichrom wire and was used to heat the whole space in the furnace uniformly up to a suitable temperature which was lower than the melting points of the sample by about 200°C. The value of resistance of the heater is 17Ω (3.5Ω/m) and can provide maximum

A

B

C

D

E

F

G

H

I

J

K

L

M

N

O

Figure 2-2. The structure of the furnace.

A stainless-steel wire

B copper block cover

C pyrex glass

D ceramic tube

E stainless-steel tube

F stainless-steel dewar

G heater (H-OUT)

H thermocouples for temperature control (T-A - T-D)

I heaters (H-1 - H-4)

J thermocouples for temperature control (T-OUT)

K sample

L thermocouples for temperature moniter

M pulley 4 cm diameter)

N synchronous motor (4 rpd)

O glass-wool container

electric power of 500 W. The whole heater system was surrounded by asbestos and glass wool. The main part of the furnace consists of a ceramic tube (D) with four independent heaters (I) and four independent thermocouples (H) as shown in Figure 2-3b. The values of resistance of the heaters H-1, H-2, H-3, and H-4 are 15, 16, 18, and 21Ω respectively. Using these heates (H-1 - H-4) the maximum electric power of 2300 W can be obtained. The heater H-1 was used to melt the sample. The currents of the heaters H-2 and H-3 were independently regulated using the temperature controllers TYPE A described in Section 2-2-3 to obtain a sharp temperature gradient in the narrow area between the positions of the thermocouple T-B and of T-C. The heater H-4 was used to anneal the product compound. The Chromel-Alumel thermocouples were used as temperature sensor to attain large electromotive force and high stability around 800 K. The innermost pyrex glass tube was used to fix thermocouples for monitoring temperature. The positions of thermocouple are shown in Figure 2-3c.

2-2-3 Temperature controller

Two types of temperature controllers were constructed.

(1) TYPE A

Two temperature controllers of this type[12,13]

Figure 2-3. Practical wiring scheme of the heaters H-OUT, H-1 - H-4, and the thermocouples T-A - T-D, T-OUT, T-1 - T-6, indicate vertical positions of thermocouples and heaters. a: the outer stainless-steel tube. b: the ceramic tube. c: the pyrex glass tube.

were constructed and employed to regulate the current of heaters H-2 and H-3 independently. The basic diagram of the circuit is shown in Figure 2-4. This controller is a proportional-integral contoller with a pair of thermocouples as the temperature sensor. The details of the DC amplifier, the reference voltage generator, the prportional-integral controller and the current output circuit are given in Figures 2-5,2-6,2-8 respectively. The emf of the thermocouples T-2 and T-3 are amplified by the DC amplifier, compared with the reference voltage suitably divided with the resistance network and fed into the logic circuit of the proportional-integral controller. The control signal from the logic circuit drives the triac which provides the proportional-integral controlled current to the heaters H-2 or H-3. The electrical characteristic of the logic circuit is shown in Figure 2-7. The wave form of the each part of the output circuit is schematically shown in Figure 2-9. Using this controller system it was revealed that the temperature can be controlled to within ± 1 K at about 800 K, which corresponds nearly to the melting points of the specimens, for more than 7 days.

(2) TYPE B

Three regulators of this type[14] were constructed and used to regulate the currents of the heaters H-1 and H-4 and the outer heater independently. The circuit

Figure 2-4. Block diagram of temperature controller
(TYPE A).

Figure 2-5. Circuit diagram of the reference voltage generator and DC amplifier in TYPE A temperature controller.

Figure 2-6. Circuit diagram of logic calculation unit.

Figure 2-7. Principle of operation of PI logic calculation unit. T_s is the setting temperature of the furnace. The current of a heater is controlled to very linearly to the temperature deviations from T_s.

Figure 2-8. Circuit of power output system. It can provide maximum power of 500 W into a furnace heater with 17 Ω resistance.

Figure 2-9. Waveforms at the portions 1-5 of output circuit 5:Output voltage.

is simple on-off regulator as shown in Figure 2-10. The controller can stabilize the temperature to within 5 - 10 K. which is sufficient in the present experiment.

2-2-4 Operation and performance

The five control system mentioned above were set so as to attain the temperature distribution shown in Figure 2-11 by adjusting the potentiometer in individual controllers. This temperature distribution was confirmed to be maintained without significant change for a week or more. The temperature fluctuation during the operation was less than ± 1 K at the positions 3 and 4. The sample sealed in a pyrex ampoule was put in the position 1 for two days in order to get complete mixing of the two components. Then the sample was lowered gradually at the rate of 12 cm/day using a synchronous motor (4 rpd.). The crystallization occurred from the bottom and proceeded as the sample was passed through the steep temperature gradient between the points T-3 and T-4. After 5 days the sample reached the position 6, where it was annealed for a day. Then the temperature of the furnace was lowered to the room temperature in one day.

Figure 2-10. Circuit of current supply (TYPE B temperature controller) to the heaters, H-1, H-4, and H-OUT in Figure 2-3. Setting of the current for each heater is done by adjusting the potentiometers.

Figure 2-11. Ideal temperature distribution inside the furnace. 1-6 are sensing positions of thermocouples T-1 - T-6. T_m is melting point of sample. Melt sample is moved down through this steep temperature gradient.

2-3 Spectrometer

2-3-1 Organization of spectrometer

One of the purpose of the present work is to measure precisely the NQR frequencies and the spin-lattice relaxation time of ^{81}Br (or ^{79}Br) of the title compounds over wide temperature range. Kind et al.[6] reported that the ^{81}Br NQR signals of these substances lie between 50 MHz and 120 MHz. Therefore a variable frequency pulsed NQR spectrometer working in this frequency range was constructed. The block diagram of the spectrometer is shown in Figure 2-12. An RF carrier from a signal generator is divided into two channels by a power divider. One channel leads, through an attenuator and a phase shifter, to a broadband receiver for phase sensitive detection and another to an RF gate which is controlled by a pulse programmer. The RF pulse signals from the gate is used to drive an RF power amplifier. This amplifier can supply RF pulses of the power of 1 kW to the sample coil via matching network. The free induction decay (FID) signal after the strong RF pulse is picked up by the coil and amplified by a tuned pre-amplifier and a broadband receiver. The amplified signal is then converted into a video signal by a video amplifier with the phase sensitive detection. An active and an passive [15] dampers are inserted between the probe and the pre-amplifier to

Figure 2-12. Block diagram of pulsed NQR spectrometer. The circuit between the rf-swich and the wideband amplifier represents a three stage tuned pre-amplifier.

protect the receiver from the high power RF pulses and to supress the dead time of the pre-amplifier. An active damper is also controlled by the pulse programmer. The details of the matching network and the pulse programmer will be described in Sections 2-3-2, and 2-3-3, respectively. The other components used in the present study are as follows:

1) A stable RF signal generator (Hewlett-Packard, 608C, or Waveteck, Model 3000): The frequency drift is less than one part in 10^6 per 10 minutes.

2) Frequency counter (Hewlewtt-Packard, 5314A) to measure the resonance frequency, which was also used to measure the time interval between two pulses.

3) RF power amplifier or RF transmitter (Matec, 525).

4) RF gated modulator (Matec, 5100)

5) Diode expander (Matec, DX-3), which was used so that the transmitter is electrically isolated from the matching unit in the detection period of the FID signal.

6) Pre-amplifier (Matec, 254)

7) Wideband amplifier (Matec, 625)

8) Oscilloscope (Tektronics, 7904) to display FID signal .

9) RF Attenuator (RA-74)

2-3-2 Pulse programmer

The detail circuits of the pulse programmer together with the quench are shown in Figure 2-13. The repetition period for the pulse sequence is determined by the use of the timer comprised in the RF gated modulator . The pulse sequence for the two pulses for the T_1 measurements is genarated by TTL logic circuit. Its interval and width can be adjusted with monostable multivibrators. The chart showing the timing of the gate pulses and the quench pulses for active damper is shown in Figure 2-14.

2-3-3 Matching circuit

The matching network containing the sample coil is the most important part in the NQR apparatus. It must satisfy the following conditions:

1. It transmits the RF power from the power amplifier to the probe coil as efficiently as possible.
2. Ringing after the high RF power as well as spurious noise should be supressed very quickly in order to detect FID signal immediately after the RF pulses.
3. The quality factor Q of the network should be very high in the detection period in order to detect very weak FID signal.

Figure 2-13. The circuit of pulse programmer.

Figure 2-14. The timing chart of pulse at positions a-d of the pulse programmer. b is the gate pulse and d the quench pulse.

Figure 2-15. The circuit of quench pulse generator. It shapes the input pulse to a special waveform output pulse to accomplish efficient quenching and rapid recovery of the detector system.

4. The above condition should be realized over very
    wide frequency range (50 - 100 MHz).

In order to design a practical matching network we
will begin with the analysis of a very simple LC
circuit given in Figure 2-16. The tuning frequency f is
determined by the equation

$$f = \frac{1}{2\pi \sqrt{L \cdot C}}$$

where L and C are the inductance and the capacitance of
the tank circuit. In an actual NQR experiment one
connects the coil immersed in a cryostat and the
matching network which is located outside of the
cryostat with a long coaxial cable. In such a case the
stray capacitance of few pF usually exists in the
cable. This stray capacity is comparable with or lager
than C in the above equation at a frequency above
50 MHz. So it may become impossible to tune the whole
circuit to the NQR frequency at high frequencies. This
difficulty can be avoided by putting the whole matching
network circuit into the cryostat. Since the output
impedance of the transmitter is 50 Ω in the present
work, the maximum RF power can be provided to the
probe coil if one can match the impedance of the
matching circuit to 50Ω. Consider two types of matching
circuits as shown in Figures 2-17a and 2-17b which are
called tapped parallel tuned circuit and tapped series
tuned circuit,[16] respectively. The input impedance of
tapped parallel tuned circuit is given by

Figure 2-16. Parallel tuning circuit.

Figure 2-17. Tapped parallel (a) and tapped series (b) matching networks.

$$Z = -jX_{c2} + \frac{X_{c1} \cdot X_L - jX_{c1} \cdot R_L}{R_L + j(X_L - X_{c1})}$$

$$X_{c1} = (\omega_o C_{c1})^{-1}$$

$$X_{c2} = (\omega_o C_{c2})^{-1}$$

$$X_L = \omega_o L$$

Using the condition $Z = 50\,\Omega$, the following solutions can be obtained with an appropriate approximation:

$$C_{c1} = [\frac{\omega_o X_L \cdot (50 + \sqrt{50 \cdot R_L})}{50 - R_L}]^{-1}$$

$$C_{c2} = [\frac{\omega_o X_L \cdot (50 + \sqrt{50 \cdot R_L})}{R_L + \sqrt{50 \cdot R_L}}]^{-1}$$

For the case of tapped series tuned circuit input impedance is

$$Z^{-1} = \frac{j}{X_{c2}} + \frac{1}{R_L + j(X_L - X_{c1})} \quad .$$

Using the condition $Z = 50\,\Omega$, the following solutions can be obtained with an appropriate approximation:

$$C_{c1} = [\omega_o (X_L - \sqrt{50 \cdot R_L})]^{-1}$$

$$C_{c2} = [\omega_o \sqrt{50 \cdot R_L}]^{-1}$$

Substituting the following values C_{c1} and C_{c2} are estimated.

$$f_o = \omega_o/2\pi = 60\,MHz \quad , \quad L = 0.4\,\mu H \, , \quad R_L = 5\,\Omega$$

For tapped parallel tuned circuit, C_{c1} and C_{c2} are both about 10 pF. For tapped series tuned circuit, C_{c1} is about 20 pF and C_{c2} is about 100 pF. Hence the tapped parallel tuned circuit is adopted because small size condition is preferable to be comprized in the limited space of the cryostat.

The overall diagram of the probe is shown in

Figure 2-18. J is variable condenser and its capacity value can be varied remotely by handling the knob (B). The detail of the condenser is shown in Figure 2-19. The coaxial cylindrical condensers of 10 pF and 20 pF were constructed. The capacitance of this type of condenser is given by

$$C = \frac{2\pi \varepsilon_0 \ell}{\log (b/a)}$$

2-3-4 Operation and Performance

The impedance of the matching unit was adjusted using a system shown in Figure 2-20. The reflected RF is monitored on an oscilloscope and the variable condensers are adjusted so as to minimize the reflected RF.

In the tapped parallel tuned circuit mentioned in Section 2-3-3 the impedance matching could not be realized because of large stray capacity even when the matching unit was placed in the cryostat. This difficulty can be overcome by two methods. The first method is to insert a resistance in series with the coil. This lowers the Q of the sample coil. And larger capacity is needed in order to satisfy the matching condition. Then, the impedance matching can be realized. But sensitivity of the tank circuit to detect the FID signal becomes poor because of low quality

Figure 2-18. The sample prove.

A BNC connector

B condenser tuning knob

C liquid nitrogen inlet tube

D copper can

E sample

F RF coil

G thermocouple junction for temperature measurement

H heater

I thermocouple for temperature control

J variable condenser

K teflon insulator

Figure 2-19. Variable condenser.

1 copper outer electrode

2 teflon insulator

3 brass support

4 tuning knob

5 brass inner electrode with the following dimensions

	5 pF	10 pF	20 pF
a/mm	15	15	30
b/mm	9	14	14
c/mm	5.5	11.5	11.5

Figure 2-20. Block diagram of the impedance matching network.

factor due to the resistance in series to the coil. The other method is to insert another condenser series to the whole tank circuit. This method proved useful because the signal loss is small. The whole matching unit constructed in the present work is shown in Figure 2-21. The length of a coaxial cable is varied so as to match the measuring frequency. For example, its length is 10 cm at 90 MHz, and 60 cm at 60 MHz.

The performance of the matching unit was tested by measuring the NQR signal of ^{121}Sb in SbCl$_3$. The ^{121}Sb (I=5/2) resonance frequencies in SbCl$_3$ are 58.08 and 112.5 MHz at 304 K.[17] For the signal at 112.5 MHz, the 90° pulse width was 20 micro sec and the pulse height was 500 V, peak-to-peak. Signal to noise ratio was about 20 which is comparable with the value obtained using a very short probe. Therefore, the undesirable effect of the long cable which connects the sample coil and the transmitter on the NQR signal can be negligibly small. The dead time of this system is 10 micro sec which is short enough for this experiment because T_2^* of the compounds studied in the present research are longer than 30 micro sec.

2-4 Pulsed FT spectrometer

2-4-1 General design of FT spectrometer

Figure 2-21. Matching network. The portion indicated
by ---is the coaxial cable made from stainless-steel
tubes of about 40 cm length.

In incommensurate phase the NQR signal is expected to be very small and so the accumulation and the averaging of the signal is necessary. Furthermore the line shape and linewidth measurements are necessary. For these purposes a pulsed FT spectrometer was constructed to throw light into the structure of the IC phase.

In the signal enhancement by data accumulation the pulsed FT method is superior to usual CW method because it can collect the signal very quickly and, by Fourier-transform (FT) of the FID signal, the frequency spectrum with high S/N ratio can be obtained. The FT'd signal is equivalent to the CW absorption spectrum, when the following conditions are satisfied.[18]

(1) All spins are equally excited, that is, the power of the RF pulse as high enough to invert all spins simultaneously.

(2) High temperature approximation is satisfied for spin system.

In the present work the pulsed FT technique was adopted to examine the NQR parameters in the IC phase. The schematic diagram of the pulsed FT spectrometer system is shown in Figure 2-22. Almost all parts of this system is the same as that mentioned in Section 2-3. A transient memory, a signal averager

Figure 2-22. Block diagram of pulsed NQR FT spectrometer. A circuit inserted between the rf-swich snd the wideband amplifier indicates a tuned three stage pre-amplifier.

and a personal computer were newly introduced in order to perform the data acquision and the FT. The components used are as follows,

(1) FID is converted to digital signal and stored using a transient memory (KAWASAKI ELECTRONICA, TM-1410). The number of sampling points (N) of the transient memory used was 1024, and minimum sampling interval was 1 micro sec. If the sampling interval is 1 micro sec, sampling time is totally 1024 micro sec. As the inverse of the sampling time corresponds to the resolution of frequency spectrum,[19] the resolution is 1 kHz in this case. This condition leads to sufficiently reliable data in the present study because the line width of ^{81}Br NQR signal is generally about 20 kHz - 40 kHz. With the sampling interval of 1 micro sec there is not any difficulty that arises from distortion of the FT'd signal because the time constant (T_2^*) of FID of ^{81}Br NQR signal is 40 - 100 micro sec.

(2) The digitized signals stored in the transient memory were accumulated by an averager (KAWASAKI ELECTRONICA, TMC-300). This averager can accumulate the data up to 1024 times but the number of accumulation was not sufficient to obtain NQR signal with high S/N ratio in incommensurate phase, so after accumulation of 1024 times the digital data in the averager was transferred to a personal computer, and accumulation was continued in the transient memory.

(3) Digital signal of averager was transferred through an interface (CONTEC, PIO-1616(98)) to a personal computer system (NEC, PC-9801E). The final data is monitored on a CRT (NEC, pc-8841), hard-copied on a printer (EPSON, RP-80II) and stored in the floppy disk of the computer (NEC,PC-8881).

2-4-2 FID processing program

Flow chart of program is shown in Figure 2-23.

OFFSETCORRECTION : The digital data have only positive values, so baseline of FID must be shifted to zero before FT.

FFT : Two base FFT algorithm[20] was used. It takes five minutes to get the Fourier transform of 1024 points.

PHASECORRECTION : FID is expressed theoretically by the expression

$$f(t) = A \cdot \exp(-t/T_2^*) \cdot \cos 2\pi (f_{RF} - f)t$$

where f_{RF} is the carrier frequency and f is the NQR resonance frequency. Its Fourier transform produces pure absorption in real part and pure dispersion respectively shown in Figure 2-24. But in a real system FID is usually expressed by the expression

$$f(t) = A \exp(-t/T_2^*) \cdot \cos[2\pi(f_{RF} - f)t + P]$$

```
          ┌─────────────────────────────┐
          │   INPUT INITIAL PARAMETER    │
          └─────────────────────────────┘
                        │
          ┌─────────────────────────────┐
          │      SUB DATAINPUT           │
          └─────────────────────────────┘
                        │
          ┌─────────────────────────────┐
          │   SUB OFFSETCORRECTION       │
          └─────────────────────────────┘
                        │
          ┌─────────────────────────────┐
          │   GRAPHIC FID DISPLAY ?      ├───┐
          └─────────────────────────────┘   │
                        │                    │
          ┌─────────────────────────────┐   │
          │   SUB GRAPHICFIDDISPLAY      │   │
          └─────────────────────────────┘   │
                        │◄───────────────────┘
          ┌─────────────────────────────┐
          │   SUB DATAREARRANGEMENT      │
          └─────────────────────────────┘
                        │
          ┌─────────────────────────────┐
          │     FID DATA DISPLAY ?       ├───┐
          └─────────────────────────────┘   │
                        │                    │
          ┌─────────────────────────────┐   │
          │     SUB FIDDATADISPLAY       │   │
          └─────────────────────────────┘   │
                        │◄───────────────────┘
          ┌─────────────────────────────┐
          │    FID DATA PRINT-OUT ?      ├───┐
          └─────────────────────────────┘   │
                        │                    │
          ┌─────────────────────────────┐   │
          │    SUB FIDDATAPRINTOUT       │   │
          └─────────────────────────────┘   │
                        │◄───────────────────┘
          ┌─────────────────────────────┐
          │    FID DATA FILE-OUT ?       ├───┐
          └─────────────────────────────┘   │
                        │                    │
          ┌─────────────────────────────┐   │
          │    SUB FIDDATAFILEOUT        │   │
          └─────────────────────────────┘   │
```

Figure 2-23. Flow chart of FID processing procedure.

Figure 2-24. The effect of the signal truncation on the FID components due to RF pulse and the dead time of the detector. a: ideal FID. b: truncated FID. Absorption and dispersion signals are mixed and both are distorted. But the absolute amplitude of the signal remains unchanged

where the phase p is introduced for purely instrumental reason that the initial part of FID cannot be observed due to the dead time of receiver system. Fourier transform of such a signal gives a spectrum which is a mixture of the absorption and the dispersion. In such a case the center of the resonance line can be determined by calculating the modulus

$$M = (\text{Im}(\mathcal{J}f(t)))^2 + (\text{Re}(\mathcal{J}f(t)))^2$$

The program is given in Appendix 1. All is written in BASIC language.

2-5 Temperature controller

In the present study the temperature of the specimen in the cryostat was controlled using the circuit shown in Figure 2-25. The temperature of the cryostat was monitored by a pair of thermocouple. The difference between the emf of the thermocouples and the output voltage of a mV generator (Ohkura Elec. Co. Ltd., I-8160), which was preset to the temperature of measurement, was amplified by a D.C. amplifier (Ohkura Elec. Co. Ltd., AM-1001) and fed into the proportional current controller.[21] With this system the temperature of the probe was controlled within ±0.01 K for few hours.

Figure 2-25. Block diagram of temperature controlling system for NQR measurements.

References

1. R. Blinc, Phys. Rev., $\underline{79}$, 331 (1981).

2. R. Ambrosetti, R. Angelone, and A. Colligiani, Phys. Rev., B$\underline{15}$, 4318 (1977).

3. I.P. Aleksandrova, R. Blinc, B. Topic, S. Zumer, and A. Rigamonti, Phys. Status Solidi, (a)$\underline{61}$, 95 (1980).

4. T.P. Das, and E.L. Hahn, "Nuclear Quadrupole Resonance Spectroscopy", Solid State Physics, Supplement 1, Seitz and Turnbull, ed. New York: Academic Press Inc., 1958.

5. R.L. Armstrong, Phys. Rep., $\underline{57}$, 343 (1980).

6. S. Plesko, R. Kind, and H. Arend, Phys. Status Solidi, (a)$\underline{61}$, 87 (1980).

7. V.K. Fillippov, and K.A. Agafanova, Zh. Prikl. Khim., $\underline{50}$(7), 1529 (1977). (J. Appl. Chem. USSR, $\underline{50}$(7), 1473 (1977).)

8. V.K. Fillippov, K.A. Agafanova, and M.A. Yakimov, Zh. Neorg. Khim., $\underline{19}$(6), 1663 (1974). (Russ J. Inorg. Chem., $\underline{19}$(6), 905 (1974).)

9. C. Sinistri, R. Reccadi, and A. Magistris, Ber. Bunsenges. Phys. Chem., $\underline{71}$(4), 376 (1967).

10. V.I. Pakhomov, P.M. Fedorov, Yu A. Polyakov, and V.V. Kirilenko, Zh. Neorg. Khim., $\underline{22}$(1), 188-92 (1977). (Russ. J. Inorg. Chem., $\underline{22}$(1), 103 (1977).)

11. P.W. Bridgeman, Proc. Amer. Acad., $\underline{60}$, 306 (1925).

12. Y. Tajima, Transistor Technique, $\underline{9}$, 389 (1981).

13. National Semiconductor, "Liniear application"

vol. 1 and vol. 2

14. General Electric Company ed. "Silicon Controlled
   Rectifier manual" , 1967.

15. H.T. Stokes, Rev. Sci. Instrum., $\underline{49}$, 1011 (1978).

16. P.D. Murphy, and B.C. Gerstein, The report of
   energy office of basic energy science,
   W-7405-eng-82 (1978).

17. H.Chihara,N. Nakamura, and H. Ohkuma, J. Phys.
   Soc. Jpn., $\underline{24}$, 306 (1968).

18. R.R. Ernst, and W.A. Anderson, Rev. Sci. Instrum.,
   $\underline{37}$, 93 (1966).

19. D. Shaw, "Foureir Transform NMR Spectroscopy",
   Elsevier North-Holland Inc.: New York, 1976.

20. J.W. Cooley, and J.W. Tukey, Math. Comput., $\underline{19}$, 297
   (1965).

21. K. Negita, Dctoral Dissertation, Osaka University,
   1980.

Chapter 3   Sample preparation and measurements

3-1 Sample preparation

3-1-1 Cs_2HgBr_4

CsBr (GR) and $HgBr_2$ (GR, >99 %) were purchased
from Nakarai Chemical Co., Ltd. A sample of 10.642 g of
CsBr and 8.993 g of $HgBr_2$ were put in a pyrex glass
ampule and evacuated for one day and sealed in vacuum.
As melting points of $HgBr_2$ and Cs_2HgBr_2 are 511 K and
708 K, respectively, a pyrex glass ampule was used as
the sample tube. As Cs_2HgBr_4 melts at 708 K,[1]
temperatures at the points 3 and 4 of Figure 2-3b
were set   at 748 K and 636 K within ±1.0 K,
respectively. The electric currents of the heaters H-1,
H-2, H-3, H-4 were regulated around 0.8, 1.2, 0.3, 0.6
A respectively. Temperature was raised to   758 K
to make the sample melt, kept there for two days in
order to get complete mixing, and then the sample tube
was lowered at a rate of 12 cm/day along the steep
temperature gradient described in Section 2-2-1. After
5 days, a colorless, transparent single crystal of
1.0*1.0*1.0 cm was obtained. The crystal was identified
by oscillation, Weisenberg, and precession photograph
of the single crystal. The samples obtained were ground
and sealed in a glass ampule with helium gas of 60 mmHg

(8.0 kPa) to be used for NQR measurements.

3-1-2 Cs_2CdBr_4

CsBr of Reagent Grade was purchased from Nakarai Chemical Co., Ltd. Anhydrous $CdBr_2$ of stated purity better than 99.99 % was purchased from Kojundo Kagaku Kenkyusho.

As $CdBr_2$ is hygroscopic, 16.518 g of CsBr and 10.564 g of $CdBr_2$ were put in a silica ampule in a dry box filled with dry nitrogen gas. As the melting point of $CdBr_2$ is 853 K a silica tube was used. It was evacuated for two days and sealed in vacuum. The sample of Cs_2CdBr_4 was grown by the similar procedure to the case of Cs_2HgBr_4 expect the initial temperature was at 913 K as melting point of Cs_2CdBr_4 is 702 K.[2] Sample were ground and sealed in a sample tube with helium gas of 58 mmHg (7.7 kPa) for NQR measurements.

3-1-3 Cs_2ZnBr_4

CsBr of Reagent Grade and $ZnBr_2$ of Reagent Grade were purchased from Nakarai Chemical Co., Ltd. Colorless, transparent crystals were obtained by slow evaporation at room temperature of aqueous solution of the stoichiometric amounts of CsBr and $ZnBr_2$.[3] The sample was recrystallized twice from aqueous solution,

ground and sealed in an ampule with the outer diameter
of 1.2 cm with 60 mmHg (8.0 kPa) helium gas for NQR
measurements.

3-1-4 $(CH_3NH_3)_2CdBr_4$

CH_3NH_3 (40 % aqueous solution) was purchased from
Tokyo Kasei Kogyo Industry Co.,Ltd. $CdBr_2 \cdot 4H_2O$ (GR,
> 98 %) was purchased from Wako Pure Chemical
Industries, Ltd. HBr (GR, 47 - 48 %) was purchased from
Nakarai Chemical Co., Ltd.

Sample was prepared in two steps.[4,5] First
CH_3NH_3Br was prepared in the following way: Hydrobromic
acid was added slowly to aqueous CH_3NH_2 solution . This
reaction is very exothermic. By slow evaporation at
333 K colorless, transparent crystals of CH_3NH_3Br were
obtained. Next, the stoichiometric amounts of
$CdBr_2 \cdot 4H_2O$ and CH_3NH_3Br were disolved in water. By slow
evaporation at room temperature colorless, transparent
poly-crystals were deposited. The sample was purified
by recrystallization from aqueous solution, ground and
sealed in a glass ampule with the outer diameter of
1.2 cm without He gas for NQR measurements.

3-2 NQR Measurements

3-2-1 Spin-lattice relaxation time, T_1,

and the resonance frequency, ν_Q

The spin-lattice relaxation time (T_1) and the resonance frequency (ν_Q) were measured by the pulsed spectrometer described in Section 2-3. Since the temperature coefficients of the NQR frequencies were large, the temperature of sample was controlled to within ± 0.05 K so as to prevent the frequency shift and/or broadening of the resonance line that might occur during each measurement. Also, the impedance matching of the probe was made by the method mentioned in section 2-2 in every measurement, to keep the optimum condition of the matching unit. The $90°$ pulse width was about 20 micro sec and pulse height was about 500 V peak-to-peak in all the runs. The spin-lattice relaxation time was measured by either $90°$ -t-$90°$ method or $180°$ -t-$90°$, depending on the situation. Both methods gave consistent results. Recovery of the magnetization was always represented by a single exponential function with respect to the evolution time. So the spin-lattice relaxation time was unambiguously determined at every temperature. At high temperatures above 200 K the FID signal became weak. Therefore, the S/N ratio was made to increase by accumulating the FID using a transient memory and a

signal averager. For $(CH_3NH_3)_2CdBr_4$, two upper resonance frequencies of the four were closely spaced so that the spin-lattice relaxation time could not be measured by the direct method at a certain temperature range. In such a case the pulsed FT method (see in Section 2-4) was used to measure T_1.

3-2-2 Line width

Line width was measured by the pulsed FT spectrometer. The sampling interval of the FID was 1 micro sec, and the pulse width was 20 micro sec. The line shape was very sensitive to temperature. Therefore, the temperature was controlled to within ± 0.01 K during each measurement. The FID signals were accumulated 1024 times or more prior to the Fourier transform.

3-2-3 Resonance frequency in the incommensurate phase

The resonance frequency was searched using the pulsed FT spectrometer described in Section 2-3. Since the FID signal could not be detected in the incommensurate phase without accumulation, the following procedure was used to measure the resonance. First, the spectrometer was set in the optimum condition by observing the FID just below the

incommensurate-commensurate transition temperature. The optimum condition was attained at the $90°$ -pulse width of 23 micro sec and for the pulse height of 400 V_{p-p}. Next the temperature was brought to the range of the incommensurate phase and, keeping the above condition of the spectrometer system, the FID signals were accumulated 10240 times with the repetition period, 0.1 s, and then Fourier-transformed. As the pulse width was 23 micro sec, the spins which resonate at a frequency lying within ($f_{RF}\pm40$) kHz can be excited (f_{RF} is the carrier frequency). Therefore, search was made in steps of 40 kHz. A typical example of the observed signal is shown in Figure 3-1 by changing the carrier frequency.

$T = 234.6\,K$

$\nu_f = 92.6473\,MHz$

Figure 3-1. Typical FID of ^{81}Br NQR line in Cs_2HgBr_4 in the incommensurate phase. The RF 90° pulse was applied to the sample at t=0 for 20 micro sec and a quench pulse as shown in Figure 2-15 was applied to the detector system the length of which was 30 micro sec. After 30 micro sec FID signal is detected. If the quench pulse is absent FID signal appeared after 50 micro sec. Thus the application of the quench pulse can make the dead time shorten by 20 micro sec.

References

1. V.I. Pakhomov, P.M. Fedorov, Yu A. Polyakov, and V.V. Kirilenkv, Zh. Neorg. Khim., 22(1), 188 (1977). (Russ. J. Inorg. Chem., 22(1), 103 (1977).)

2. C. Sinistri, R. Reccadi, and A. Magistris, Ber. Bunsenges. Phys. Chem., 71(4), 376 (1967).

3. B. Morroson, and E.C. Lingafelter, Acta Cryst., 12, 744 (1959).

4. P.A. Daoud, and R. Perret, Soc. Chim., 5, 5 (1973).

5. H. Arend, W. Huber, F.H. Mischgofsky, and G.K. Richter-van Leuwen, J. Cryst. Growth, 43, 213 (1978).

Chapter 4 Experimental results

4-1 Cs_2HgBr_4

4-1-1 Temperature dependence of ^{81}Br NQR frequencies

Phase relation determined by Yamada[1] and that determined by Kind[2] is inconsistent in Cs_2CdBr_4. And Kind showed the similar phase relation in Cs_2HgBr_4[2-4] to that in Cs_2CdBr_4. Therefore the temperature dependence of ^{81}Br NQR frequencies was reinvestigated and the result is shown in Figure 4-1. Our result agrees with the result by Kind[2] within±20 kHz in the whole temperature range of measurement. Our transition temperatures shown in Figure 4-2 agree with those determined by Kind[2] within 2 K. Selected resonance frequencies in each phase are tabulated in Table 4-1. In the normal high temperature phase above 245 K, three resonance lines were observed and the signal intensity of the lowest resonance frequency line ν_3 was about twice as strong as that of the other two signals, ν_1 and ν_2. These results are consistent with the X-ray structure data[4]: There exist three crystallographically nonequivalent bromine sites. Two bromines (site 1 and site 2) are on the mirror plane and the number of the equivalent atoms in the unit cell is 4 for each site. The other bromine (site 3) is at general positions and the number of the equivalent

Figure 4-1. Temperature dependence of ^{81}Br NQR frequencies in Cs_2HgBr_4. ^{81}Br NQR frequencies in the incommensurate phase (between 230 K and 243 K) will be shown in Figure 4-6.

Figure 4-2. Phase relation of Cs_2HgBr_4.

Table 4-1

^{81}Br NQR frequencies in Cs_2HgBr_4

T/K	ν/MHz	T/K	ν/MHz
Normal phase		Commensurate phase	
280.0	91.549	200.4	93.679
280.1	81.099	200.2	84.480
280.5	78.469	200.1	80.662
		200.1	80.464
IC phase			
232.7	92.742	Low temp phase	
233.7	92.703	105.1	97.149
235.0	92.664	98.9	94.111
	92.454	100.2	88.546
236.1	92.624	100.2	87.542
236.2	92.436	100.4	86.298
237.2	92.582	100.7	83.812
237.5	92.403	100.7	80.223
238.5	92.463	100.2	78.055
240.0	92.485		
239.8	92.362		
241.2	92.325		
242.0	92.403		
243.0	92.300		

atoms in the unit cell is 8. Therefore signal intensity ratio of 1:1:2 is expected. The lowest resonance frequency line ν_3 can obviously be assigned to the site 3. Assignment of the other sites were made by referring to the results of the Zeeman experiment on Cs_2CdBr_4[5] which is isomorphous with Cs_2HgBr_4[6]. Thus the highest frequency line ν_1 was assigned to the site 1, and the medium frequency line ν_2 assigned to the site 2.The resonance frequencies in the incommensurate phase were measured by the FT pulsed spectrometer and will be described in Section 4-1-4. In the low temperature commensurate phase four signals were observed. Bromines which are related to each other by the mirror symmetry in the normal phase become inequivalent in this phase because of the loss of the mirror symmetry. So the four atoms in $[HgBr_4]^{2-}$ are inequivalent in this phase. The frequency difference of lower two resonance lines ν_C and ν_D became small on cooling, and, coalesce into a single line at the transition point between the commensurate and the low temperature phase. On further cooling through the commensurate - low tempeature phase transition at 165 K, each one of four lines ν_A - ν_D splits into two lines and so eight resonance lines were observed below 165 K. The lower four resonance lines ν_5 - ν_8 could not be observed near the phase transition point at 165 K for, perhaps, the following reason. The temperature coefficients of these resonance lines are

Figure 4-3. Line widths at the half maximum of ^{81}Br NQR lines in Cs_2HgBr_4 in the commensurate and the normal phases.

extremely large (100 kHz/K) near the phase transition

point so that the lines become very broad even if only

slight temperature gradient exists through the sample.

The fact that there is no discrete change in the

resonance frequency at the transition point indicates

that the transition is of second-order.[7]

4-1-2 Line width

In order to examine the critical nature of the

phase transition in the normal-incommensurate and the

incommensurate-commensurate phase transitions, the line

width of each line was measured in the normal and the

commensurate phases by the pulsed FT spectrometer

mentioned in Section 2-4. Results are shown in Figure

4-3. In the commensurate phase, the line width of the

four resonance lines were almost constant except near

the commensurate-low temperature phase transition

point. Especially, any significant line broadening was

not detected near the lock-in transition temperature.

This fact and also the fact that the resonance

frequencies show discrete change at the commensurate-

incommensurate transition suggest that the lock-in

transition of this compound is of first-order.[7] This

is consistent with the widely-accepted notion that the

lock-in transition is of first order.[8] In the normal

phase, line broadening of the lowest frequency line was

observed, while the upper two lines showed no critical

broadening. These facts suggest that the normal-incommensurate phase transition is of second-order[7] with anisotropic critical fluctuation. The full discussion on the nature of this phase transition will be given in Section 4-1-4 in relation to the NQR parameters in the incommensurate phase near T_I.

4-1-3 Temperature dependence
        of spin lattice relaxation time

In order to throw light into dynamical properties of the successive phase transitions in the Cs_2HgBr_4, the spin-lattice relaxation time T_1 was measured as a function of temperature. The results are shown in Figure 4-4. In the incommensurate and normal phases, spin-lattice relaxation times were shorter than 100 micro sec, which was the limit of the measurement. In the low temperature phase, the spin-lattice relaxation times for ν_1 and ν_2 were almost the same, decreasing monotonously on heating, and both show no anomaly in the commensurate - low temperature phase transition region. This fact indicates that the relaxation in the low temperature phase is governed by librational motion of the $[HgBr_4]^{2-}$ tetrahedron.[9] It can be seen in Figure 4-4 that in the low temperature region of the low temperature phase the spin-lattice relaxation times for the ν_3 and ν_4 lines are significantly different

Figure 4-4. Temperature dependence of ^{81}Br NQR spin-lattice relaxation times in Cs_2HgBr_4. The numbers are referred to the line numbers in Figure 4-1.

from each other. But on approaching the commensurate -
low temperature phase transition point the difference
between their T_1's becomes smaller: The temperature
variation of the difference resembles that of the
so-called order parameter of a second-order phase
transition. There are many substances in which the T_1's
of NQR show some interesting critical decrease
associated with their phase transitions[10]. But there
has not been found any compounds in which T_1's behave
like an order parameter of phase transition: Cs_2HgBr_4
is the first example which shows such a behavior. It is
supposed that the peculiar temperature dependence of T_1
in this material is closely related to the mechanism of
the phase transition between the low temperature and
the commensurate phases. The T_1's of $\nu_5 - \nu_8$ tend to
behave like those of ν_3 and ν_4 on heating but they
could not be determined accurately near T_C due to poor
signal intensities. Near the lock-in transition
temperature there was not any significant anomaly,
probably suggesting that the spin-lattice relaxation
due to stochastic origin is very efficient and overcome
the critical contribution in the commensurate phase.

4-1-4 ^{81}Br NQR frequencies in incommensurate phase

In order to characterize the structure of the
incommensurate phase, the ^{81}Br nuclear quadrupole
resonance signals were searched by pulsed FT

spectrometer described in Section 2-4. Only a pair of resonance lines were observed near 92.5 MHz. A typical spectrum is shown in Figure 4-5. The temperature dependence of the resonance frequencies in the incommensurate phase together with those in the normal and the commensurate phases is shown in Figure 4-6. Three characteristic features are seen in this figure: First, the normal-incommensurate phase transition is of second-order, corroborating the previous postulate in Section 4-1-2. The second is that the lower frequency line in the incommensurate phase can be connected smoothly to the line in the normal phase at T_I. The third character is that the higher frequency line in the incommensurate phase is , on the other hand, smoothly connected to the line ν in the commensurate phase at T_c. Furthermore, the fact that any resonance line which correspond to either of two lower lines in the normal phase could not be observed in the incommensurate phase is also an important information. These characteristics will be more fully discussed in relation to the mechanism of the successive phase transitions in the material in Chapter 5.

$$T = 234.9 \,\text{K}$$

$$\nu_f = 92.6473 \,\text{MHz}$$

$$(\nu - \nu_f)/\text{kHz}$$

Figure 4-5. Typical FT spectrum of a ^{81}Br NQR line in Cs$_2$HgBr$_4$ in the incommensurate phase obtained by 10240 times signal averaging. On the deformed base line spectrum is seen at the frequency separated by about 25 kHz from the carrier frequency ν_f.

Figure 4-6. Temperature dependence of [81]Br NQR frequencies in Cs_2HgBr_4 in the incommensurate, the normal, and the commensurate phases.

4-2 Cs_2CdBr_4

4-2-1 Temperature dependence of ^{81}Br NQR frequencies

This material is isomorphous to Cs_2HgBr_4[4,6] and NQR parameters in both compounds behave similarly to each other. The temperature dependence of the ^{81}Br nuclear quadrupole resonance frequencies is shown in Figure 4-7. The data agree with the result by Kind[2,5] within 100 kHz in the whole temperature range measured. Comparison of the data in this figure with those in Figure 4-1 shows that this substance behaves similarly to Cs_2HgBr_4. The transition temperatures determined shown in Figure 4-8 agree with those by Kind[2,5] within 2 K. Typical resonance frequencies in each phase are tabulated in Table 4-2. The absolute value of the frequencies are reduced by factor of about 7/10 from those in Cs_2HgBr_4 probably due to the difference of the electronic structure in the two $[MBr_4]^{2-}$ tetrahedrons. The normal phase gives three resonance lines with the intensity ratio 1:1:2 as in Cs_2HgBr_4: ν_1, ν_2, ν_3 were assigned to the bromine at the sites 1, 2, and 3 by referring to the previous Zeeman experimental result.[5] The resonance frequencies in the incommensurate phase will be shown later. On cooling the sample through the commensurate-low temperature phase transition each of four lines ν_A - ν_D split into two lines and so eight resonance lines

Figure 4-7. Temperature dependence of ^{81}Br NQR frequencies in Cs_2CdBr_4. ^{81}Br NQR frequencies in the incommensurate phase (between 237 K and 252 K) will be shown in Figure 4-11.

Figure 4-8. Phase relation of Cs_2CdBr_4.

Table 4-2

[81]Br NQR frequencies in Cs_2CdBr_4

T/K	ν/MHZ	T/K	ν/MHz
Normal phase		Commensurate phase	
279.6	66.051	200.3	67.347
278.7	59.914	201.5	62.038
279.5	57.520	200.5	60.227
		201.3	58.347
IC phase			
240.4	66.685	Low temp phase	
240.4	66.554	100.9	69.399
242.2	66.648	100.9	68.099
242.2	66.527	100.7	64.505
244.0	66.610	101.0	63.791
244.0	66.504	100.6	62.226
245.8	66.571	100.6	61.399
245.9	66.479	100.9	60.872
249.4	66.478	100.7	57.519
249.4	66.432		
251.2	66.418		
251.4	66.407		

were observed. The resonance lines ν_7 and ν_8 were not observed near the transition temperature for the same reason as in Cs_2HgBr_4. The commensurate - low temperature phase transition is of the second-order.

4-2-2 Line width

The results of the line width measurement are shown in Figure 4-9. In the commensurate phase the line width of four resonance lines were almost constant and no significant line broadening was observed near the lock-in transition temperature. This suggests that the lock-in transition in this compound is also the first-order as in Cs_2HgBr_4. In the normal phase the highest frequency line did not show any anomaly in the line width whereas the other two lines broadened near T_I due probably to an anisotropic critical fluctuation as in the case of Cs_2HgBr_4.

4-2-3 Temperature dependence
of spin-lattice relaxation time

The Results of the T_1 measurements are shown in Figure 4-10. As in Cs_2CdBr_4 the spin-lattice relaxation times were too short to measure in the incommensurate and the normal phases. Therefore T_1 were measured only in the commensurate and the low temperature phases. The

Figure 4-9. Line widths at the half maximum of ^{81}Br NQR lines in Cs_2CdBr_4 in the commensurate and the normal phases.

Figure 4-10. Temperature dependence of [81]Br NQR spin-lattice relaxation times in Cs_2CdBr_4. The numbers correspond to the line numbers in Figure 4-7.

spin-lattice relaxation time of ν_1, ν_2, and ν_A behave similarly to those of Cs_2CdBr_4, suggesting that the relaxation is governed by librational motion of $[CdBr_4]^{2-}$ tetrahedron[9]. Although order parameter-like behavior of T_1 was not recognized in the low temperature phase contrary to the case of Cs_2HgBr_4, steep decrease of T_1 was observed for ν_B and ν_C in the commensurate phase near T_I.

4-2-3 ^{81}Br nuclear quadrupole resonance frequency
in the incommensurate phase

Only two resonance lines were observed near 66.6 MHz. Temperature dependence of the resonance frequencies in the incommensurate phase together with those in the normal and the commensurate phases is shown in Figure 4-11. The characteristic features of the frequency data are the same as those in Cs_2HgBr_4, i.e.,

(1) The normal-incommensurate phase transition is of the second order.

(2) The frequency of the lower resonance line in the incommensurate phase is smoothly connected to that in the normal phase at T_I.

(3) The frequency of the higher resonance line is smoothly connected to that in the commensurate phase at T_C.

Figure 4-11. Temperature dependence of ^{81}Br NQR frequencies in Cs_2CdBr_4 in the incommensurate, the normal, and the commensurate phases.

(4) The resonance lines corresponding to the two lower lines, ν_2 and ν_3, in the normal phase could not be observed.

4-3 Cs_2ZnBr_4

4-3-1 Temperature dependence of ^{81}Br nuclear quadrupole resonance frequencies

In order to elucidate the mechanisms of the successive phase transitions including the incommensurate transitions on the basis of dynamical nature of the crystal lattices as studied by, for example, NQR it is of help to compare the NQR data of Hg- and Cd-salts mentioned above with the other isomorphous compounds which do not undergo any phase transition. Cs_2ZnBr_4 is chosen for such a reference substance and the temperature dependence of its nuclear quadrupole resonance frequencies and the spin-lattice relaxation times were measured. Temperature dependence of the nuclear quadrupole resonance frequencies is shown in Figure 4-12. Three resonance lines were observed in the temperature range between 77 K and 300 K as expected from the X-ray structure data [11]. Their frequencies decrease monotonously with temperature with no indication of phase transition in the whole temperature range of the measurement. Our frequency

Figure 4-12. Temperature dependence of [81]Br NQR frequencies in Cs_2ZnBr_4.

Table 4-3

^{81}Br and ^{79}Br NQR frequencies in $(CH_3NH_3)_2CdBr_4$

Nuclear	T/K	ν/MHz
79	119.9	76.803
	119.9	76.821
	120.1	68.577
	120.0	68.099
81	119.9	64.160
	119.9	64.177
	120.1	57.286
	120.0	56.890
79	220.0	75.528
	219.9	75.470
	220.0	69.338
	220.2	67.808
81	220.1	63.095
	220.1	63.045
	220.0	57.925
	220.1	56.646

data are consistent with those by Kind [2] within 100 kHz in the temperature range measured.

4-3-2 Temperature dependence of ^{81}Br

spin-lattice relaxation time, T_1

Temperature dependence of the spin-lattice relaxation time is shown in Figure 4-13. According to the theory of quadrupole relaxation by librational motion[9], the spin-lattice relaxation rate, T_1^{-1} is expressed as

$$T_1^{-1} = (\frac{e^2Qq}{h})^2 T^2 \cdot [\cdots] .\qquad (4-1)$$

where the last term is dependent on the librational mode. The temperature dependece of the relaxation time obeys this $T_1^{-1} = C*T^2$ law for all the lines. Therefore, relaxations of Bromine nuclei at all sites are governed by the librational motion of the $[ZnBr_4]^{2-}$ tetrahedron in the temperature range between 78 K and 300 K. The spin-lattice relaxation time of the highest frequency line ν_1 is long compared with those of the ν_2 and ν_3 lines. The quadrupole coupling constant, e^2Qq/h, is related to ν by the expression[7]

$$\nu = (\frac{e^2Qq}{2h}) \cdot (1 + \frac{1}{3}\eta^2)^{\frac{1}{2}} .\qquad (4-2)$$

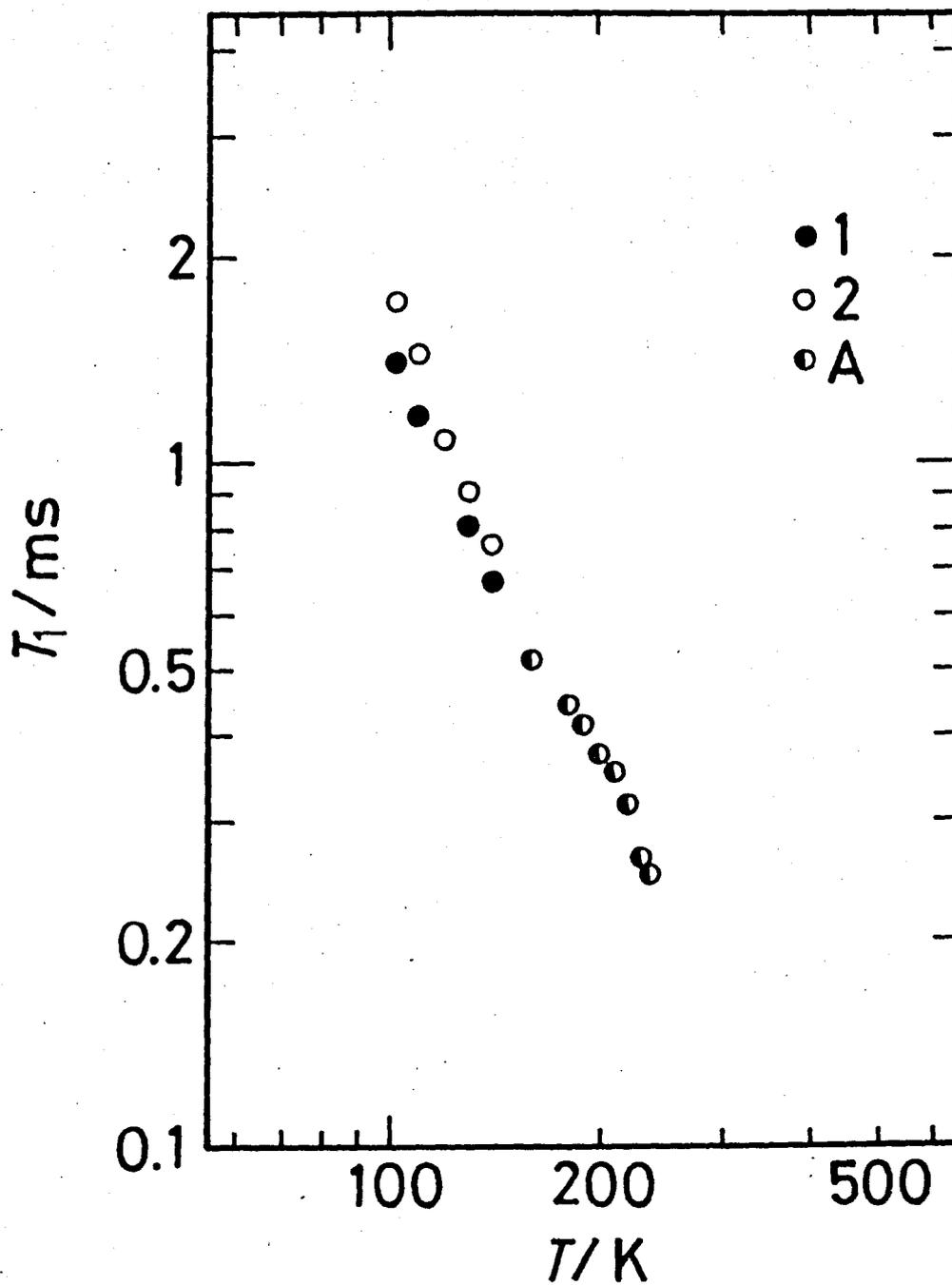The asymmetry parameter , η , is zero if the nucleus interested is located at the three-fold symmetry site. And ν is equal to e^2Qq/h. If the last terms in the

Figure 4-13. Temperature dependence of ^{81}Br NQR spin-lattice relaxation times in Cs_2ZnBr_4.

Equation 4-1 are the same for all the lines, the
Equation 4-1 expect the following relation
$T_1^{-1}(\nu_1):T_1^{-1}(\nu_2):T_1^{-1}(\nu_3)= \nu_1^2:\nu_2^2:\nu_3^2$. And the
relaxation time of the ν_1 line should be shorter than
those of the other lines, ν_2 and ν_3. And the result
that the relaxation time of the ν_1 line is relatively
longer than those of the other lines, ν_2 and ν_3, can
not be explained, if the last term is different for
each line. This result indicates that an anisotropic
librational motion is excited. The line intensity of
the ν_3 line is twice as large as that of ν_1 or ν_2 line.
Therefore the ν_3 line is assigned to the site 3. The
frequency of the ν_i (i= 1-3) line in Cs_2CdBr_4 is
approximately equal to the frequency of the v_i line in
Cs_2ZnBr_4 at room temperature. Therefore, the same site
assignments are allowed for both compounds. The ν_1 line
is assigned to site 1. The Cd-Br(1) axis is parallel to
the a-axis. The libration about this axis may cause
only small fluctuation of the main components of EFG
at the site 1, but large fluctuation may result for ν_2
and ν_3 lines. The fluctuation of EFG brings about the
quadruoplar relaxation[7]. Therefore, such an
anisotropic librational mode does not cause efficient
quadrupole relaxation at the site 1, but can bring
about strong quadrupole relaxation at the other sites.
This mechanism therefore accounts qualitatively the
order of the experimental T_1 values. Hence we can

conclude that these librational amplitude about the a-axis is large compared with other two modes. This mode is mainly excited. As will be mentioned in Chapter 5, the rotation of $[MBr_4]^{2-}$ (M=Hg, Cd) about the a-axis is causes the normal-incommensurate phase transition . Therefore in three isomorphous compounds, Cs_2ZnBr_4, Cs_2CdBr_4, and Cs_2HgBr_4, the libration about the a-axis plays an important role for their physical properties.

4-4 $(CH_3NH_3)_2CdBr_4$

4-4-1 Temperature dependence of ^{81}Br and ^{79}Br
nuclear quadrupole resonance frequencies

A preliminary X-ray analysis[6] of $(CH_3NH_3)_2CdBr_4$ revealed that the anionic motion is highly anisotropic with a large amplitude in the direction of the crystallographic a-axis and then predicted that this compound is a candidate of special family which undergoes incommensurate phase transition. Furthermore a recent differential scanning calorimetry work [12] reported that this compound undergoes a first order phase transition with large enthalpy of transition at 167 K and another one at 400 K. Hence the ^{81}Br and ^{79}Br NQR measurements on this material were undertaken to examine these phase transitions. The frequencies of four resonance lines found in this compound vary smoothly with temperature and didnot show any anomaly

between 77 K and 300 K, indicating that there is no phase transition, contrary to the previous DSC result in this temperature range [12]. There are four crystallographically inequivalent sites by X-ray analysis[6], being consistent with the number of the resonance lines in the present work. The resonance frequencies at selected temperatures were shown in Table 4-3. The temperature dependence of the ^{81}Br and ^{79}Br nuclear quadrupole resonance frequencies are shown in Figures 4-14 ans 4-15, respectively. Below 200 K the frequencies of the upper two resonance lines , ν_1 and ν_2, almost coincide with each other: The frequency differences between these two lines are plotted in Figure 4-14 and 4-15 in an enlarged scale. At about 80 K and 180 K two frequencies cross each other accidentally . The frequencies of the ν_3 and ν_4 lines behave in a curious manner, i.e., the resonance frequency of ν_4 assumes a maximum value at about 120 K and the resonance frequency of the ν_3 increases monotonously with an increase in temperature up to 300 K. Such an anomolous temperature dependence has been observed in systems in where the hydrogen atom is involved in hydrogen bonds[13]. The anomalous behavior of ν_3 and ν_4 will be analyzed later together with the spin-lattice relaxation data.

4-4-2 Temperature dependence of the ^{81}Br and ^{79}Br

Figure 4-14. Temperature dependence of [79]Br NQR frequencies in $(CH_3NH_3)_2CdBr_4$. The difference of frequencies between v_1 and v_2 is shown in the upper figure to distinguish the closely located two lines.

Figure 4-15. Temperature dependence of ^{81}Br NQR frequencies in $(CH_3NH_3)_2CdBr_4$. The difference of frequencies between v_1 and v_2 is shown in the upper figure to distinguish the closely located two lines.

nuclear quadrupole spin-lattice relaxation time

In order to learn the static as well as dynamic nature of possible hydrogen bond and molecular motion the spin-lattice relaxation time for both ^{81}Br and ^{79}Br were measured as a function of temperature. The results are shown in Figures 4-16, 4-17, 4-18, and 4-19. Because the frequency difference between ν_1 and ν_2 was very small below 200 K, their spin-lattice relaxation times could not be measured accurately. The temperature dependence of the spin-lattice relaxation times of ν_3 and ν_4 suggest that the librational motion of $[CdBr_4]^{2-}$ governs the spin-lattice relaxation below 200 K, which fact will be discussed in Appendix 2. But above 200 K a sharp decrease in the spin-lattice relaxation time was observed due probably to the onset of some reorientational motion[14]. The T_1 of ν_1 and ν_2 also show a steep decrease though experimental errors were relatively large.

As was pointed out above the physical properties of this compounds are apparently different from those of the other three compounds. Therefore the close examination of the NQR data for this compound will be deferred to Appendix 2.

Figure 4-16. Temperature dependence of ^{79}Br and ^{81}Br NQR spin-lattice relaxation times of v_1 lines in $(CH_3NH_3)_2CdBr_4$.

Figure 4-17. Temperature dependence of ^{79}Br and ^{81}Br NQR spin-lattice relaxation times of v_2 lines in $(CH_3NH_3)_2CdBr_4$.

Figure 4-18. Temperature dependence of ^{79}Br and ^{81}Br NQR spin-lattice relaxation times of ν_3 lines in $(CH_3NH_3)_2CdBr_4$.

Figure 4-19. Temperature dependence of ^{79}Br and ^{81}Br NQR spin-lattice relaxation times of v_4 lines in $(CH_3NH_3)_2CdBr_4$.

References

1. Y. Yamada, and N. Hamaya, J. Phys. Soc. Jpn., <u>52</u>, 3466(1983).

2. S. Plesko, R. Kind, and H. Arend, Phys. Status Solidi, (a)<u>61</u>, 87 (1980).

3. S. Plesko, V. Dvorak, R. Kind, and A. Treindl, Ferroelectrics, <u>36</u>, 331 (1981).

4. G.K. Semin, I.M. Alymov, V.M. Burbelo, V.I. Pakhomov, and P.M. Fedorov, Izv. Akad. Nauk. SSSR, Ser. Fiz. <u>42</u>, 2095 (1978).

5. S. Plesko, R. Kind, and H. Arend, Ferroelectrics, <u>26</u>, 703 (1980).

6. D. Altermatt, A. Niggli, W. Petter, and H. Arend, Mat. Res. Bull., <u>14</u>, 1391 (1979).

7. H. Chihara, and N. Nakamura, "Advances in Nuclear Quadrupole Resonance" vol. 4, J.A.S. Smith ed. London, Hyden & Son Ltd, 1980.

8. T. Atake, K. Nomoto, B.K. Chaudhuri, and H. Chihara, J. Chem. Thermodyn. <u>15</u>, 339 (1983).

9. J. van Kranendonk, M.B. Walker, Phys. Rev. Lett., <u>18</u>, 701 (1967).

10. H.M. van Driel, M. Wiszniewska, B.M. Moores, and R.L. Armstrong, Phys. Rev., B<u>6</u>, 1596 (1972).

11. B. Morosin, and E.C. Lingafelter, Acta Cryst., <u>12</u>, 744 (1959).

12. C.N.R. Rao, S. Gaaguly, H.R. Swamy, and I.A. Oxton, J. Chem. Soc., Faraday Trans. 2, <u>77</u>, 1825 (1981).

13. K. Negita, N. Nakamura, and H. Chihara, Chem. Phys.

Lett., <u>63</u>, 187 (1979).

14. S. Alexander, A. Tzalmona, Phys. Rev., A<u>138</u>, 845 (1965).

Chapter 5   Structure of incommensurate phase

5-1 Introduction

The NQR of Cs_2HgBr_4 and Cs_2CdBr_4 revealed the four following features of the incommensurate phases as mentioned in Sections 4-1-4 and 4-2-4.

(1) The normal-incommensurate phase transition is of the second-order.

(2) Among a pair of resonance lines detected the lower frequency line in the incommensurate phase is smoothly connected to the highest resonance line of the normal phase at T_I.

(3) The higher frequency line in the incommensurate phase is, on the other hand, smoothly connected to the resonance line of the commensurate phase at T_c.

(4) Resonance lines corresponding to the other two lower lines, ν_2 and ν_3, in the normal phase were undetectable in the incommensurate phase.

Nuclear quadrupole resonance frequency is in general very sensitive to environment around the nuclei of interest.[1] Therefore, the above features (2) - (4) are considered to reflect the structure of the incommensurate phase in these compounds. In this chapter the incommensurate structure in these two substances is examined on the basis of NQR data by two different approaches: The first is to analyze the NQR

frequencies in the incommensurate phase by applying a phenomenological theory of transition.[2] The second approach is to perform a model calculation of the electric field gradient at the bromine sites aiming at the microscopic nature of the incommensurate phase.

5-2 Analysis by phenomenological theory

5-2-1 Brief review of theory[2]

The resonance frequency of a given atomic species in the incommensurate phase can be expressed as

$$\nu = \nu_0 + a_1 u + \frac{1}{2} a_2 u^2 + \cdots \quad (u = A \cos p(x)) \quad (5-1)$$

where u is the displacement of the atom at a given site from the original position in the normal phase, ν_0 the resonance frequency in the normal phase and a_1 and a_2 are some constants. Equation 5-1 can be a good approximation only when the wavelength of the incommensurate modulation is sufficiently long compared with the region of the atoms which contribute to the EFG significantly. In order to calculate ν the analytical expression of u is necessary. The theoretical treatments so far proposed for usual incommensurate structure may be classified into two: One is a model which expresses u as a "plane wave" and the other introduces a "phase soliton" concept to

represent u. In the present compounds X-ray analysis[3]
suggests that the incommensurate modulation is one
dimensional and so it is believed that a simple one
dimensional model will be considered below.

(1) plane wave model

   According to the plane wave model

$$u = A \cos p(x) = A \cos (k_I x + p_0)$$ (5-2)

where p is a linear function of x, the coordinate of
the atom measured from an appropriate origin along the
direction of the modulation, and k_I is the
incommensurate modulation wave vector. Inserting
Equation 5-2 into Equation 5-1 we obtain

$$\nu = \nu_0 + a_1 A \cos p(x) + \tfrac{1}{2} a_2 A^2 \cos^2 p(x) + \cdots$$ (5-3)

The density of spectral line $f(\nu)$ is obtained from

$$f(\nu) d\nu = \rho(p) dp$$ (5-4)

where $\rho(p)$ is the phase density. The incommensurate
phase is characterized by the atomic displacements
which vary from an atom to another atom almost
continuously. In other words, this situation is
represented by $\cos p(x)$ which varies continuously between
+1 and -1. In such a case $\rho(p)$ assumes a constant value
over the domain of p. By reducing the domain of p to
the intervnal (0, 2π) the relation, $\rho(p) = 1/2\pi$, is
obtained. Hence

$$f(\nu) = 1 / (2\pi \, d\nu/dp)$$ (5-5)

The derivative of Equation 5-3 is

$$\frac{d\nu}{dp} = - (\nu_1^* + \nu_2^* \cos p + \cdots) \sin p .$$ (5-6)

where $\nu_1^* = a_1 * A$ and $\nu_2^* = a_2 * A^2$.

(i) linear case

Let us consider that the nucleus occupies a general position in the normal phase and assume that only the linear term is dominant. Then

$$\nu = \nu_0 + \nu_1^* \cos p(x) .$$

The frequency distribution can be obtained from Equation 5-5 as

$$f(\nu) = \frac{1}{2\pi \nu_1^* |\sin p|} = \frac{1}{2\pi \nu_1^* (1 - (\frac{\nu - \nu_0}{\nu_1^*})^2)^{\frac{1}{2}}} .$$

The edge singularities appear at

$$\nu = \nu_0 \pm \nu_1^* .$$

$f(\nu)$ is shown in Figure 5-1a.

(ii) quadratic case

Let us consider that the nucleus occupies a special position in the normal phase and assume that only the quadratic term is dominant. Then

$$\nu = \nu_0 + \frac{1}{2} \nu_2^* \cos^2 p(x)$$

The frequency distribution can be obtained from Equation 5-5 to be

$$f(\nu) = \frac{1}{2\pi \nu_2^* |\cos p \cdot \sin p|} = \frac{1}{2\pi \nu_2 ((\frac{\nu - \nu_0}{\nu_2^*/2})(1 - \frac{\nu - \nu_0}{\nu_2^*/2}))^{\frac{1}{2}}}$$

$f(\nu)$ is shown in Figure 5-1b. The edge singularities occur at $\nu = \nu_0$ and $\nu = \nu_0 + \nu_2^*/2$.

(2) soliton case

In the soliton model,[4] p(x) is one of the

Figure 5-1. Theoretical lineshape in one-dimensionally modulated incommensurate structure in the plane wave limit: (a) linear case, (b) quadratic case.

solutions of one-dimensional time-independent Sine-Gordon equation:

$$\frac{d^2p}{dx^2} - \alpha^2 \sin(\ell x) = 0 \qquad (u = A\cos p(x))$$

For single soliton

$$p_s(x) = \frac{4}{\ell} \arctan \exp(-\alpha\sqrt{\ell x})$$

For multi-soliton case, the solution can be approximately described as

$$p(x) = \frac{2\pi}{\ell}\hbar + p_s(x - \hbar b) \qquad \hbar = 1, 2, \cdots$$

By differentiating the Equation 5-1

$$\frac{dv}{dx} = -(v_1^* + v_2^* \cos p(x) + \cdots) \cdot \sin p(x) \cdot \frac{dp}{dx}$$

In the soliton case the commensurate line which corresponds to $\frac{dp}{dx} \approx 0$ will appear because $\frac{dv}{dx}$ becomes zero and edge singurarity appears. The schematic $f(\vec{v})$ is shown in Figure 5-2.

5-2-2 Application of phenomenological theory

to Cs_2HgBr_4 and Cs_2CdBr_4

According to the theory mentioned above a broad NQR line with sharp singular edges will be expected in the incommensurate phase. The width between two edges corresponds to $2v_1^*$ or v_2^* depending on the theoretical model. In the present experiment, however, only a pair of weak resonance lines were observed (Figures 5-3 and 5-4).

This experimental result may be interpreted in three ways: The first is to consider that the two lines observed in the incommensurate phase are due to [81]Br in

Figure 5-2. Typical lineshape in an incommensurate system where soliton plays the main role.

Figure 5-3. Temperature dependence of [81]Br NQR frequencies in Cs_2HgBr_4 in the incommensurate phase.

Figure 5-4. Temperature dependence of ^{81}Br NQR frequencies in Cs_2CdBr_4 in the incommensurate phase.

crystallographically different sites generated by the normal-incommensurate transition. If this interpretation is true the incommensurate phase might have the distinctly defined atomic sites contrary to the widely-accepted models of the incommensurate phase in which the atomic positions are modulated in an incommensurate manner. In such case, however, the intensity of the pair of the lines should be comparable with those in the normal or the commensurate phase. The fact that the line intensity is very low in the incommensurate phase excludes the above idea. The second interpretation is to regard the incommensurate phase as some mixture of the normal or the commensurate phase and the highly defective incommensurate phase and to assume that the NQR lines come only from the normal phase. With such a model of the incommensurate phase the poor NQR signals may be accounted for. But this model demands that the fraction of the incommensurate phase is decreased on heating so that the increment in the intensity of the lines with temperature is predicted. This expectation conflicts with the fact that the line intensity does not vary significantly with temperature. The third interpretation is to accept the previous uniform model of the incommensurate phase but, on account of a large amplitude of the incommensurate modulation, the NQR line as seen in Figures 5-3 and 5-4 broadened to an extent that the

central lower intensity part can not be observed and so only the parts of the high singular edges were detected.

The maximum line splittings were 300 kHz and 400 kHz in Hg- and Cl-salts, respectively, while the line width of ν_1 in the normal phase was about 20 kHz and so the intensity of the incommensurate phase is expected to become 1/20 of those in the normal phase. Therefore the above interpretation that the central part of the NQR line is lost into the noise level whereas the singular edges have poor but detectable intensities can be accepted.

Comparison of the experimental data with the theoretical line shape in Figure 5-1 shows that the structure of the incommensurate phase in both Hg- and Cd-salts can be described by the plane wave model in which the quadratic term is dominant and no soliton effect exists. As was mentioned in Chapter 4 the signal in the incommensurate phase comes from those atoms which would be at the site 1 in the normal phase which is a special position in the mirror plane. From group theoretical consideration, the rotation of the $[MBr_4]^{2-}$ tetrahedrons which move the bromine atom at the site 1 out of the mirror plane is represented by the quadratic term as appeared in Equation 5-3. Hence the incommensurate phase transition in both salts is associated with the rotation of the anion groups. This behavior is similar to $NaNO_2$,[5] but different from

Rb_2ZnBr_4 and Rb_2ZnCl_4.[6] That is, in $NaNO_2$ [14]N resonance line splits into two lines in the incommensurate phase, and the low resonance line is smoothly connected to the line in the normal phase at T_I. On the other hand, in Rb_2ZnBr_4 and Rb_2ZnCl_4, [87]Rb lines show the behavior predicted by the linear case of the phenomenological theory.

The splitting of frequency

$$\Delta \nu = \frac{\nu_2^*}{2} = \frac{1}{2}\alpha_2 A^2$$

is proportional to the square of the amplitude of the incommensurate distortion wave which can be clearly taken as the order parameter of the incommensurate transition[7]: According to the Landau-type phenomenological theory of the incommensurate transition the order parameter A forms the leading term of the Helmholtz free energy when expanded as the function of the displacement and is simply expressed by

$$A \sim (T - T_I)^{\frac{1}{2}}$$

In many real systems, however, such a simple relation fails and instead A can be represented by a more general form,

$$A \propto (T - T_I)^{\beta}$$

where β is the critical exponent for the order parameter. β is a very important quantity relating to the mechanism of phase transition on the basis of the scaling law, i.e. any proper theory on the transition will be required to reproduce the value of the

parameter . Using the above general expression, $\Delta \nu$ can be written as

$$\Delta \nu = (T - T_I)^{2\beta}$$

By fitting the experimental ν to this relation β's were determined to be 0.27 for both Cs_2CdBr_4 and Cs_2HgBr_4, which is similar to the value 0.36 for Rb_2ZnBr_4 and Rb_2ZnCl_4.[6]

5-3 Model calculation

In the preceding section the NQR frequencies ν in the incommensurate phase was used to look into the structural characteristics of the incommensurate phase of Hg- as well as Cd-salts: There was revealed that the incommensurate modulation is expressed by a plane wave which is generated by some rotation of the $[MBr_4]^{2-}$ anions. However, about which axis does each anion rotate ? In order to answer this question a model calculation of the electric field gradient at each bromine site in a model incommensurate structure was made.

5-3-1 Method of calculation

Before considering the model, the method of calculating the efg will be described. In order to calculate the electrostatic potential, electric field, and electric field gradient in ionic crystals one must take the lattice sum over the particles undergoing the

Coulomb interaction. It is well known that convergency
of such a lattice sum is poor in the real space.
Usually the lattice sum is calculated using the Ewald
method[8] which takes the lattice sum over the real
space in one part and over the reciprocal space in
another part to obtain a rapid convergence. On the
other hand, Bertaut[9-11] proposed another ingenious
method which calculates the lattice sum over the whole
reciprocal space. The convergence in this method is
much more efficient than the usual Ewald method. Here
the Bertaut method is applied to calculate electric
field gradients in the incommensurate phase.

The Bertaut method introduces a sphero-symmetrical
continuous charge densities $q_j \sigma(\vec{r} - \vec{r}_j)$ to obtain rapid
convergence instead of point charge $q_j \delta(\vec{r} - \vec{r}_j)$. This
treatment is valid according to a well-known theorem
in electrostatics. In the following a brief account of
the method will be reviewed. The charge distribution in
a crystal lattice can be expressed as

$$\rho(\vec{r}) = \sum_j q_j \sigma(\vec{r} - \vec{r}_j)$$

$$= V_c^{-1} \cdot \sum F(\vec{h}) \Phi(\vec{h}) \exp(-2\pi i \vec{h} \cdot \vec{r}) .$$

Here $\Phi(\vec{h})$ is the Fourier transform of $\sigma(\vec{r} - \vec{r}_j)$, the
distribution of charge around any atomic site $\vec{r}_j$, and
$F(\vec{h})$ is the structure factor of point charge
corresponding to the reciprocal lattice vector $\vec{h}$

$$F(\vec{h}) = \sum_j q_j \exp(2\pi i \vec{h} \cdot \vec{r}_j)$$

Using these quantities the electrostatic interaction

energy between ions in the entire crystal is expressed

as

$$W = \frac{1}{2} \cdot \frac{1}{4\pi\varepsilon_0} \sum_{i,j} \frac{q_i q_j}{r_{ij}}$$

$$= \frac{1}{4\pi\varepsilon_0} \left\{ (2V_c)^{-1} \sum_{\vec{h}}{}' \frac{|F(\vec{h})\Phi(\vec{h})|^2}{|\vec{h}|^2} - (2\pi)^{-1} \int \frac{|\Phi(\vec{h})|^2}{|\vec{h}|^2} dh^3 \sum_j q_j^2 \right\} .$$

Here q_j is a charge at $\vec{r_j}$ in the unit cell, q_i is the

charge of ion at a lattice site i in the crystal, and

V_c is the volume of the unit cell in the real space.

The summation $\sum_j$ is taken over all the charges in the

unit cell. The electrostatic potential at the j site is

derived from W as

$$V(\vec{r_j}) = \frac{1}{4\pi\varepsilon_0} \left\{ (\pi V_c)^{-1} \sum_{\vec{h}}{}' F(\vec{h}) \frac{|\Phi(\vec{h})|^2}{|\vec{h}|^2} \exp(-2\pi i \vec{h} \cdot \vec{r_j}) - q_j (\pi)^{-1} \int \frac{|\Phi(\vec{h})|^2}{|\vec{h}|^2} d^3\vec{h} \right\} ,$$

where V_c is the volume of an unit cell in real lattice,

and the electric field,

$$\vec{E}(\vec{r_j}) = - \text{grad } V(\vec{r_j})$$

$$= \frac{1}{4\pi\varepsilon_0} \left\{ -2\pi V_c^{-1} \sum_{\vec{h}} F(\vec{h}) \frac{|\Phi(\vec{h})|^2}{|\vec{h}|^2} \vec{h} \exp(-2\pi i \vec{h} \cdot \vec{r_j}) - 2i V_c^{-1} \sum q_j \frac{|\Phi(\vec{h})|^2}{|\vec{h}|^2} |h| \right\}.$$

This expression is rewritten as follows:

$$\vec{E}(\vec{r_j}) = \frac{1}{4\pi\varepsilon_0} \left\{ -2V_c^{-1} \sum_{\vec{h}} \sum_i q_i \sin 2\pi \vec{h} \cdot (\vec{r_i} - \vec{r_j}) \frac{|\Phi(\vec{h})|^2}{|\vec{h}|^2} \vec{h} \right\}$$

The gradient of $\vec{E}(\vec{r_j})$ in the direction of a unit vector

$\vec{n}$ is given by

$$\text{grad}_{\vec{n}} \vec{E}(\vec{r_j}) = \sum_{\vec{h}} g(\vec{h}) \vec{h} (\vec{h} \cdot \vec{n})$$

Here $g(\vec{h})$ is defined by

$$g(\vec{h}) = \frac{1}{4\pi\varepsilon_0} \left\{ 4\pi V_c^{-1} \cdot (F(\vec{h}) - q_j \exp(2\pi i \vec{h} \cdot \vec{r_j})) \frac{|\Phi(\vec{h})|^2}{|\vec{h}|^2} \exp(-2\pi i \vec{h} \cdot \vec{r_j}) \right.$$

The components of the efg tensor $\theta_{\alpha\beta}$ in the reciprocal

space is finally given, using $g(\vec{h})$, by

$$\theta_{\alpha\beta} = \sum_{\vec{h}} g(\vec{h}) h_\alpha h_\beta$$

To calculate the potential, the electric field,

and the electric field gradient with efficient convergence a suitable distribution of $\sigma(\vec{r})$ must be selected. Previous works[9] employed the parabolic charge density distribution

$$\sigma(\vec{r}) = 15(R-r)^2/(2\pi R^5)$$

as one of the best functions to obtain rapid convergence. Here the charge is non-zero within the sphere of radius R from the site of interest. In this case $\phi(\vec{h})$ is calculated to be

$$\phi(\vec{h}) = 60 [\alpha\cos\alpha - 3\sin\alpha + 2\alpha]/\alpha^5$$

with

$$\alpha = 2\pi |\vec{h}|/R$$

As seen from this expression $\phi(\vec{h})$ varies as the inverse of $|\vec{h}|$ to the power four. Therefore, convergence is good compared with the point charge model where $\phi(h)=1$ is assumed. Bertaut confirmed that the Madelung constant of NaCl can be accurately calculated by taking the lattice sum up to only (h,k,l)=(5,3,1) with the parabolic charge distribution.

5-3-2 Structural model in the incommensurate phase

In order to define the model used, possible displacement of each atom on cooling the normal phase through T_I will be considered. At room temperature, the space group is Pnma[12,13] and three ^{81}Br resonance lines were observed. In the commensurate phase four

resonance lines were observed indicating that no cell-doubling occurs owing to the phase change. According to the Landau theory the irreducible representation at the point of the reciprocal lattice in the first Brillouin zone is associated with the hypothetical direct phase change, from the normal phase to the commensurate phase. Irreducible representation at the Γ point is shown in Table 5-1. The ν_3 line in the normal phase splits into two lines in the commensurate phase. This indicates that the mirror plane symmetry m_y is lost in the commensurate phase. Therefore, one of the representations $\Gamma_3^+, \Gamma_4^+, \Gamma_1^-$ and Γ_2^- is concerned with the phase transition. These representations correspond to the space groups $P2_1/a$, $P2_1/n$, $P2_12_12_1$, and $Pn2_1a$, respectively. Recent X-ray analysis of the commensurate phase[13] determined the space group to be $P2_1/n$. Therefore the representation Γ_4^+ brings about the phase change from the normal to the commensurate phase. This representation corresponds to an in-phase rotation of all $[MBr_4]^{2-}$ tetrahedrons about the a-axis. Figures 5-3 and 5-4 show that the NQR line shifted by ν_2 (i.e. one of the edge singularities) from the "normal" line in the incommensurate phase connects smoothly to the intrinsic line ν in the commensurate phase at T_c. This suggests that the rotational displacement of $[MBr_4]^{2-}$ anions that has taken place in the commensurate phase corresponds to the upper limit of the incommensurate modulation amplitude. Hence the calculation of the efg

Table 5-1

Irreducible representation at the Γ-point of Brillouin zone for the space group Pnma

	$\bar{I}$	2_z	2_y	2_x	I	m_z	m_y	m_x
Γ_1^+	1	1	1	1	1	1	1	1
Γ_2^+	1	-1	1	-1	1	-1	1	-1
Γ_3^+	1	1	-1	-1	1	1	-1	-1
Γ_4^+	1	-1	-1	1	1	-1	-1	1
Γ_1^+	1	1	1	1	-1	-1	-1	-1
Γ_2^+	1	-1	1	-1	-1	1	-1	1
Γ_3^+	1	1	-1	-1	-1	-1	1	1
Γ_4^+	1	-1	-1	1	-1	1	1	-1

in the incommensurate phase was carried out by referring to the structure of the commensurate phase in which the magnitude of the rotation angle of the anion is known. The angular displacement in the commensurate phase is schematically shown in   Figure 5-5: All the $[MBr_4]^{2-}$ tetrahedrons rotate about the a-axis in the same direction by 7.5° from the original orientation in the normal phase.

The X-ray diffraction experiment on the incommensurate phase [3] revealed that the incommensurate wave vector $\vec{q} = 0.15\vec{a}^*$ which is close to $(1/7)a^*$. Therefore the calculation of the structure factor $\vec{F}(\vec{h})$ was performed by assuming $q=(1/7)a^*$ ($0.143a^*$) which corresponds to the unit cell super lattice with seven subcells, that is (7a*b*c). Here a, b, and c are the lattice constants in the normal phase. The rotation angle about the a-axis, which is taken as the order parameter, is expressed as;

$$\theta = A \sin\left(\frac{2\pi}{7} \cdot L + P_0\right) \qquad L = 0, \cdots, 6 \qquad \left(P = \frac{2\pi}{7}L + P_0\right)$$

Here A is the maximum angle of rotation, i.e., the amplitude of modulation and P is the phase constant. By choosing an appropriate value of P_0, various displacements for each of the seven sites can be realized. This idea is confirmed like this. As shown in Figure 5-6 the efg value is only dependent on θ, that is, on rotation angle of the interested atom around a-axis. By choosing P_0 efg of an atomic site in various

Figure 5-5. Typical displacement in incommensurate phase (c).

Figure 5-6. Calculated NQR frequency at the site 1 in the incommensurate phase as a function of $(\theta/A)^2$ where θ is the rotation angle of the $[CdBr_4]^{2-}$ about the Cd-Br axis which is nearly parallel to the a-axis: $\theta = A \cdot \sin((2\pi/7) \cdot L + P_o)$ where $A = 7.5°$, $L = 0, \sim, 6$. The calculated frequencies in the normal and the commensurate phases are indicated by RT and LT, respectively.

environment can be realized. For example, when P_0 is equal to zero , θ will be

0, 0.78A, 0.97A, 0.43A, -0.43A, -0.97A, -.78A.

When P_0 is equal to $\pi/14$, θ will be

0.22A, 0.9A, 0.9A, 0.22A, -0.62A, -A, -0.62A.

If P_0 is chosen to be $\pi/28$, θ will be

0.11A, 0.86A, 0.94A, 0.33A, -0.53A, -0.99A, -0.71A.

In this way , the electric field gradient at the bromine site which involved in the large unit cell can be calculated in various phase constant . L is the site number along the a-axis, that is, the number of the subcell contained in the incommensurate unit cell. A assumes an angle between $0°$ and $7.5°$ because in the commensurate phase the rotation angle is about $7.5°$.[13] Original fractional atomic coordinates in the normal phase are shown in Table 5-2.[12] Atomic coordinates of the bromines were generated in the incommensurate superlattice in the following way. The anions were rotated about the axis which runs through Cd of $[CdBr_4]^{2-}$ tetrahedron and parallel to the a-axis. The cadmium and cesium atoms were fixed in their original positions in the normal phase. The coordinates in the b and c directions of the bromine site is given by the following expressions:

YC = (Y(Br)-Y(Cd))*cosAA-(Z(Br)-Z(Cd))*sinAA+Y(Cd)

ZC = (Y(Br)-Y(Cd))*sinAA+(Z(Br)-Z(Cd))*cosAA+Z(Cd)

Here AA is equal to $2\pi*\theta/180°$. The coordinate XC along the a-axis was left unchanged. Formal charges on the

Table 5-2

Atomic parameters and the effective charges
used for model calculation

atom	position			charge/e
	x/a	y/b	z/c	
Cd	.2225	.25	.4236	2.0
Br(1)	-.0243	.25	.4119	-1.0
Br(2)	.3204	.25	.5926	-1.0
Br(3)	.3209	-.0094	.3426	-1.0
Cs(1)	.1236	.25	.0960	1.0
Cs(2)	-.0170	.25	.6762	1.0

component atoms shown in Table 5-2 were employed in the calculation.

The FORTRAN program for the EFG calculation was used. Calculation was carried out using ACOS-1000 (NEC) of the Computer Center of Osaka University. The lattice sums for the potential, the electric field, the electric field gradient were calculated for each bromine site in the modulated structure for running the indices h, k, l between ±105, ±15, and ±15, respectively. The convergence of the sum is sufficiently good and the significant figure is four.

5-3-3 Results and discussion

In order to examine the validity of the model calculation the electric field gradient were first calculated for the normal phase. The electric field at the bromine sites, and the principal components of electric field gradients obtained are shown in Table 5-3. The NQR frequency can be related to the nuclear quadrupole coupling constant e^2Qq_{zz} and the asymmetry parameter η,

$$\nu_Q = \frac{1}{2}\frac{e^2Qq}{h}(1+\frac{1}{3}\eta^2)^{\frac{1}{2}}(1-\gamma^\infty)$$

$$\eta = \frac{q_{xx}-q_{yy}}{q_{zz}}$$

for the nuclear spin I=3/2[14], where

$$|q_{zz}| \geq |q_{yy}| \geq |q_{xx}|$$

Table 5-3

EFG tensor of principal component calculated

φ	q_{xx}	q_{yy}	q_{zz}
site 1			
Normal phase			
	-.29922	.14910	.15011
Commensurate phase			
	-.29804	.14761	.15043
IC phase			
A=7.5° 0	-.29916	.14860	.15056
2π/7	-.29850	.14876	.14974
4π/7	-.29816	.14800	.15016
6π/7	-.29897	.14817	.15080
8π/7	-.29895	.14886	.15009
10π/7	-.29814	.14838	.14976
12π/7	-.29852	.14791	.15062
π/28	-.29914	.14869	.15045
9π/28	-.29838	.14868	.14970
17π/28	-.29822	.14794	.15028
25π/28	-.29905	.14828	.15078
33π/28	-.29885	.14887	.14998
41π/28	-.29811	.14827	.14983
49π/28	-.29864	.14794	.15070
1π/14	-.29910	.14877	.15033
9π/14	-.29829	.14859	.14969
17π/14	-.29831	.14791	.15040
25π/14	-.29911	.14838	.15073
33π/14	-.29873	.14886	.14988
41π/14	-.29810	.14817	.14993
49π/14	-.29876	.14800	.15076

A=5.0°	0	-.29919	.14888	.15031
	3 /2	-.29872	.14869	.15003
A=2.5°	0	-.29921	.14905	.15016
	3 /2	-.29909	.14900	.15009

site 2

Normal phase

	.15326	.11786	-.27112

Commensurate phase

	.15366	.10935	-.26301

IC phase

A=7.5°	0	.15385	.11787	-.27172
	2 π/7	.15374	.11266	-.26641
	4 π/7	.15349	.10945	-.26294
	6 π/7	.15369	.11608	-.26978
	8 π/7	.15385	.11635	-.27021
	10 π/7	.15360	.10959	-.26319
	12π/7	.15352	.11234	-.26586

A=5.0°	0	.15352	.11786	-.27139

A=2.5	0	.15333	.11786	-.27139
	π/2	.15328	.11689	-.27016

site 3
  Normal phase

| | .10665 | -.26567 | .15901 |

  Commensurate phase

| | .11387 | -.28771 | .17384 |
| | .10626 | -.24857 | .14231 |

  IC phase

A=7.5°	0	.10892	-.26727	.15835
		.10517	-.26474	.15957
	2π/7	.11291	-.28410	.17119
		.10507	-.25091	.14584
	4π/7	.11288	-.28631	.17343
		.10709	-.24904	.14195
	6π/7	.10762	-.27424	.16661
		.10765	-.25803	.15038
	8π/7	.10433	-.25625	.15193
		.11908	-.27701	.16602
	10π/7	.10632	-.24875	.14243
		.11370	-.28715	.17345
	12π/7	.10729	-.25187	.14458
		.11061	-.28191	.17130
A=5.0°	0	.10808	-.26666	.15858
		.10557	-.26497	.15940
A=2.5°	0	.10733	-.26613	.15880
		.10607	-.26528	.15921
	π/2	.10837	-.27312	.16476
		.10574	-.25874	.15300
	3π/2	.10574	-.25874	.15300
		.10837	-.27312	.16476

and γ^∞ is the Sternheimer's antishielding constant.[15] We can calculate $\nu_Q(1-\overset{\circ}{\gamma})/eQ$ and η from the table. The Sternheimer's anti-shielding factor, γ^∞, obtained from the experimental ν_Q and the calculated q_{zz} was -66, which is larger than the reported value -35 for the Br^- ion[16]. The γ^∞ is related to the shielding effect of the inner shell electron density of Br, which is very sensitive to the bond structure. As the simplest charge density was adopted in our model calculation in $[CdBr_4]^{2-}$ complex anion, the two values fall within a reasonable range of agreement. The calculation of the absolute value of ν_Q needs the knowledge of Q and γ^∞, but the latter varies depending on the bonding nature, the configuration of the surrounding ions, etc. Moreover the covalency between the central metal and the bromine contributes to some extent to q as well as the surrounding charge distribution does. Therefore the absolute values of calculated ν_Q may contain some ambiguities. We will hereafter discuss the relative values of ν_Q at the three different sites. The calculated ν_Q' were 0.2992 at the site 1, 0.2719 at the site 2, and 0.2674 at the site 3. The largest value was obtained for the site 1, and the smallest value for the site 3. The relative order of the values agrees with the experimental results. Furthermore, the experimental frequency ratio at 300 K is 1:0.908:0.873 whereas the frequency ratio obtained in the model calculations is

1:0.909:0.894. The agreement between the experimental and the calculated frequency ratios is suprisingly good in spite of the crudeness of the model.

Next, the electric field gradients in the incommensurate phase were calculated at the site 1. The efg's were computed, as a function of the orientation of the anion, for three modulation amplitudes, $A = 2.5°$, $5.0°$,and $7.5°$. The results of the computation of the electric field gradient are recorded in Table 5-3. In order to compare the values of efg with ϑ_2 in the phenomenological theory (Section 5-2-2), ϑ_Q', which were calculated from Equation 5-9 are plotted against $\sin^2 p$ in Figure 5-6. The approximately linear relation is obvious. The frequencies distribute between the highest frequency where $p=0$ and the lowest one where $p=\pi/2$ or $(3/2)\pi$. Furthermore, the highest frequency where $p=0$ appears near the frequency in the normal phase. These results are in good accord with the phenomenological theory. In order to evaluate the frequencies at the edge singularities the calculation of the only the electric field gradients at the site where $p=0$ and $p=\pi/2$ or $(3/2)\pi$ are necessary. Hence the calculation of the efg for $A=5.0°$ and $A=2.5°$ was performed only in the cases where $p=0$ and $\pi/2$.

In order to reproduce the observed temperature dependence of the frequencies at the edge singularities the computed frequencies were plotted against A^2, in

Figure 5 - 7.   .   The frequency difference is
proportional to the square of A in agreement with the
phenomenological theory. The temperature dependence
could be reproduced except that the one singularity
edge leading to the ν_1 of the commensurate phase and
calculated ν_1 itself come on the lower side of the
other edge, opposite to the experimental result. Except
for this, this Figure reproduces the temperature
dependence of the frequencies. That is, one resonance
line is smoothly connected to the resonance line in the
normal phase at T_I and the other resonance line is
smoothly connected to the resonance line in the
commensurate phase at T_c. Furthermore the maximum
frequency difference relative to the frequency, $\Delta\nu/\nu$
where p=0 is calculated to be $3.5*10^{-3}$, which is
compared with the experimental value of $2.3*10^{-3}$. The
agreement between them is very good. Therefore the
behavior of the NQR parameters in the incommensurate
phase is accounted for by this model satisfactorily.
The above analysis of the NQR data leads to an
important conclusion about the structure of the
incommensurate phase: The tetrahedral anions are
rotated about the a-axis. The model that the angle of
the rotation of each anion is regularly modulated by a
sinusoidal wave with a period of about 7a and the
maximum angle, i.e. , the amplitude of the modulation
varies linearly from zero at T_I to about $7.5°$ at T_c upon

Figure 5-7. Calculated NQR frequencies in the incommensurate phase for the site 1 plotted against A^2. This figure represents the temperature dependence of NQR frequencies: $\theta = A \sin((2\pi/7) \cdot L + \rho)$ is used.

cooling can produce the experimental NQR data.

In order to find the reason why the signal corresponding to the sites 2 and 3 in the normal phase could not be observed in the incommensurate phase, the electric field gradients in the incommensurate phase were calculated at the sites 2 and 3 using the same model as for the site 1. The results of the computation are shown in Figures 5-8, 5-9, and 5-10. In order to compare with the phenomenological theory, ν'_Q are plotted against $\sin^2 p$ for site 2 and against $\sin P$ for the sites 3 and 4. These two sites correspond to ν_C and ν_D in the commensurate phase. For the site 2 a linear relation between ν_Q and $\sin^2 P$ holds approximately as can be shown in Figure 5-8. The frequency difference in Figure 5-8 roughly proportional to A^2. Therefore the ν_2 line is considered to behave similarly to ν_1 in the incommensurate phase but the splitting between the two edge singularities is larger than that of ν_1 by a factor of 10. As to ν_3 and ν_4 plotted against $\sin^2 P$ (Figure 5-11) an obvious deviation from the phenomenological theory is observed. The reason for this discrepancy is not clear in the present stage. Anyway, the splitting between the edge singularities amounts to 100 times that at the ν_1. It is therefore suggested that the large broadening of the line at sites 2, 3, and 4 weaken the signal intensities of these lines by less than 10 and so no signal was

Figure 5-8. Calculated NQR frequencies in the incommensurate phase for the site 1 vs $(\theta/A)^2$ where θ is the rotation angle of the $[CdBr_4]^{2-}$ about the Cd-Br axis which is nearly parallel to the a-axis together with frequency in the normal phase (RT) and the commensurate phase (LT).

Figure 5-9. Calculated NQR frequencies in the incommensurate phase for the site 3 and 4 vs θ/A where θ is the rotation angle of the $[CdBr_4]^{2-}$ about the Cd-Br axis which is nearly parallel to the a-axis together with frequency in the normal phase (RT) and the commensurate phase (LT).

Figure 5-10. Calculated NQR frequencies in the incommensurate phase for the site 2 v.s A^2 which corresponds to the temperature dependence of NQR frequency in the incommensurate phase together with frequencies in the normal and commensurate phases.

Figure 5-11. Calculated NQR frequencies in the incommensurate phase for the site 3,4 $v.s$ A^2 which corresponds to the temperature dependence of NQR frequency in the incommensurate phase together with frequencies in the normal and commensurate phases.

detected for these sites.

In this way, the spectrum in the incommensurate phase can be well accounted for by the above model calculation: It is first confirmed that the rotation of the anions about the a-axis occurs in the incommensurate phase and the rotation angle of each site is regularly modulated by the incommensurate wave. This picture also accounts for the difference of line broadening at each site near the normal-incommensurate phase transition temperature. In this temperature range, the fluctuation of the rotational mode of anions becomes large and its amplitude may be larger when the amplitude of the incommensurate wave is larger. Due to such a fluctuating mode the electric field gradients at the sites 2 and 3 fluctuate very effectively, compared with that at the site 1 at which the incommensurate wave has the smallest amplitude. Therefore relatively large line-broadening occurs at the sites 2 and 3, but negligible at the site 1. In Cs_2ZnBr_4, anisotropy of spin-lattice relaxation is observed. This can be also accounted for by the large amplitude libration about the a direction. That is, this mode fluctuates the electric field gradient at the sites 2 and 3 more effectively than that at the site 1. Therefore, the spin-lattice relaxation time at the site 1 is longer than that at the sites 2 and 3. It was thus revealed in Cs_2HgBr_4 and Cs_2CdBr_4, that the motion of the $[MBr_4]^{2-}$ is is highly anisotropic in the normal phase and its

libration about the a-axis becomes the incommensurate modulation wave at the incommensurate transition. The anisotropic librational motion was also observed in Cs_2ZnBr_4 which is isomorphous with the above two substances as was already mentioned in Section 4-4.

References

1. R.L. Armstrong, Phys. Rep., $\underline{57}$, 343 (1980).

2. R. Blinc, I.P. Aleksandrova, A.S. Chaves, F. Milia, V. Rutar, J. Seliger, and S. Zumer, J. Phys. C, $\underline{15}$, 547 (1982).

3. S. Plesko, R. Kind, and H. Arend, Phys. Status Solidi, (a)$\underline{61}$, 87 (1980).

4. W.L. McMillan, Phys. Rev., B$\underline{14}$, 1496 (1976); W.L. McMillan, Phys. Rev., B$\underline{12}$, 1187 (1975).

5. R. Ambrosetti, R. Angelone, and A. Colligiani, Phys. Rev., B$\underline{15}$, 4318 (1977). I.P. Aleksandrova, R. Blinc, B. Topic, S. Zumer, and A. Rigamonti, Phys. Status Solidi, (a)$\underline{61}$, 95 (1980).

6. R. Blinc, V. Ruter, B. Topic, F. Milia, I.P. Aleksandrova, A.S. Chaves, and R.S. Gazzinilli, Phys. Rev. Lett., $\underline{46}$, 1406 (1981).

7. R. Blinc, Phys. Rep., $\underline{79}$, 331 (1981).

8. P.P. Ewald, Ann. Phys., $\underline{64}$, 253 (1921).

9. E.F. Bertaut, J. Phys. Chem. Solids, $\underline{39}$, 97 (1978).

10. E.F. Bertaut, J. Phys. Rad., $\underline{13}$, 499 (1952).

11. J.W. Weenk, and H.A. Harwig, J. Phys. Chem. Solids, $\underline{36}$, 783 (1975).

12. D. Altermatt, A. Niggli, W. Petter, and H. Arend, Mat. Res. Bull., $\underline{14}$, 1391 (1979).

13. D. Altermatt, H. Arend, V. Gramlich, A. Niggli, and W. Petter, Acta Cryst., B$\underline{40}$, 347 (1984).

14. T.P. Das, and E.L. Hahn, "Nuclear Quadrupole

Resonance Spectroscopy", Solid State Physics,

Supplement 1, Seitz and Turnball, ed. New York:

Academic Press Inc., 1958.

15. R.M. Sternheimer, Phys. Rev., 80, 102 (1950).

16. G. Burns, and E.G. Wikner, Phys. Rev., 121, 155

(1961); K.D. Sen, and P.T. Narasimhan, "Advances in

Nuclear Quadrupole Resonance", vol. 1, J. A. S.

Smith ed. London: Heyden & Son Ltd, 1974.

Chapter 6 Classification of compounds of A_2BX_4 type

Since the report was published on the existence of an incommensurate-commensurate phase transition in K_2SeO_4[1], the variety of compounds which exhibit similar transitions have been found. These are classified into the following types.

1) A_2BX_4[2]

2) $(TMA)_2BX_4$[2]

3) $NaNO_2$[3]

4) thiourea[4], biphenyl[5]

and so on.

The series of compounds of the type A_2BX_4 are especially interesting in that they assume isomorphous structures (β-K_2SO_4) with the space group Pmna and undergo similar sequence of transitions to each other. Three compounds studied in the present work, i.e., Cs_2HgBr_4[6], Cs_2CdBr_4[7], and Cs_2ZnBr_4[8] belong to this group. As shown in Chapter 5 Cs_2HgBr_4[9] and Cs_2CdBr_4[10] show successive phase transitions and become incommensurate in some temperature region. Their physical properties, for example the transition temperatures, the length and direction of the incommensurate wave vectors, the behavior below T_c, etc., are very similar. On the other hand, Cs_2ZnBr_4[9] shows no phase transition although the crystal structure at room temperature is isomorphous to Cs_2HgBr_4 and Cs_2CdBr_4. In other member of the compounds

of A_2MX_4 type such an extreme, essential difference between substances exists that is some compounds undergo successive phase changes whereas some others do not show any transition despite that their composition as well as the structural data resemble one another: These facts suggest that the structure of any crystal of this type of substance is realized on a very delicate balance of intermolecular or interionic forces and that the phase transition phenomena happen to occur when such an intricate balance is destroyed. Hence it will be an essential point to understand the phase change phenomena in order to examine possible correlation between the crystal structures of the above series of materials and the presence of phase transitions in them and to find out some factors which govern the phase transition.

The space group of the highest temperature phase of each of A_2BX_4 type compounds (A= K, Na, Rb, Cs; B= Hg, Cd, Zn, Co, Mn, Cu; X= Cl, Br, I) is listed in Table 6-1. From this table two interesting characteristics can be extracted.

1) A_2CoX_4 and A_2ZnX_4 have the same space group when A and X are common. Thus, the space group of both Cs_2CoCl_4[11] and Cs_2ZnCl_4[12] is Pnma, and the space group of Rb_2CoI_4[13] and Rb_2ZnI_4[14] is $P2_1/m$. The lattice constants and bond lengths in A_2CoX_4 and A_2ZnX_4 are almost the same as shown in Table 6-2. The similar

Table 6-1

Space group for various compounds

anion complex	cation			
	Na	K	Rb	Cs
$HgCl_4$				Pnma
$HgBr_4$				Pnma
HgI_4				$/P2_1$
$CdCl_4$	Pbam			I4/mmm
$CdBr_4$				Pnma
CdI_4				
$ZnCl_4$	Pnma	Pnma	Pnma	Pnma
$ZnBr_4$			Pnma	Pnma
ZnI_4			$P2_1/m$	Pnma
$CoCl_4$	Pnma	Pnma	Pnma	Pnma
$CoBr_4$		$Pnma/P2_1/m$	Pnma	Pnma
CoI_4		$P2_1/m$	$P2_1/m$	Pnma

relations can be seen between A_2HgX_4 and A_2CdX_4 in Table 6-1. The above experimental facts and close examination of the structure of other substances in Table 6-1 and Table 6-2 strongly suggest that the compounds with the common cation and with the anion of the same or almost same size crystallize in the same space group even if the central metals are chemically quite different.

2) This kind of structural correlation is also reflected on the nature of the incommensurate phase in some compounds which undergo the normal to the incommensurate structure. For example, both Rb_2ZnBr_4 and Rb_2ZnCl_4[15], assume a translationally modulated incommensurate structure whereas Cs_2HgBr_4 and Cs_2CdBr_4 undergo a transition into rotationally modulated incommensurate structure. There must be something more involved than the simple law of isomorphism. Hence we can first assume that the crystal structure of the highest temperature phase, and the existence and the mode of the modulation in the incommensurate phase are governed by the relative sizes of the cation and the complex anion.

3) Table 6-3 also suggests that the condition for a highest temperature phase to undergo a phase transition, not restricted to the incommensurate transition, concerns the relative size of cation and complex anion. In order to elucidate such a condition in somewhat quantitative manner a simple calculation of

Table 6-2

Space group and lattice parameters of A_2ZnX_4 and A_2CoX_4

compound	space group	lattice constant		
		$a/\overset{\circ}{A}$	$b/\overset{\circ}{A}$	$c/\overset{\circ}{A}$
Na_2ZnCl_4	Pnma	8.053	6.402	13.695
Na_2CoCl_4	Pnma	8.073	6.428	13.713
K_2ZnCl_4	Pnma	8.926	7.256	12.402
K_2CoCl_4	Pnma	8.933	7.240	12.421
Rb_2ZnCl_4	Pmcn	7.282	12.726	9.257
Rb_2CoCl_4	Pmcn	7.283	12.723	9.272
Cs_2ZnCl_4	Pnma	9.758	7.400	12.970
Cs_2CoCl_4	Pnma	9.737	7.392	12.972
Rb_2ZnBr_4	Pmcn	7.656	13.343	9.708
Rb_2CoBr_4	Pmcn	7.651	13.371	9.718
Cs_2ZnBr_4	Pnma	10.196	7.770	13.517
Cs_2CoBr_4	Pnma	10.181	7.723	13.492
Rb_2ZnI_4	$P2_1/m$			
Rb_2CoI_4	$P2_1/m$	10.383	8.144	7.657
Cs_2ZnI_4	Pmcn	8.29	14.45	10.84
Cs_2CoI_4	Pmcn	8.297	14.414	10.833

Table 6-3

Existence of phase transition or transitions in A_2MX_4 compounds

	cation			
anion complex	Na	K	Rb	Cs
$HgCl_4$				YES
$HgBr_4$				YES
HgI_4				NO
$CdCl_4$				
$CdBr_4$				YES
CdI_4				
$ZnCl_4$	?	YES	YES	NO
$ZnBr_4$			YES	NO
ZnI_4				YES
$CoCl_4$	?	?	?	NO
$CoBr_4$		?	?	?
CoI_4		?	?	?

the relative sizes of the cation and the anion was made on each of a series of compounds shown in Figure 6-1.[16-27] The structural data and the information about the phase transitions are recorded in Table 6-2 and Table 6-3. The ionic radii for A^+ were taken from ref. 28 as 1.52 A for K^+, 1.66 A for Rb^+, and 1.81 A for Cs^{+}[28]. The ionic radii of $[MX_4]^{2-}$ complex anion was obtained by adding the interatomic distance of M-X and the atomic radius of X atom[29]. The ratio between the ionic radii, $R([MX_4]^{2-})/R(A^{2+})$ was calculated from these data and is shown in Figure 6-1, where the solid lines represent compounds which undergo any phase transitions and the broken lines those without transition, although small overlap exists. This graph indicates that the compounds with the ratio between 1.9 and 2.2 shows phase transition but for one exception (Cs_2ZnBr_4). Next, the volume occupied by the cation is plotted against the volume occupied by the complex anion, both reduced by the unit cell volume, in Figure 6-2. This Figure reveals that only compounds with $V([MX_4]^{2-})/V_{unit\ cell}$ larger than $1.72*10^{-1}$ undergo some phase transition irrespective of the value $V(A^{2+})/V_{unit\ cell}$.

Above calculations revealed that $V([MX_4]^{2-})/V_{unit\ cell} = 1.72*10^{-1}$ is an important critical value for compounds with A_2MX_4 type as an index for existence to undergo a phase transition. However, this result

Figure 6-1. Ratio of the effective radius of the complex anion $[MX_4]^{2-}$ to the radius in cation A^+ for various compounds. —— indicates a compound which has phase transition. and - - - indicates a compound which has no phase transition.

Figure 6-2. The effective volume of the complex anion $[MX_4]^{2-}$ is plotted against the volume of the cation A^+ both reduced by the volume of the unit cell. ● indicates a compound which has phase transition and ○ indicates a compound which has no phase transition.

does not provide any informations about the effect of the anisotropic nature of the crystal on the phase change phenomena whereas the incommensurate transition which is the main interest of the present work depends on a highly anisotropic properties of the crystal. In order to examine such anisotropic nature of the correlation between the phase transition and the crystal stability. The ionic radius $R(A^+)$ or $R([MX_4]^{2-})$ reduced by each one of the lattice constants was drawn in Figure 6-3. The compounds with and without any phase transitions were distinguished by the solid and broken lines, respectively. These show that the compound which is composed of a cation with a small size and complex anion with large size compared with either one of the lattice constants undergo a phase change. This tendency is distinct in the quantity $R([MX_4]^{2-})/a$, i.e., only compounds with this ratio greater than about $3.5*10^{-1}$ undergo som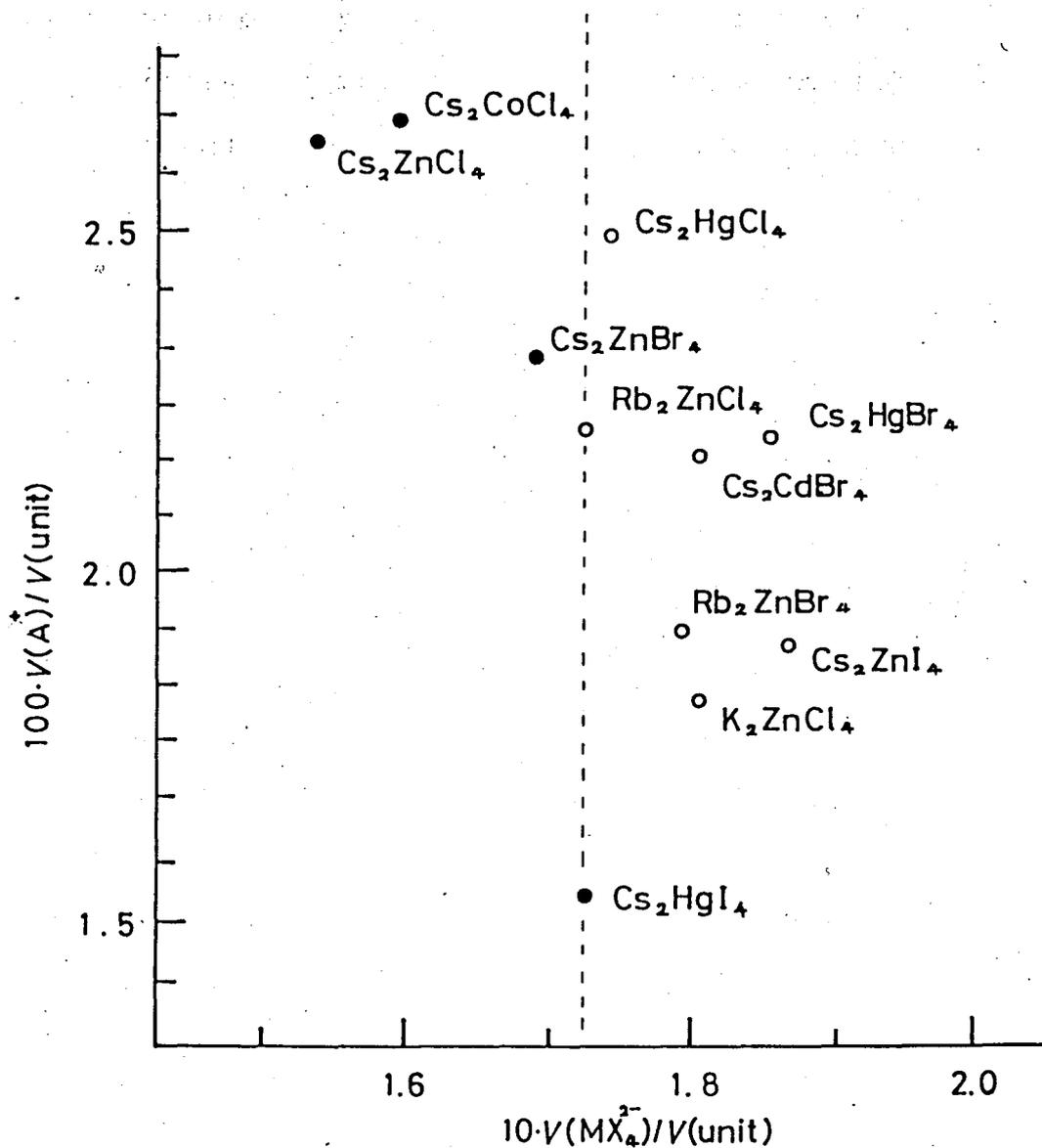e kind of phase transition. This fact looks very significant for the transition to occur because the crystal data of several substances show that the incommensurate wave vector or soft mode vector is directed in the a-direction. Moreover, the cell tripling, if occurs at the transition, occurs along the a-direction at a low temperature.

This finding is consistent with recent microscopic theoretical research on incommensurate phase. Bak et al. presented an anisotropic Ising model with

Table 6-4

Space group, lattice constants of the normal phase, and
the axis along which the cell multiplication occurs
on the transition to the low temperature phase

compound	space group	lattice constant			axis
		$a/\text{Å}$	$b/\text{Å}$	$c/\text{Å}$	
Cs_2HgCl_4	Pnma	9.798	7.585	13.384	?
Cs_2CdBr_4	Pnma	10.237	7.918	13.882	a
Cs_2CdBr_4	Pnma	10.235	7.946	13.977	a
K_2ZnCl_4	Pnam	8.926	12.402	7.256	a
Rb_2ZnCl_4	Pmcn	7.282	12.726	9.257	c
Rb_2ZnBr_4	Pmcn	7.656	13.343	9.708	c
Cs_2ZnBr_4	Pnma	10.196	7.770	13.517	no
Cs_2CoCl_4	Pnma	9.737	7.392	12.972	no
Cs_2ZnI_4	Pmcn	8.29	14.45	10.84	?
Cs_2ZnCl_4	Pnam	9.758	12.970	7.400	no

Table 6-5

Lattice parameters, and calculated ionic radii

compound	lattice parameter			$R(MX_4)/\text{Å}$	$R(A)/\text{Å}$
	$a/\text{Å}$	$b/\text{Å}$	$c/\text{Å}$		
Cs_2HgCl_4	9.798	7.585	13.384	3.46	1.81
Cs_2HgBr_4	10.237	7.918	13.384	3.68	1.81
Cs_2CdBr_4	10.235	7.946	13.977	4.04	1.81
K_2ZnCl_4	8.926	7.256	12.402	3.26	1.52
Rb_2ZnCl_4	9.257	7.282	12.726	3.29	1.66
Rb_2ZnBr_4	9.708	7.656	13.343	3.49	1.66
Cs_2ZnBr_4	10.196	7.770	13.517	3.51	1.81
Cs_2CoCl_4	9.737	7.392	12.972	3.29	1.81
Cs_2ZnI_4	10.84	8.29	14.45	3.87	1.81
Cs_2ZnCl_4	9.758	7.400	12.970	3.25	1.81

MX$_4^{2-}$

1 Cs$_2$HgCl$_4$

2 Cs$_2$HgBr$_4$

3 Cs$_2$CdBr$_4$

4 K$_2$ZnCl$_4$

5 Rb$_2$ZnCl$_4$

6 Rb$_2$ZnBr$_4$

7 Cs$_2$ZnBr$_4$

8 Cs$_2$CoCl$_4$

9 Cs$_2$ZnI$_4$
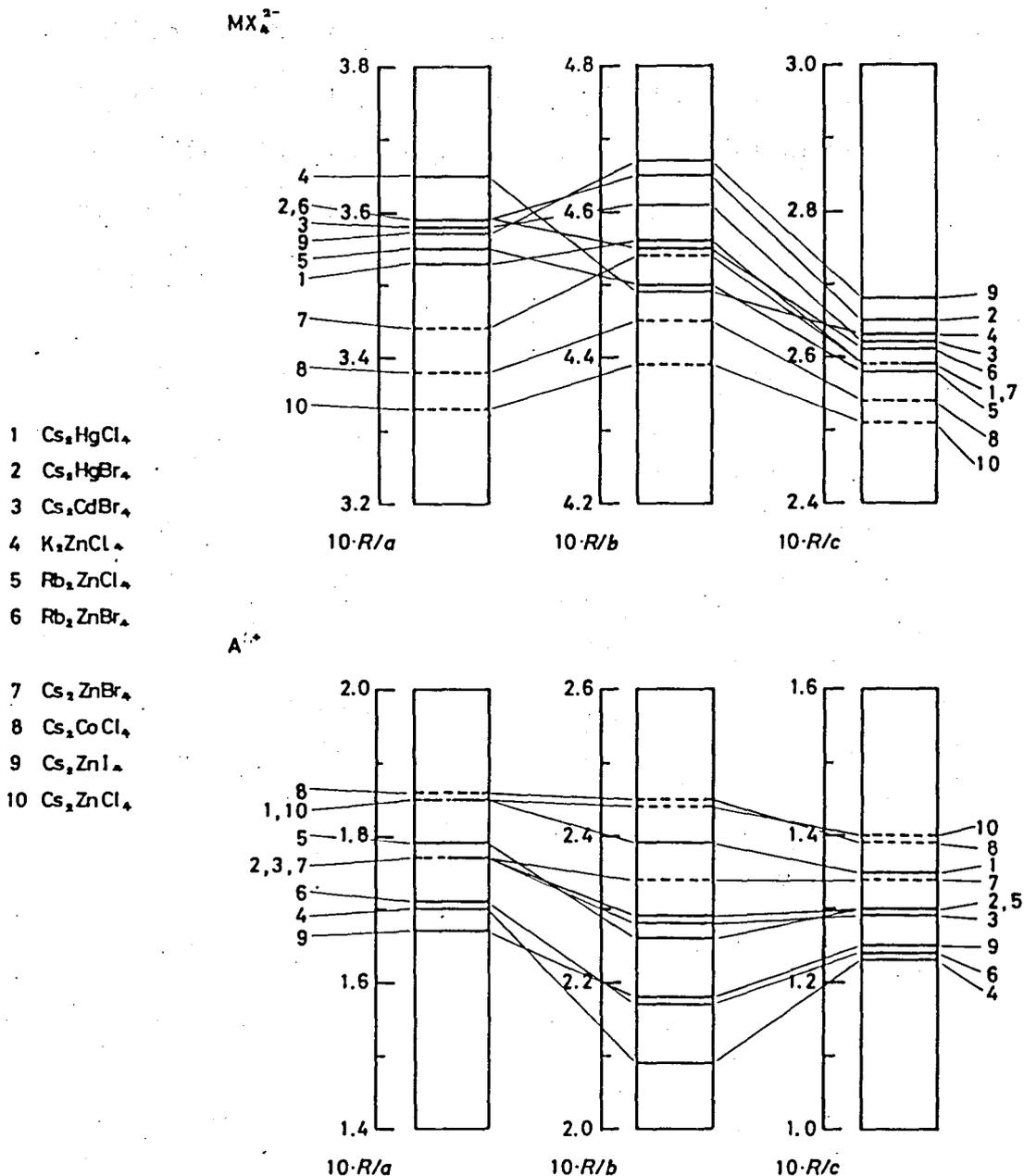
10 Cs$_2$ZnCl$_4$

A$^+$

Figure 6-3. Ratio of the radius of the complex anion [MX$_4$]$^{2-}$ and that of to the cation A$^+$ to the individual lattice constants in various compounds are shown in the upper and the lower figures, respectively. ⎯⎯ indicates a compound which has phase transition. and - - - indicates a compound which has no phase transition.

competing interactions (ANNNI model)[30] to interpret
the occurrence of various types of incommensurate
phases. The ANNNI model is shown in Figure 6-5. An
assembly of spins S which can assume the value +1 or -1
interact with one another through a ferromagnetic
nearest neighbour interaction J_1 in two or three
dimensions. In a particular direction, however, there
acts between two spins, in addition to J_1, an
antiferromagnetic next-nearest-neighbour interaction
J_2. The calculation of the phase diagram by Bak et al.
indicated that the competition between J_1 and J_2 works
to stabilize various structures.   The work of Bak et
al. therefore points out that highly anisotropic
interaction is important for the crystal to undergo an
incommensurate phase change, being consistent with the
present result. Using this conclusion the following two
deductions can be made.

1) One can predict the presence of some phase
transition in a compound with A_2BX_4 structure (Pnma) by
examining the relative size of the complex $[MX_4]^{2-}$
anion to its lattice parameter a. For compounds
Na_2ZnCl_4,[31] Na_2CoCl_4,[32] K_2CoCl_4,[13] K_2CoBr_4,[33]
Rb_2CoCl_4,[34] Rb_2CoBr_4,[33] Cs_2CoBr_4,[33] Cs_2CoI_4,[13]
which are space group Pnma, $R([MX_4]^{2-})/a$ is plotted in
Figure 6-5.

2) It is also predicted that compounds in which the
value of $R([MX_4]^{2-})/a$ is slightly samller than 0.35 is

(a)   (b)

Figure 6-4. ANNNI model for two dimensional (b) and three dimensional (a) lattices. J_0 and J_1 represent the nearest neighbor interactions and J_2 the next nearest neighbor interaction.

Figure 6-5. Ratio of the radius of the complex anion $[MX_4]^{2-}$ to the lattice constant (a) in various compounds. —— indicates a compound which is expected to have phase transition. and - - - indicates a compound which is expected to have no phase transition, - - - —— indicates the compound on the boader line.

a condidate which undergoes a phase transition at high pressure, because the ratio can be increased up to >0.35 by pressure. If the complete crystal structure data are not available on some particular substances the quantity $R([MX_4]^{2-})/R(A^+)$ as shown in Figure 6-6 can be used to predict whether it undergoes any phase change or not. As an example $R([MX_4]^{2-})/R(A^+)$ is plotted in Figure 6-6 for various substances including compounds whose crystal structure are unknown. We can thus predict that Rb_2CoBR_4, Cs_2CoI_4, and Rb_2CoCl_4 have at least one phase trans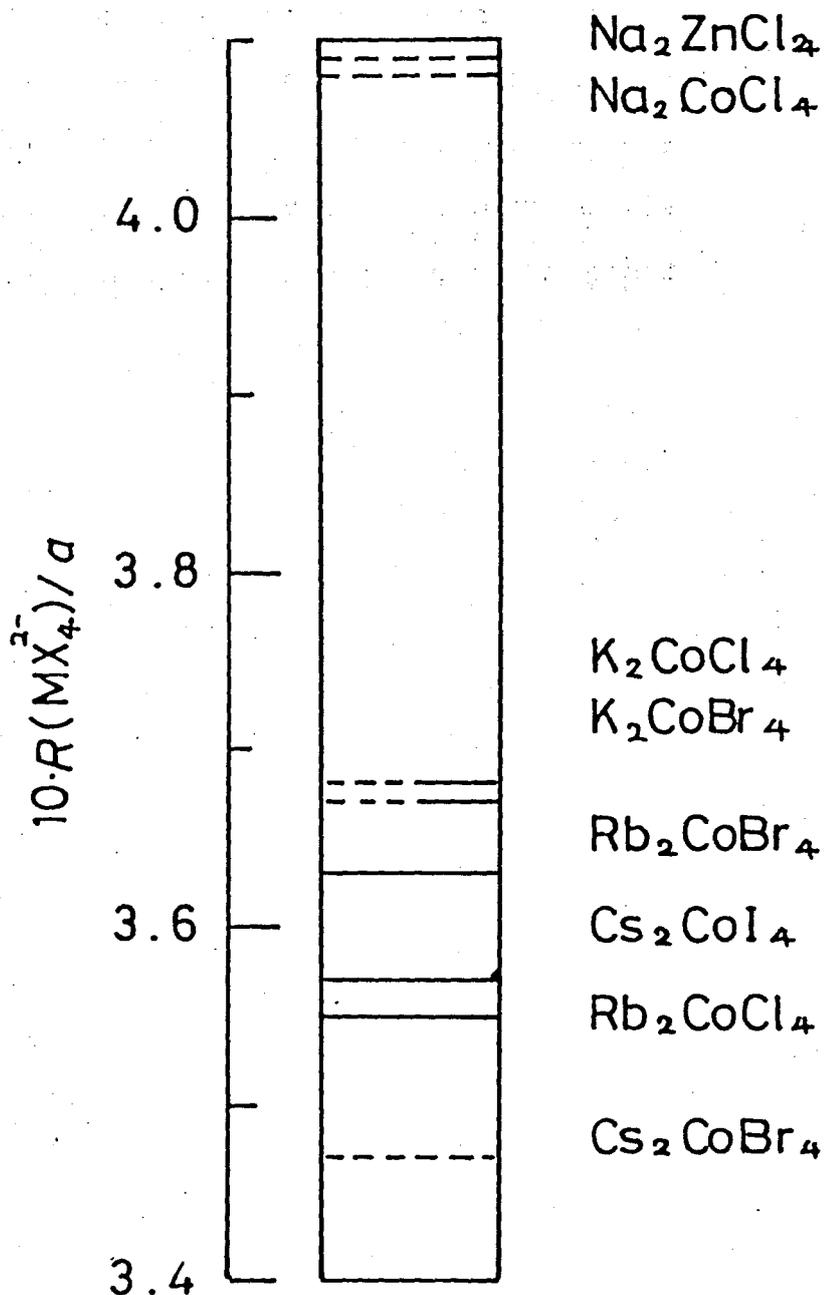ition below room temperature. In this way, we can interpret the fact that both Cs_2HgBr_4 and Cs_2CdBr_4 undergo successive phase transitions while Cs_2ZnBr_4 isomorphrous to the former two compounds does not exibit any phase change. The anisotropic interaction along the crystallographic a-axis in Cs_2ZnBr_4 is smaller than the crystal one representedby $R([MX_4]^{2-})/a = 0.35$ whereas in the former compounds a strong interaction along the a-axis drives these materials to undergo phase transitions on cooling.

Figure 6-6. Ratio of the radius of the complex anion $[MX_4]^{2-}$ to the radius of the cation A^+ in various compounds. ——— indicates a compound which is expected to have phase transition. and - - - indicates a compound which is expected to have no phase transition, - - ——— indicates the compound on the boader line.

References

1. M. Iizumi, J.D. Axe, G. Shirane, and K. Shimaoka, Phys. Rev., B15, 4392 (1977).

2. Y. Yamada, N. Hamaya, J Phys. Soc. Jpn., 52, 3466 (1983).

3. I.P. Aleksandrova, R. Blinc, B. Topic, S. Zumer, and A. Rigamonti, Phys. Status Solidi, (a)61, 95 (1980).

4. K. Gesi, and M. Iizumi, J. Phys. Soc. Jpn., 51, 1047 (1982); A.H. Moudden, F. Denoyer, M. Lambert, and W. Fitzgerald, Solid State Commun., 32, 933 (1979).

5. H. Cailleau, F. Moussa, and J. Mons, Solid State Commun., 31, 521 (1979).

6. G.K. Semine, I.M. Alymov, V.M. Bakhomov, and P.M. Fedorov, Izv. Akad. Nauk. SSSR, Ser. Fiz. 42, 2095 (1978).

7. D. Altermatt, H. Arend, A. Niggli, and W. Petter, Mat. Res. Bull., 14, 1391 (1979).

8. B. Morosin, and E.C. Lingafelter, Acta Cryst., 12, 744 (1959).

9. S. Plesko, R. Kind, and H. Arend, Phys. Status Solidi, (a)61, 87 (1980).

10. S. Plesko, R. Kind, and H. Arend, Ferroelectrics, 26, 703 (1980).

11. M.A. Porai-Koshits, Kristallografiya, 1, 291 (1956).

12. J.A. McGinnety, Inorg. Chem., 13, 1057 (1974).

13. Von H. Seifert, and L. Staudel, Z. Anorg. Allg.

    Chem., 429, 105 (1977).

14. W.J. Asker, D.E. Scaife, and J.A. Watts, Aust. J.

    Chem., 25, 2301 (1959).

15. T. Ueda, S. Iida, and H. Terauchi, J. Phys. Soc.

    Jpn., 51, 3953 (1982).

16. O.P. Lamba, M.B. Patel, S. Ram, Prem Chand, and

    H.D. Bist, Solid State Commun., 50, 321 (1984).

17. V.V. Petrov, V.G. Pitsyuga, V.A. Bogdanova,

    M.A. Bagina, and Yu Khalakhan, Fiz. Tverd. Tela.,

    25, 3465 (1983).

18. S.A. Linde, A. Ya Mikhailova, V.I. Pakhomov, and

    V.G. Shulliga, Koord. Khim., 9, 998 (1983).

19. I. Mekhail, and K. Peters, Acta Cryst., B35, 1200

    (1979).

20. F. Milia, R. Kind, and J. Slak, Phys. Rev., B27,

    6662 (1983).

21. M. Wada, A. Sawada, and Y. Ishibashi, J. Phys.

    Soc. Jpn., 47, 1185 (1979).

22. T. AtaKe, K. Nomoto, B.K. Chaudhuri, and H. Chihara,

    J. Chem. Thermodyn., 15, 339 (1983).

23. C.J. de Peter, Acta Cryst., B35, 299 (1979).

24, T.P. Melia, R. Merrifield, J. Chem. Soc. (A), 1259

    (1971).

25. D.E. Scaife, Aust. J. Chem., 24, 1315 (1971).

26. R.D. Shannon, and C.T. Prewitt, Acta Cryst., B25,

    925 (1969).

27. G.K. Semine, I.M. Alymov, V.M. Burbelo,
    V.I. Pakhomov, and P.M. Fedorov, Izv. Akad. Nauk.
    SSSR, Ser. Fiz. 42, 2095 (1978).

28. P. Bak, Phys. Rev., B21, 5297 (1980).

29. C.J.J. van Loon, and D. Visser, Acta Cryst., B33,
    188 (1977).

30. H.J. Seifert, and I. Al-Khudair, J. Inorg. Nucl.
    Chem., 37, 1625 (1975).

31. M. Amit, A. Horowitz, and J. Mokovsky, Israel J.
    Chem., 10, 715 (1972).

32. N. Krauzman, and J.P. Mathieu, C. R. Acad. Sci.,
    Ser. B272, 955 (1971).

33. C.J.J. van Loon, and D.J.W. Iido, Acta Cryst.,
    B31, 770 (1975).

34. S. Siegel, and, E. Gebert, Acta Cryst., 17, 790
    (1964).

```
10 ' NQR FID PROCESSING ROUTINE
20 CLEAR ,&H1C00
30 DEF SEG=&H1C00
40 WIDTH 80,25:CONSOLE 0,25,0,0:CLS 3
45 DD$=DATE$:TT$=TIME$
47 PRINT "***** Welcome to NQR FID PROCESSING ROUTINE *****"
50 INPUT "Counts of sampling points";CS
60 INPUT "Sampling interval/micro sec";SI:RES=1000/(CS*SI)
70 INPUT "Counts of accumulation";CA
80 INPUT "Registry number";REG
90 DIM XF(CS+137),YF(CS+137),ZF(CS+137)
100 INPUT "Frequency/MHz";FREQ
110 INPUT "Temperature/mV";TEMP
120 INPUT "Pulse separation";TAU,TAU$
130 GOSUB *DATAINPUT
140 GOSUB *OFFSETCORRECTION
150 INPUT "Do you need graphic FID display ?(Y or N)";A$
160 IF A$="N" GOTO 180
170 GOSUB *GRAPHICFIDDISPLAY
180 GOSUB *DATAREARRANGEMENT
190 INPUT "Do you need FID data display ?(Y or N)";A$
200 IF A$="N" GOTO 220
210 GOSUB *FIDDATADISPLAY
220 INPUT "Do you need FID data print-out ?(Y or N)";A$
230 IF A$="N" GOTO 250
240 GOSUB *FIDDATAPRINTOUT
250 INPUT "Do you need FID data file-out ?(Y or N)";A$
260 IF A$="N" GOTO 280
270 GOSUB *FIDDATAFILEOUT
280 INPUT "Do you need FFT ?(Y or N)";A$
290 IF A$="N" GOTO 440
300 GOSUB *FFT
310 GOSUB *PHASECORRECTION
320 INPUT "Do you need graphic SPECTRUM display ?(Y or N)";A$
330 IF A$="N" GOTO 350
340 GOSUB *GRAPHICSPECTRUMDISPLAY
350 INPUT "Do you need SPECTRUM data display ?(Y or N)";A$
360 IF A$="N" GOTO 380
370 GOSUB *SPECTRUMDATADISPLAY
380 INPUT "Do you need SPECTRUM data print-out ?(Y or N)";A$
390 IF A$="N" GOTO 410
400 GOSUB *SPECTRUMDATAPRINTOUT
410 INPUT "Do you need SPECTRUM data file-out ?(Y or N)";A$
420 IF A$="N" GOTO 440
430 GOSUB *SPECTRUMDATAFILEOUT
440 END
```

***** subroutine OFFSET CORRECTION *****

```
2990 '
3000 *OFFSETCORRECTION
3010 INPUT "First number of sampling point for offset correction(0-20
F:XOF=0
3020 FOR I=NOF TO CS-1:XOF=XOF+XF(I)/(CS-NOF):NEXT I
3030 FOR I=0 TO CS-1:XF(I)=XF(I)-XOF:NEXT I
3040 RETURN
```

***** subroutine GRAPHIC FID DISPLAY *****

```
3990 '
4000 *GRAPHICFIDDISPLAY
4010 SCREEN 2,0,0,0:CONSOLE 0,25,0,0:CLS 3
4020 INPUT "Initial and final number of sampling points for display(0
;NGDI1,NGDF1
4030 INPUT "Vertical scale";VS:CLS 1
4040 WINDOW(NGDI1,-100*VS)-(NGDF1,100*VS)
4050 VIEW(72,40)-(584,360)
4060 LINE(0,0)-(CS-1,0):LINE(0,100)-(0,-100)
4070 L1=((CS-1)/50)
4080 FOR L=1 TO L1:LINE(50*L,2)-(50*L,-2):NEXT L
4090 FOR I=0 TO CS-1:XP1=-100*XF(I):PSET(I,XP1):NEXT I:SCREEN 2,0,0,1
4091 LOCATE 0,0 :PRINT "FID of ";REG
4092 LOCATE 50,0 :PRINT "Date ";DD$
4094 LOCATE 50,1 :PRINT "Time ";TT$
4100 LOCATE 50,3 :PRINT "Frequency=";FREQ;"MHz"
4110 LOCATE 50,4 :PRINT "Tau=";TAU;TAU$
4120 LOCATE 50,5 :PRINT "Temperature=";TEMP;"mV"
4130 LOCATE 50,7 :PRINT "Sampling points=";CS
4140 LOCATE 50,8 :PRINT "Sampling interval=";SI;"micro S"
4150 LOCATE 50,9 :PRINT "Accumulation=";CA
4160 MI1=INT(NGDI1/50)+1:MF1=INT(NGDF1/50)
4170 FOR I=MI1 TO MF1
4180 XG=INT((I*50-NGDI1)*512/(NGDF1-NGDI1)):XGI=INT((XG+72)/8)
4190 LOCATE XGI-1,13:PRINT INT(I*50*SI)
4200 NEXT I
4210 LOCATE 73,12:PRINT "micro S":CONSOLE 23,2,0,0
4220 LOCATE 0,23:INPUT "Do you need more display ?(Y or N)";A$
4230 IF A$="N" GOTO 4250
4240 SCREEN 2,0,0,0:CLS 3:GOTO 4010
4250 CONSOLE 0,25,0,0:CLS 3
4260 RETURN
```

***** subroutine OFFSET CORRECTION *****

```
2990 '
3000 *OFFSETCORRECTION
3010 INPUT "First number of sampling point for offset correction(0-2047ma>
F:XOF=0
3020 FOR I=NOF TO CS-1:XOF=XOF+XF(I)/(CS-NOF):NEXT I
3030 FOR I=0 TO CS-1:XF(I)=XF(I)-XOF:NEXT I
3040 RETURN
```

***** subroutine GRAPHIC FID DISPLAY *****

```
3990 '
4000 *GRAPHICFIDDISPLAY
4010 SCREEN 2,0,0,0:CONSOLE 0,25,0,0:CLS 3
4020 INPUT "Initial and final number of sampling points for display(0-2047
;NGDI1,NGDF1
4030 INPUT "Vertical scale";VS:CLS 1
4040 WINDOW(NGDI1,-100*VS)-(NGDF1,100*VS)
4050 VIEW(72,40)-(584,360)
4060 LINE(0,0)-(CS-1,0):LINE(0,100)-(0,-100)
4070 L1=((CS-1)/50)
4080 FOR L=1 TO L1:LINE(50*L,2)-(50*L,-2):NEXT L
4090 FOR I=0 TO CS-1:XP1=-100*XF(I):PSET(I,XP1):NEXT I:SCREEN 2,0,0,1
4091 LOCATE 0,0 :PRINT "FID of ";REG
4092 LOCATE 50,0 :PRINT "Date ";DD$
4094 LOCATE 50,1 :PRINT "Time ";TT$
4100 LOCATE 50,3 :PRINT "Frequency=";FREQ;"MHz"
4110 LOCATE 50,4 :PRINT "Tau=";TAU;TAU$
4120 LOCATE 50,5 :PRINT "Temperature=";TEMP;"mV"
4130 LOCATE 50,7 :PRINT "Sampling points=";CS
4140 LOCATE 50,8 :PRINT "Sampling interval=";SI;"micro S"
4150 LOCATE 50,9 :PRINT "Accumulation=";CA
4160 MI1=INT(NGDI1/50)+1:MF1=INT(NGDF1/50)
4170 FOR I=MI1 TO MF1
4180 XG=INT((I*50-NGDI1)*512/(NGDF1-NGDI1)):XGI=INT((XG+72)/8)
4190 LOCATE XGI-1,13:PRINT INT(I*50*SI)
4200 NEXT I
4210 LOCATE 73,12:PRINT "micro S":CONSOLE 23,2,0,0
4220 LOCATE 0,23:INPUT "Do you need more display ?(Y or N)";A$
4230 IF A$="N" GOTO 4250
4240 SCREEN 2,0,0,0:CLS 3:GOTO 4010
4250 CONSOLE 0,25,0,0:CLS 3
4260 RETURN
```

***** subroutine DATA REARRANGEMENT *****

```
4990 '
5000 *DATAREARRANGEMENT
5010 INPUT "First number of sampling point,you need(0-2047max.)";NR
5020 FOR I=NR TO CS-1:XF(I-NR)=XF(I):NEXT I
5030 FOR I=CS-NR TO CS-1:XF(I)=0:NEXT I
5040 RETURN
```

***** subroutine FID DATA DISPLAY *****

```
5990 '
6000 *FIDDATADISPLAY
6010 CONSOLE 0,25,0,0:CLS 3
6020 INPUT "Initial and final number of sampling points for display(0-204'
     ;NDOI1,NDOF1
6030 J1=INT((NDOF1-NDOI1)/51):CLS 1
6040 PRINT "Registry number=";REG
6050 PRINT "  Frequency=";FREQ;"MHz";TAB(50);"Sampling interval=";SI;"poi₁
6060 PRINT "  Tau=";TAU;TAU$;TAB(50);"Sampling interval=";SI;"micro S"
6070 PRINT "  Temperature=";TEMP;"mV";TAB(50);"Accumulation=";CA
6080 CONSOLE 4,21,0,0
6090 FOR J=1 TO J1+1:LOCATE 0,4:PRINT " Page ";J
6100 PRINT TAB(2);"No.";TAB(7);"t/micro";TAB(15);"FID";TAB(29);"No.";TAB(∶
     micro";TAB(42);"FID";TAB(56);"No.";TAB(61);"t/micro";TAB(69);"FID"
6110 PRINT
6120 FOR I=0 TO 16:K=NDOI1+(J-1)*51+I
6130 PRINT TAB(2);K;TAB(7);K*SI;TAB(29);K+17;TAB(34);(K+17)*SI;TAB(56);K+∶
     61);(K+34)*SI
6140 LOCATE 15,I+7:PRINT USING "+#.###^^^^";XF(K)
6150 LOCATE 42,I+7:PRINT USING "+#.###^^^^";XF(K+17)
6160 LOCATE 69,I+7:PRINT USING "+#.###^^^^";XF(K+34)
6170 NEXT I
6180 INPUT Q:CLS 1
6190 NEXT J
6200 CONSOLE 0,25,0,0:CLS 1
6210 INPUT "Do you need more display ?(Y or N)";A$
6220 IF A$="Y" GOTO 6020
6230 CLS 1
6240 RETURN
```

***** subroutine FID DATA PRINT OUT *****

```
6990 '
7000 *FIDDATAPRINTOUT
7010 INPUT "Initial and final number of sampling points for print-out(0-2
)";NPOI1,NPOF1
7020 IF (NPOF1-NPOI1)<120 GOTO 7040
7030 I1=INT((NPOF1-NPOI1-120)/138)
7040 LPRINT:LPRINT:LPRINT:LPRINT:LPRINT "************** FID **********
PRINT:LPRINT "Date ";DD$
7045 LPRINT "Time ";TT$:LPRINT
7050 LPRINT "Registry No.=";REG
7060 LPRINT "   Frequency=";FREQ;"MHz";TAB(50);"Sampling points=";CS;"poin
7070 LPRINT "   Tau=";TAU;TAU$;TAB(50);"Sampling interval=";SI;"micro S"
7080 LPRINT "   Temperature=";TEMP;"mV";TAB(50);"Accumulation=";CA
7090 LPRINT :LPRINT
7100 LPRINT " Page 1"
7110 LPRINT TAB(2);"No.";TAB(7);"t/micro";TAB(15);"FID";TAB(29);"No.";TAB
/micro";TAB(42);"FID";TAB(56);"No.";TAB(61);"t/micro";TAB(69);"FID"
7120 LPRINT
7130 FOR I=0 TO 39
7140 K=NPOI1+I
7150 LPRINT USING "######";K;
7160 LPRINT USING "######.#";K*SI;
7170 LPRINT " ";
7180 LPRINT USING "+#.###^^^^";XF(K);
7190 LPRINT USING "########";K+40;
7200 LPRINT USING "######.#";(K+40)*SI;
7210 LPRINT " ";
7220 LPRINT USING "+#.###^^^^";XF(K+40);
7230 LPRINT USING "########";K+80;
7240 LPRINT USING "######.#";(K+80)*SI;
7250 LPRINT " ";
7260 LPRINT USING "+#.###^^^^";XF(K+80)
7270 NEXT I
7275 LPRINT:LPRINT:LPRINT:LPRINT:LPRINT:LPRINT:LPRINT:LPRINT
7280 IF (NPOF1-NPOI1)<120 GOTO 7490 7500
7290 FOR J=1 TO I1+1
7300 LPRINT:LPRINT:LPRINT:LPRINT:LPRINT:LPRINT:LPRINT:LPRINT:LPRINT
7310 LPRINT " Page ";J+1
7320 LPRINT TAB(2);"No.";TAB(7);"t/micro";TAB(15);"FID";TAB(29);"No.";TAB(
/micro";TAB(42);"FID";TAB(56);"No.";TAB(61);"t/micro";TAB(69);"FID"
7330 LPRINT
7340 FOR I=0 TO 45:K=NPOI1+120+(J-1)*138+I
7350 LPRINT USING "######";K;
7360 LPRINT USING "######.#";K*SI;
7370 LPRINT " ";
7380 LPRINT USING "+#.###^^^^";XF(K);
7390 LPRINT USING "########";K+40;
7400 LPRINT USING "######.#";(K+40)*SI;
```

```
7410 LPRINT " ";
7420 LPRINT USING "+#.###^^^^";XF(K+40);
7430 LPRINT USING "########";K+80;
7440 LPRINT USING "######.#";(K+80)*SI;
7450 LPRINT " ";
7460 LPRINT USING "+#.###^^^^";XF(K+80)
7470 NEXT I
7480 LPRINT:LPRINT:LPRINT:LPRINT:LPRINT:LPRINT:LPRINT:LPRINT
7490 NEXT J
7500 INPUT "Do you need more print-out ?(Y or N)";A$
7510 IF A$="Y" GOTO 7010
7520 RETURN
```

***** subroutine FID DATA FILE OUT *****

```
7990 '
8000 *FIDDATAFILEOUT
8010 INPUT "Is this the first FID data for this file ?(Y or N)";A$
8020 IF A$="N" GOTO 8040
8030 OPEN "2:FID"+STR$(REG) FOR OUTPUT AS #2:GOTO 8050
8040 OPEN "2:FID"+STR$(REG) FOR APPEND AS #2
8050 WRITE #2,DD$,TT$,REG,FREQ,TAU,TAU$,TEMP,CS,SI,CA
8060 FOR I=0 TO CS-1:WRITE #2,XF(I):NEXT I
8070 CLOSE #2
8080 RETURN
```

***** subroutine FFT *****

```
8990 '
9000 *FFT
9005 M=LOG(CS)/LOG(2)
9010 DIM S(CS/2),C(CS/2)
9020 A=0:B=3.14159*2/CS
9030 FOR I=0 TO CS/2:S(I)=SIN(A):C(I)=COS(A):A=A+B:NEXT I
9040 L=CS:H=1
9050 FOR G=1 TO M:L=L/2:K=0
9060 FOR Q=1 TO H:P=0
9070 FOR I=K TO L+K-1:J=I+L
9080 A=XF(I)-XF(J):B=YF(I)-YF(J)
9090 XF(I)=XF(I)+XF(J):YF(I)=YF(I)+YF(J)
9100 IF P=0 THEN XF(J)=A:YF(J)=B:GOTO 9120
9110 XF(J)=A*C(P)+B*S(P):YF(J)=B*C(P)-A*S(P)
9120 P=P+H:NEXT I
9130 K=K+L+L:NEXT Q
9140 H=H+H:NEXT G
9150 J=CS/2
9160 FOR I=1 TO CS-1:K=CS
9170 IF J<I THEN SWAP XF(I),XF(J):SWAP YF(I),YF(J)
9180 K=K/2:IF J>=K THEN J=J-K:GOTO 9180
9190 J=J+K
9200 NEXT I
9210 FOR I=0 TO CS-1:XF(I)=XF(I)/CS:YF(I)=YF(I)/CS:NEXT I
9220 RETURN
```

***** subroutine GRAPHIC SPECTRUM DISPLAY *****

```
9990 '
10000 *GRAPHICSPECTRUMDISPLAY
10010 FOR I=0 TO 2:SCREEN 2,0,I,0:CLS 3:NEXT I:CONSOLE 0,25,0,0:CLS 1
10015 PRINT "1-ABSORPTION 2-DISPERSION 3-ABSORPTION+DISPERSION 4-AMPLITUDE"
10016 PRINT "5-ABSORPTION+AMPLITUDE 6-DISPERSION+AMPLITUDE"
10017 PRINT "7-ABSORPTION+DISPERSION+AMPLITUDE 8-NOTHING"
10020 INPUT "Which page do you want to display ?(1-8)";P
10030 INPUT "Initial and final number of sampling points for display";NGDI2,NGI
2
10040 INPUT "Vertical scale";VS:CLS 1
10080 L2=INT((CS-1)/50)
10100 SCREEN 2,0,0,0:WINDOW(NGDI2,-100*VS)-(NGDF2,100*VS):VIEW(72,40)-(584,360)
10105 LINE(0,0)-(CS-1,0):LINE(0,100)-(0,-100):FOR L=0 TO L2:LINE(50*L,2)-(50*L,
2):NEXT L
10110 FOR I=0 TO CS-1:XP2=-1000*XF(I):PSET(I,XP2):NEXT I
10120 SCREEN 2,0,1,0:WINDOW(NGDI2,-100*VS)-(NGDF2,100*VS):VIEW(72,40)-(584,360)
10125 LINE(0,0)-(CS-1,0):LINE(0,100)-(0,-100):FOR L=0 TO L2:LINE(50*L,2)-(50*L,
2):NEXT L
10130 FOR I=0 TO CS-1:YP2=-1000*YF(I):PSET(I,YP2):NEXT I
10140 SCREEN 2,0,2,0:WINDOW(NGDI2,-100*VS)-(NGDF2,100*VS):VIEW(72,40)-(584,360)
10145 LINE(0,0)-(CS-1,0):LINE(0,100)-(0,-100):FOR L=0 TO L2:LINE(50*L,2)-(50*L,
2):NEXT L
10150 FOR I=0 TO CS-1:ZP2=-1000*ZF(I):PSET(I,ZP2):NEXT I:SCREEN 2,0, ,P
10151 LOCATE 0,0 :PRINT "SPECTRUM of ";REG
10152 ON P GOTO 10154,10155,10156,10157,10158,10159,10160,10161
10153 LOCATE 3,1:PRINT "            ":GOTO 10170
10154 LOCATE 3,1:PRINT "(ABSORPTION)":GOTO 10170
10155 LOCATE 3,1:PRINT "(DISPERSION)":GOTO 10170
10156 LOCATE 3,1:PRINT "(ABSORPTION+DISPERSION)":GOTO 10170
10157 LOCATE 3,1:PRINT "(AMPLITUDE)":GOTO 10170
10158 LOCATE 3,1:PRINT "(ABSORPTION+AMPLITUDE)":GOTO 10170
10159 LOCATE 3,1:PRINT "(DISPERSION+AMPLITUDE)":GOTO 10170
10160 LOCATE 3,1:PRINT "(ABSORPTION+DISPERSION+AMPLITUDE)":GOTO 10170
10161 LOCATE 3,1:PRINT "            ":GOTO 10170
10170 LOCATE 50,4 :PRINT "Tau=";TAU;TAU$
10175 LOCATE 50,0 :PRINT "Date ";DD$
10180 LOCATE 50,1 :PRINT "Time ";TT$
10185 LOCATE 50,3 :PRINT "Frequency=";FREQ;"MHz"
10190 LOCATE 50,4 :PRINT "Tau=";TAU;TAU$
10195 LOCATE 50,5 :PRINT "Temperature=";TEMP;"mV"
10200 LOCATE 50,7 :PRINT "Sampling points=";CS
10205 LOCATE 50,8 :PRINT "Resolution=";RES;"kHz"
10210 LOCATE 50,9 :PRINT "Accumulation=";CA
10220 MI2=INT(NGDI2/50)+1:MF2=INT(NGDF2/50)
10230 FOR I=MI2 TO MF2
10240 XG=INT((I*50-NGDI2)*512/(NGDF2-NGDI2)):XGI=INT((XG+72)/8)
10250 LOCATE XGI-1,13:PRINT INT(I*50*RES)
10260 NEXT I
10270 LOCATE 73,12:PRINT "kHz":CONSOLE 24,1,0,0
10280 LOCATE 0,24:INPUT "Do you need more display ?(Y or N)";A$
10290 IF A$="N" GOTO 10310
10300 GOTO 10010
10310 CONSOLE 0,25,0,0:FOR I=0 TO 2:SCREEN 2,0,I,0:CLS 3:NEXT I
10320 RETURN
```

***** subroutine PHASE CORRECTION *****

```
10990 '
11000 *PHASECORRECTION
11010 FOR I=0 TO CS-1:ZF(I)=SQR(XF(I)^2+YF(I)^2):NEXT I
11020 RETURN
```

***** subroutine SPECTRUM DATA DISPLAY *****

```
11990 '
12000 *SPECTRUMDATADISPLAY
12010 CONSOLE 0,25,0,0:CLS 3
12020 INPUT "Initial and final number of sampling points for display(0-2047m
";NDOI2,NDOF2
12030 J2=INT((NDOF2-NDOI2)/34):CLS 1
12040 PRINT "Registry No.=";REG
12050 PRINT "  Frequency=";FREQ;"MHz";TAB(50);"Sampling points=";CS;"points"
12060 PRINT "  Tau=";TAU;TAU$;TAB(50);"resolution=";RES;"kHz"
12070 PRINT "  Temperature=";TEMP;"mV";TAB(50);"Accumulation=";CA
12080 CONSOLE 4,21,0,0
12090 FOR J=1 TO J2+1:LOCATE 0,4:PRINT " page ";J
12100 PRINT TAB(2);"f/kHz";TAB(9);"Abs.";TAB(19);"Dis.";TAB(29);"Amp.";TAB(4
f/kHz";TAB(49);"Abs.";TAB(59);"Dis.";TAB(69);"Amp."
12110 PRINT
12120 FOR I=0 TO 16:K=NDOI2+(J-1)*34+I
12130 LOCATE 2,I+7:PRINT USING "####.#";K*RES
12140 LOCATE 42,I+7:PRINT USING "####.#";(K+17)*RES
12150 LOCATE 9,I+7:PRINT USING "+#.##^^^^";XF(K)
12160 LOCATE 19,I+7:PRINT USING "+#.##^^^^";YF(K)
12170 LOCATE 29,I+7:PRINT USING "+#.##^^^^";ZF(K)
12180 LOCATE 49,I+7:PRINT USING "+#.##^^^^";XF(K+17)
12190 LOCATE 59,I+7:PRINT USING "+#.##^^^^";YF(K+17)
12200 LOCATE 69,I+7:PRINT USING "+#.##^^^^";ZF(K+17)
12210 NEXT I
12220 INPUT Q:CLS 1
12230 NEXT J
12240 CONSOLE 0,25,0,0:CLS 1
12250 INPUT "Do you need more display ?(Y or N)";A$
12260 IF A$="Y" GOTO 12020
12270 CLS 1
12280 RETURN
```

***** subroutine SPECTRUM DATA PRINT OUT *****


```
12990 '
13000 *SPECTRUMDATAPRINTOUT
13010 INPUT "Initial and final number of sampling points for print-out(0-2
.)";NPOI2,NPOF2
13020 IF (NPOF2-NPOI2)<80 GOTO 13040
13030 I2=INT((NPOF2-NPOI2-80)/92)
13040 LPRINT:LPRINT:LPRINT:LPRINT:LPRINT "************** SPECTRUM ******
**":LPRINT:LPRINT "Date ";DD$
13045 LPRINT "Time ";TT$:LPRINT
13050 LPRINT "Regisrty No.=";REG
13060 LPRINT "  Frequency=";FREQ;"MHz";TAB(50);"Sampling points=";CS;"poir
13070 LPRINT "  Tau=";TAU;TAU$;TAB(50);"Resolution=";RES;"kHz"
13080 LPRINT "  Temperature=";TEMP;"mV";TAB(50);"Accumulation=";CA
13090 LPRINT :LPRINT
13100 LPRINT " Page 1"
13110 LPRINT TAB(2);"f/kHz";TAB(9);"Abs.";TAB(19);"Dis.";TAB(29);"Amp.";TA
"f/kHz";TAB(49);"Abs.";TAB(59);"Dis.";TAB(69);"Amp."
13120 LPRINT
13130 FOR I=0 TO 39:K=NPOI2+I
13140 LPRINT USING "######.#";K*RES;
13150 LPRINT " ";
13160 LPRINT USING "+#.##^^^^";XF(K);
13170 LPRINT " ";
13180 LPRINT USING "+#.##^^^^";YF(K);
13190 LPRINT " ";
13200 LPRINT USING "+#.##^^^^";ZF(K);
13210 LPRINT USING "########.#";(K+40)*RES;
13220 LPRINT " ";
13230 LPRINT USING "+#.##^^^^";XF(K+40);
13240 LPRINT " ";
13250 LPRINT USING "+#.##^^^^";YF(K+40);
13260 LPRINT " ";
13270 LPRINT USING "+#.##^^^^";ZF(K+40)
13280 NEXT I
13285 LPRINT:LPRINT:LPRINT:LPRINT:LPRINT:LPRINT:LPRINT:LPRINT
13290 IF (NPOF2-NPOI2)<120 GOTO 13528 13530
13300 FOR J=1 TO I2+1
13310 LPRINT:LPRINT:LPRINT:LPRINT:LPRINT:LPRINT:LPRINT:LPRINT:LPRINT
13320 LPRINT " Page ";J+1
13330 LPRINT TAB(2);"f/kHz";TAB(8);"Abs.";TAB(18);"Dis.";TAB(28);"Amp.";TA
"f/kHz";TAB(47);"Abs.";TAB(57);"Dis.";TAB(67);"Amp."
13340 LPRINT
13350 FOR I=0 TO 45:K=NPOI2+80+(J-1)*92+I
13360 LPRINT USING "######.#";K*RES;
13370 LPRINT " ";
13380 LPRINT USING "+#.##^^^^";XF(K);
13390 LPRINT " ";
13400 LPRINT USING "+#.##^^^^";YF(K);
```

```
13410 LPRINT " ";
13420 LPRINT USING "+#.##^^^^";ZF(K);
13430 LPRINT USING "########.#";(K+46)*RES;
13440 LPRINT " ";
13450 LPRINT USING "+#.##^^^^";XF(K+46);
13460 LPRINT " ";
13470 LPRINT USING "+#.##^^^^";YF(K+46);
13480 LPRINT " ";
13490 LPRINT USING "+#.##^^^^";ZF(K+46)
13500 NEXT I
13510 LPRINT:LPRINT:LPRINT:LPRINT:LPRINT:LPRINT:LPRINT:LPRINT
13520 NEXT J
13530 INPUT "Do you need more print-out ?(Y or N)";A$
13540 IF A$="Y" GOTO 13010
13550 RETURN
```

***** subroutine SPECTRUM DATA FILE OUT *****


```
13990 '
14000 *SPECTRUMDATAFILEOUT
14010 INPUT "Is this the first SPECTRUM for this file ?(Y or N)";A$
14020 IF A$="N" GOTO 14040
14030 OPEN "2:SPE"+STR$(REG) FOR OUTPUT AS #2:GOTO 14050
14040 OPEN "2:SPE"+STR$(REG) FOR APPEND AS #2
14050 WRITE #2,DD$,TT$,REG,FREQ,TAU,TAU$,TEMP,CS,SI,CA
14060 FOR I=0 TO CS-1:WRITE #2,XF(I),YF(I),ZF(I):NEXT I
14070 CLOSE #2
14080 RETURN
```

***** subroutine DATA INPUT *****

```
14990 '
15000 'DATAINPUT
15010 '                              *** DATA SAMPLING PROGRAM BY ASM ***
15020 '
15030 DEF SEG=&H1D00
15040 '
15050 INPUT "BIOMATION or KAWASAKI (B or K)";B$: IF B$="B" THEN GOTO 15070
15055 INPUT "ADD Count of KAWASAKI AVERAGER";CAA:CAB=CA:CA=CA*CAA
15060 NSAMP=1024: POKE &H0,&H1: GOTO 15080
15070 NSAMP=2048: POKE &H0,&H0:CAB=CA : CAA=1
15080 DEF SEG=&H1C00
15090 ASM=&H0
15100 RESTORE 15255
15110 FOR I=&H0 TO &HE9: READ DAT: POKE I,DAT : NEXT I
15120 '
15130 IACCUM=0
15140 DEF USR=&H100
15150 RESTORE 16340
15160 FOR I=&H100 TO &H100+&H25: READ DAT1: POKE I,DAT1: NEXT I
15170 LOCATE 2,15:PRINT "Final Count   Now":LOCATE 2,16:PRINT CA
15175 LOCATE 2,18:PRINT "Start Time   Now":LOCATE 2,19:PRINT TIME$
15180 CALL ASM
15190 '                              *** DATA TRANSFER FROM ASM TO BASIC ***
15200 FOR I=0 TO CS-1: X=USR(0): XF(I)=XF(I)+X: NEXT I
15210 '
15220 IACCUM=IACCUM+1:LOCATE 16,16:PRINT IACCUM*CAA:LOCATE 16,19:PRINT TI
     IACCUM < CAB THEN 15180
15230 FOR I=0 TO CS-1: XF(I)=XF(I)/CAB:NEXT I
15240 RETURN
15250 ' ***** MACHINE LANGUAGE PROGRAM *****   DATA INITIALIZE
15255 DATA &H50, &H51, &H52, &H56, &H1E, &H53, &H90
15260 DATA &HB8, &H00, &H1D
15265 DATA &H8E, &HD8
15270 DATA &HB8, &H10 ,&H00
15275 DATA &HA3, &H04 ,&H00
15280 DATA &HBB, &H10, &H00
15290 DATA &HB8, &H00, &H00
15300 DATA &H89, &H07
15310 DATA &H83, &HC3, &H02
15320 DATA &H81, &HFB, &H0A, &H10
15330 DATA &H77, &HF5
15340 DATA &HA0, &H00, &H00
15350 DATA &H3C, &H01
15360 DATA &H74, &H4D
15370 DATA &H90
15380 DATA &HBB, &H02, &H00
15390 DATA &HC7, &H07, &H00, &H08
15400 DATA &H90
```

```
15410 DATA &HBA, &HD1, &H00
15420 DATA &HB8, &H02, &H00
15430 DATA &HEF
15440 DATA &HB1, &H10
15450 DATA &HFE, &HC9
15460 DATA &H75, &HFC
15470 DATA &HB8, &H00, &H00
15480 DATA &HEF
15490 DATA &H90
15500 DATA &HB1, &H08
15510 DATA &HED
15520 DATA &H20, &HC8
15530 DATA &H3C, &H08
15540 DATA &H75, &HF9
15550 DATA &H90
15560 DATA &HED
15570 DATA &H20, &HC8
15580 DATA &H3C, &H08
15590 DATA &H74, &HF9
15600 DATA &HB9, &H20, &H00
15610 DATA &H49
15620 DATA &H75, &HFD
15630 DATA &H90
15640 DATA &HB8, &H10, &H00
15650 DATA &HB1, &H01
15660 DATA &HEF
15670 DATA &H90
15680 DATA &HED
15690 DATA &H20, &HC8
15700 DATA &H3C, &H01
15710 DATA &H75, &HF9
15720 DATA &HB8, &H10, &H00
15730 DATA &HBA, &HD0, &H00
15740 DATA &HEF
15745 DATA &HE9, &H42, &H00
15750 DATA &H90
15760 DATA &H90
15770 DATA &HBB, &H02, &H00
15772 DATA &HC7, &H07, &H00, &H04
15774 DATA &H90
15776 DATA &HBA, &HD1, &H00
15778 DATA &HB8, &H02, &H00
15780 DATA &HEF
15790 DATA &HB1, &H10
15800 DATA &HFE, &HC9
15810 DATA &H75, &HFC
15820 DATA &H90
15830 DATA &HB8, &H00, &H00
15840 DATA &HEF
15850 DATA &H90
15855 DATA &H90
15860 DATA &HB1, &H08
```

```
15870 DATA &HED
15880 DATA &H20, &HC8
15890 DATA &H3C, &H08
15900 DATA &H75, &HF9
15910 DATA &HED
15920 DATA &H20, &HC8
15930 DATA &H3C, &H08
15940 DATA &H74, &HF9
15950 DATA &HB8, &H10, &H00
15960 DATA &HEF
15970 DATA &HBA, &HD0, &H00
15980 DATA &HEF
15990 DATA &H90
16000 DATA &H90
16010 DATA &HB8, &H18, &H00
16020 DATA &HEF
16030 DATA &H90
16040 DATA &H90
16050 DATA &HB8, &H10, &H00
16070 DATA &HEF
16080 DATA &H90
16090 DATA &H8B, &H0E, &H02, &H00
16100 DATA &HBB, &H10, &H00
16110 DATA &HED
16120 DATA &H88, &H07
16130 DATA &H83, &HC3, &H02
16140 DATA &HB8, &H11, &H00
16150 DATA &HEF
16160 DATA &H90
16170 DATA &HB8, &H10, &H00
16180 DATA &HEF
16190 DATA &H90
16200 DATA &H90
16210 DATA &H90
16220 DATA &H90
16230 DATA &H49
16240 DATA &H75, &HEA
16250 DATA &H90
16260 DATA &H90
16270 DATA &H90
16280 DATA &HB8, &H00, &H00
16290 DATA &HEF
16300 DATA &H90
16310 DATA &HB8, &H10, &H00
16320 DATA &HA3, &H04, &H00
16325 DATA &H5B, &H1F, &H5E, &H5A, &H59, &H58
16330 DATA &HCF
16340 DATA &H50
16350 DATA &H51
16360 DATA &H52
16370 DATA &H56
16380 DATA &H1E
```

```
16390 DATA &H53
16400 DATA &H90
16410 DATA &HB8,&H00,&H1D
16420 DATA &H8E,&HD8
16430 DATA &HA1,&H04,&H00
16440 DATA &H89,&HC1
16450 DATA &H83,&HC1,&H02
16460 DATA &HBB,&H04,&H00
16470 DATA &H89,&H0F
16480 DATA &H89,&HC3
16490 DATA &H8B,&H07
16500 DATA &H5B
16510 DATA &H1F
16520 DATA &H5E
16530 DATA &H89,&H07
16540 DATA &H5A
16550 DATA &H59
16560 DATA &H58
16570 DATA &HCF
```

Appendix 2 Molecular motion in $(CH_3NH_3)_2CdBr_4$

Tetrahalometallates (II) of the type $(C_nH_{2n+1}NH_3)_2MX_4$ (M=Mn, Fe, Cd, Cu, X=Cl, Br) exibit various structural phase transitions which have attracted considerable attention in recent years.[1] Of these $(C_3H_7NH_3)_2MnCl_4$ has a reentrant incommensurate phase.[2] $(CH_3NH_3)_2CdBr_4$ was recently pointed out to be a candidate of an incommensurate material.

According to an X-ray structure analysis[3] the space group of $(CH_3NH_3)_2CdBr_4$ is monoclinic $P2_1/c$, which is a subgroup of orthorhombic Pnma, and some disorder is present with respect to the positions of carbon and bromine atoms. Recently phase transitions were discovered by DSC at 167 K and 400 K, and their enthalpies of transitions being 3.0 kJ/mol and 1.1 kJ/mol, respectively.[4] These results suggest that this compound is a potential incommensurate material being derived from the A_2BX_4 type structure classified in Chapter 6.

Present NQR frequency measurements found no evidence of phase transition betwen 77 K and 300 K and no anomaly was observed at about 167 K. And my DTA experiment found also no evidence of phase transition between 77 K and 400 K. As was mentioned in Section 4-4 the NQR measurements revealed four crystallographically inequivalent bromine sites in agreement with the X-ray result.[3] The spin-lattice relaxation time of each of

two nuclear species ^{79}Br and ^{81}Br shortened drastically above 200 K, as was shown in Figures 1 and 2. The T_1's for v_3 and v_4, for example, can be reproduced by the following expressions:

$$T_1^{-1}(v_3, ^{79}Br)/ms^{-1} = 8.97 \times 10^{-6} \times T^2 + 9.91 \times 10^3 \cdot exp \ (-19.3 \ kJ \ mol^{-1}/RT) \quad (1)$$

$$T_1^{-1}(v_3, ^{81}Br)/ms^{-1} = 5.77 \times 10^{-6} \times T^2 + 1.95 \times 10^3 \cdot exp \ (-16.6 \ kJ/mol^{-1}/RT) \quad (2)$$

$$T_1^{-1}(v_4, ^{79}Br)/ms^{-1} = 1.52 \times 10^{-5} \times T^2 + 8.56 \times 10^4 \cdot exp \ (-23.1 \ kJ \ mol^{-1}/RT) \quad (3)$$

$$T_1^{-1}(v_4, ^{79}Br)/ms^{-1} = 1.02 \times 10^{-5} \times T^2 + 8.56 \times 10^4 \cdot exp \ (-23.1 \ kJ \ mol^{-1}/RT) \quad (4)$$

In each equation the first term assumes a T^2 dependence. This means that the librational motion of $[CdBr_4]^{2-}$ tetrahedron governs the relaxation rate below 200 K.[5] According to the theory of the magnetic relaxation the spin-lattice relaxation rate is expressed as

$$T_1^{-1} \propto (e^2 Q q)^2$$

when the nuclear quadrupole interaction governs the T_1 while

$$T_1^{-1} \propto (\gamma_i \gamma_j I(I+1))^2$$

when the dipolar interaction dominates the relaxation where γ_i and γ_j are the gyromagnetic ratio of the nuclear species i and j. Since the ^{79}Br and ^{81}Br nuclei are in the same environment, the ratio of the T_1 of these two nuclear species should be expressed as

$$\frac{T_1^{-1}(^{79}Br)}{T_1^{-1}(^{81}Br)} = \left(\frac{Q(^{79}Br)}{Q(^{81}Br)} \right)^2$$
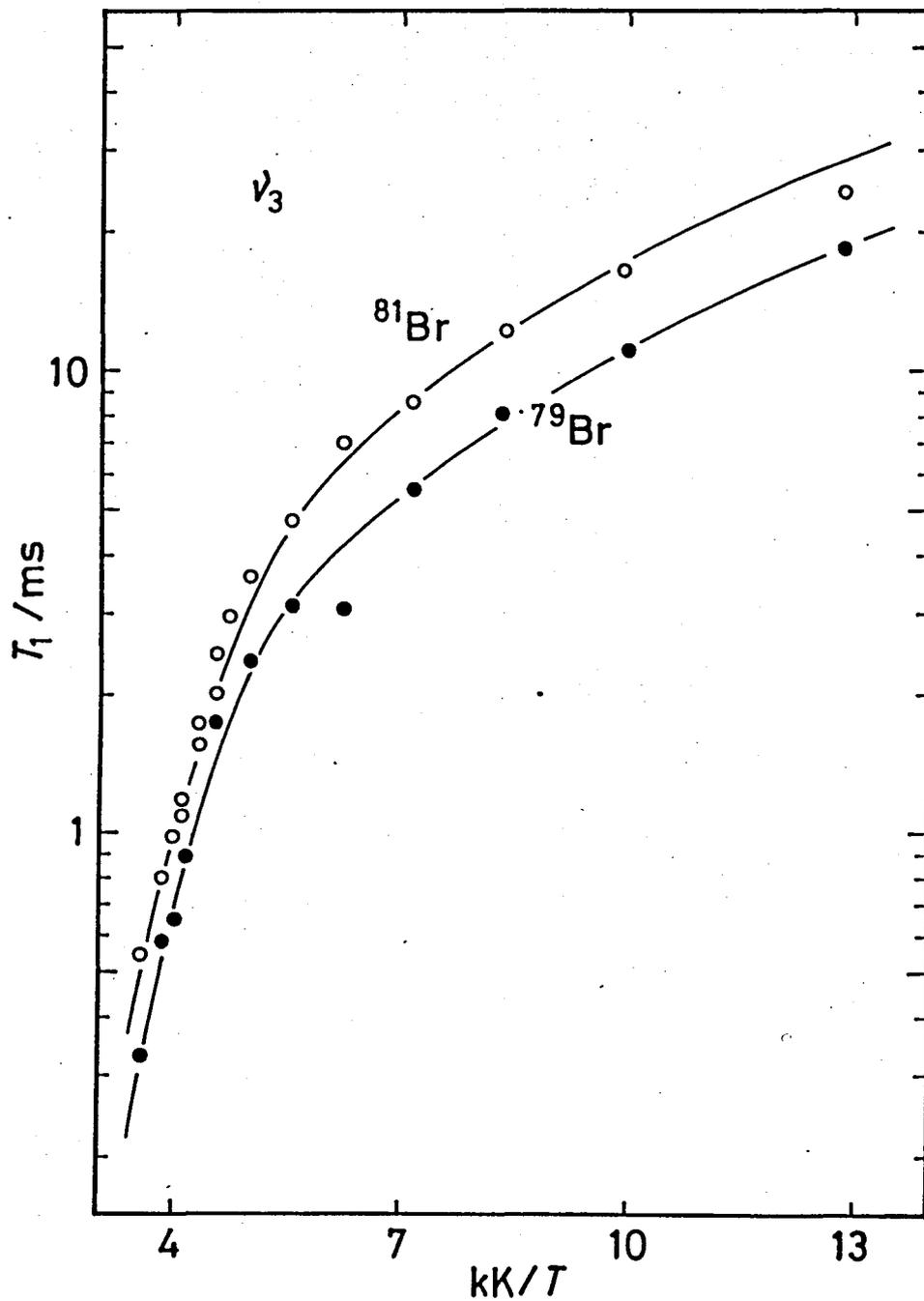
for the quadrupolar relaxation and

Figure A-1. Temperature dependence of ^{79}Br and ^{81}Br spin-lattice relaxation times for ν_3 of $(CH_3NH_3)_2CdBr_4$. Solid lines were T_1 calculated from Equation A-1 and A-2.
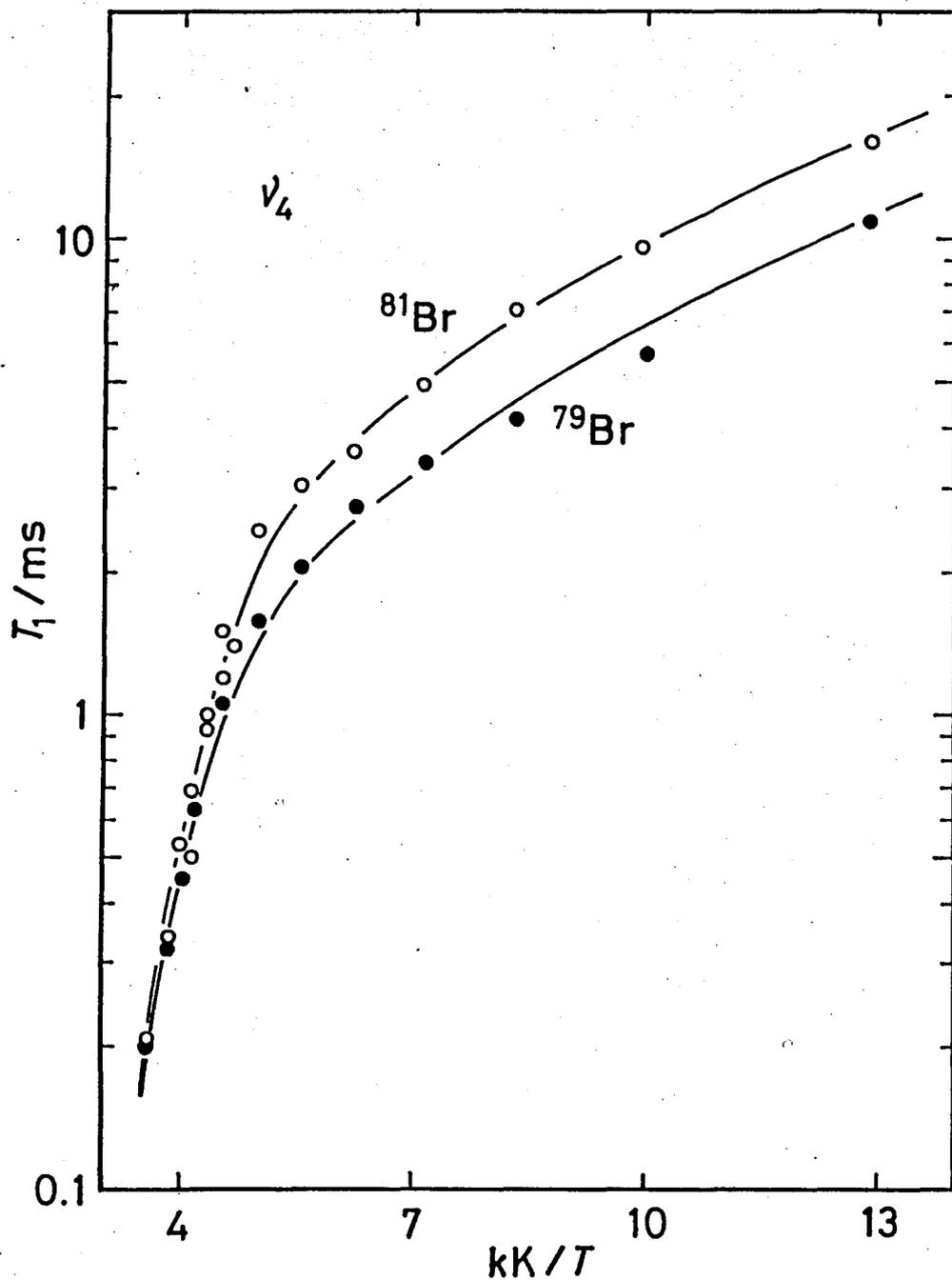
Figure A-2. Temperature dependence of ^{79}Br and ^{81}Br spin-lattice relaxation times for v_4 of $(CH_3NH_3)_2CdBr_4$. Solid lines were T_1 calculated from Equation A-3 and A-4.

$$\frac{T_1^{-1}(^{79}Br)}{T_1^{-1}(^{81}Br)} = \left(\frac{\sigma(^{79}Br)}{\sigma(^{81}Br)}\right)^2$$

for the dipolar relaxation. For the ν_3 and ν_4 lines, $T_1^{-1}(^{79}Br)/T_1^{-1}(^{81}Br)$ are equal to 1.55 and 1.49, respectively in agreement wih 1.433 of the square of the quadrupole moments. In the case of dipolar interaction $T_1^{-1}(^{79}Br)/T_1^{-1}(^{81}Br)$ is expected to be 0.59 inconsistent with the present results. Therefore, in the low temperature region below 200 K the relaxation is mainly caused by the modulation of the quadrupole interaction due to the librational motions of $[CdBr_4]^{2-}$ tetrahedron.[5] The excess relaxation rate above 200 K is plotted in Figures 3 and 4 for the ν_3 and ν_4 lines, respectively. From these plots the activation energy was determined to be 23.1 kJ/mol for ν_4. For ν_3 somewhat large scatter of T_1 values introduces a larger experimental error in the activation energy which, however, lies between 16.6 and 19.3 kJ/mol in agreement with that for the ν_4 line. For ν_1 and ν_2 the experimental error was large so that their T_1's were not used to determine the activation parameters. The activation energy of 20 ± 3 kJ/mol is interpreted in two ways. First is the reorientation of $[CdBr_4]^{2-}$ tetrahedron. The second is the N - H --- Br hydrogen bond switching by the reorientation of cation. The observed activation energy seems to be fairly small for the first case.

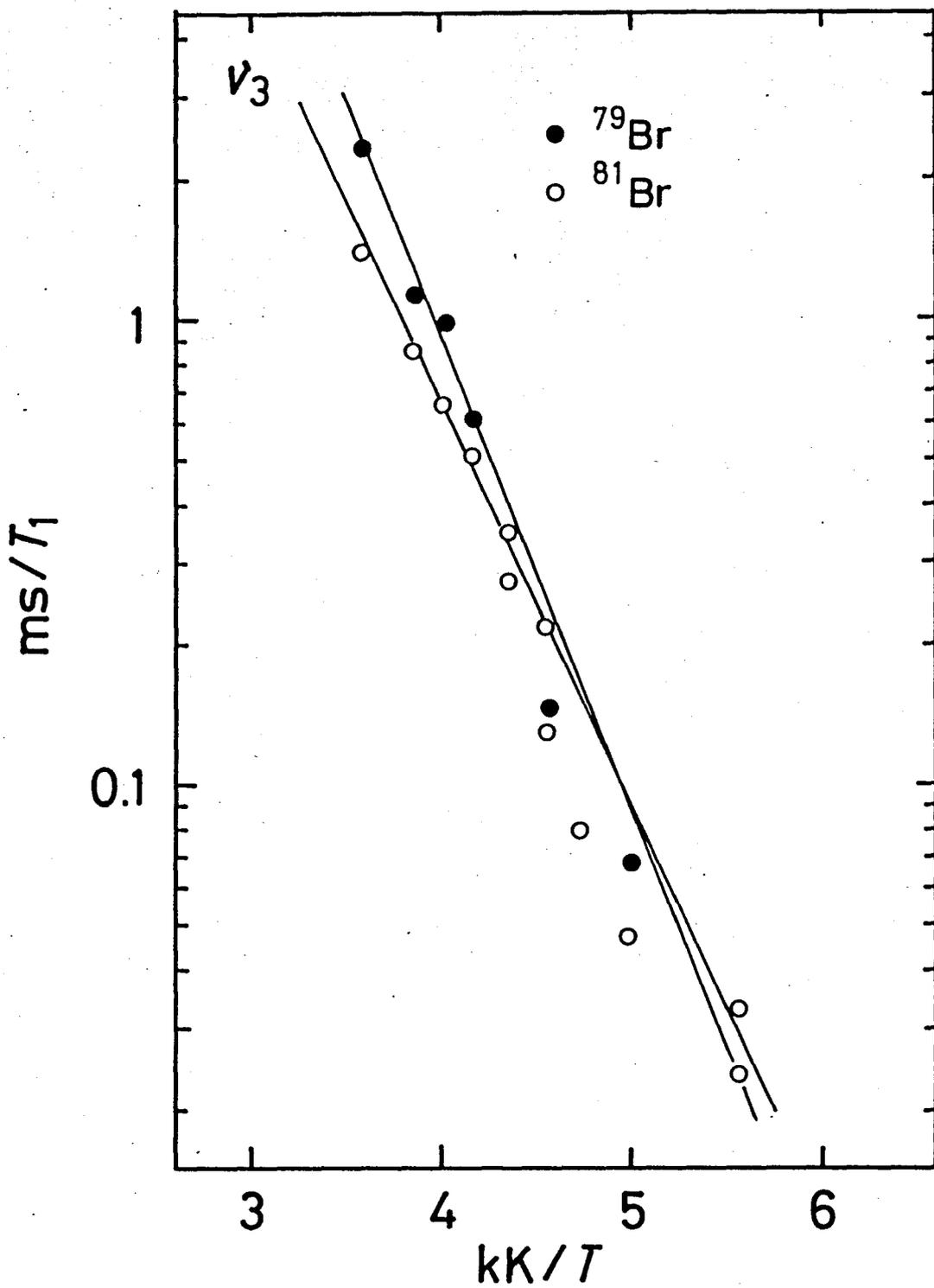The four resonance frequencies in $(CH_3NH_3)_2CdBr_4$

Figure A-3. Relaxation rate for v_3 line deduced by removing the librational contribution.
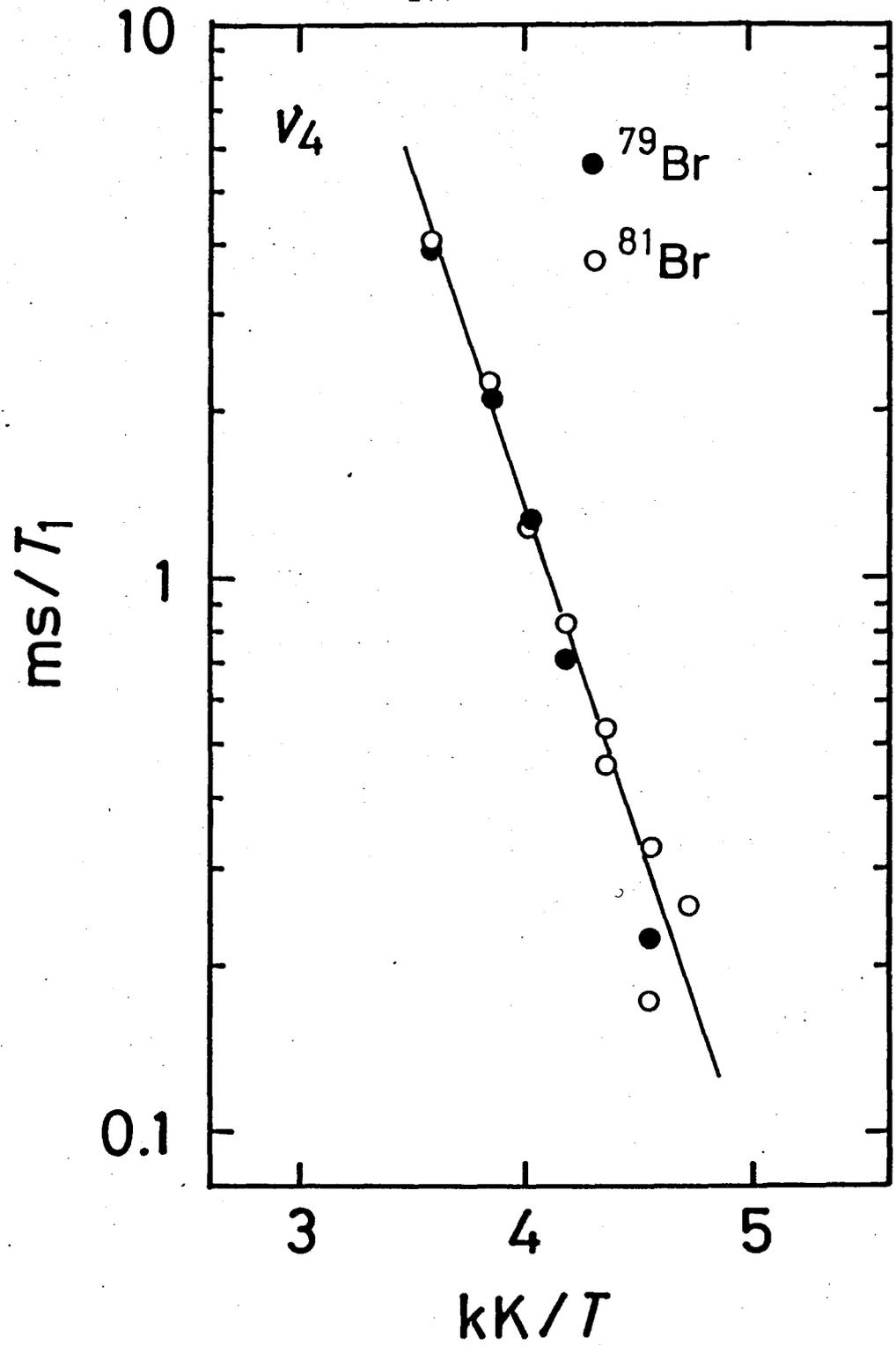
Figure A-4. Relaxation rate for v_4 line deduced by removing the librational contribution.

show a peculiar temperature dependence. According to

the Bayer type theory[7] NQR frequency decreases

monotonously in heating the sample due to increased

vibrational averaging of the efg. But in the present

compound ν_3 increases with increase in temperature in

the whole tmperature region of measurement. Such an

anomalous behavior of the resonance line may be

interpreted as follows:[8] There is formed an inter or

intra-molecular "extra" bond such as CT bond or

hydrogen bond between the resonant nucleus and another

nearby atom so that the efg at the former site is

decreased to some extent, causing NQR frequency to

decrease. When the temperature raises the molecular

tharmal vibrational amplitudes increases and , as a

result, the extra weak bonding is partially broken.

This brings about a positive temperature coefficient of

the NQR frequency. This mechanism may apply to the

system because the nearest distances between either of

two inequivalent nitrogen and every one of four

bromines are distributed between 3.37 and 3.76 $\overset{\circ}{A}$ and

therefore the formation of some hydrogen bond[9] of

type N-H ---Br in $(CH_3NH_3)_2CdBr_4$ is possible. These

hydrogen bonding may be broken as the cation rotates or

reorients about its three-fold axis at the high

temperature (The activation energy for such rotation

is 10 kJ/mol in $(CH_3NH_3)_2TeCl_6$, for example).

Moreover, as was mentioned above, the cations and the

bromines are in some disordered state at room temperaure. If we assume that disordering process proceeds gradually with increase in temperature without the specimen experiencing any phase transition it modulates the structure around the resonant nucleus so as to bring about a change in the efg at the nucleus in an anomalous manner. Some other experimental works such as IR and Raman studies on this compound is desirable to confirm the above mechanism.

References

1. L. Ricard, and J.C. Lassegues, J. Phys. C, $\underline{17}$, 217 (1984); L.J. de Tongh, and A.R. Miedema, Adv. Phys., $\underline{23}$, 1 (1974).

2. P. Muralt, and R. Kind, Helv. Phys. Acta, $\underline{56}$, 689 (1983); W. Depmeier, Acta Cryst., B$\underline{37}$, 330 (1981).

3. D. Altermatt, A. Niggli, W. Petter, and H. Arend, Mat. Res. Bull., $\underline{14}$, 1391 (1979).

4. C.N.R. Rao, S. Ganguly, H.R. Swamy, and I.A. Oxton, J. Chem. Soc., Faraday Trans. 2, $\underline{77}$, 1825 (1981).

5. J. van Kranendonk, and M.B. Walker, Phys. Rev. Lett., $\underline{18}$, 701 (1967); J. van Kranendonk, and M.B. Walker, Can. J. Phys., $\underline{46}$, 2441 (1968).

6. Y. Furukawa, H. Kiriyama, and R. Ikeda, Bull. Chem. Soc. Jpn., $\underline{54}$, 103 (1981).

7. H. Chihara, and N. Nakamura, "Advances in Nuclear Quadrupole Resonance" vol. 4, J. A. S. Smith ed. London, Heyden & Son Ltd, 1980.

8. K. Negita, N. Nakamura, H. Chihara, Chem. Phys. Lett., $\underline{63}$, 187 (1979).

9. G.C. Pimentel, and A.L. McClellan, "The Hydrogen Bond", Freeman, San Francisco, 1960.